8-9-2022

Experimental study on CO2-sensitive polyacrylamide as potential in-situ sealing agent for CO2 leakage pathways in geological storage sites

Iris Laihmen Quan Lopez
Mississippi State University, ilq1@msstate.edu

Experimental study on CO_2-sensitive polyacrylamide as potential in-situ sealing agent for CO_2 leakage pathways in geological storage sites

By

Iris Laihmen Quan Lopez

Approved by:

Maryam Mirabolghasemi (Major Professor)
Kelsey Crane
Amin Amirlatifi
Julie Jessop
Bill Elmore (Graduate Coordinator)
Jason Keith (Dean, Bagley College of Engineering)

A Dissertation
Submitted to the Faculty of
Mississippi State University
in Partial Fulfillment of the Requirements
for the Degree of Doctor of Philosophy
in Chemical Engineering
in the Dave C. Swalm School of Chemical Engineering

Mississippi State, Mississippi

August 2022

Name: Iris Laihmen Quan Lopez

Date of Degree: August 9, 2022

Institution: Mississippi State University

Major Field: Chemical Engineering

Major Professor: Maryam Mirabolghasemi

Title of Study: Experimental study on CO_2-sensitive polyacrylamide as potential in-situ sealing agent for CO_2 leakage pathways in geological storage sites.

Pages in Study: 160

Candidate for Degree of Doctor of Philosophy

ABSTRACT

As the world pushes for 'greener' technologies and carbon neutrality, efforts have focused on creating novel ways to mitigate humankind's carbon footprint. Carbon capture and storage (CCS) has become a prevalent technique that has proven to be an effective long-term method to safely relocate excess carbon dioxide (CO_2) into subsurface formations. However, CCS is a newer technique which requires constant monitoring due to potential leakage pathways present in CO_2 storage sites; therefore, a preventive approach to seal leakage pathways is recommended. This dissertation explores the potential of CO_2-sensitive polyacrylamide (CO_2-SPAM) as a novel sealing agent for enhanced oil recovery (EOR) and CCS applications. This manuscript explores the strength and weaknesses of various CO_2-triggered chemicals and selects the appropriate fit for subsurface in-situ sealing. Relevant literature shows that CO_2-SPAM can significantly reduce permeability in porous media. Additionally, organically cross-linked polyacrylamide-based gels, of which CO_2-SPAM is one, are thermally stable, resistant to low pH levels, highly injectable, and widely used in various industrial processes. These characteristics make CO_2-SPAM a suitable candidate for in-situ sealing. Further studies were performed to

comprehend the chemical mechanism, rheological behavior, and injection effects of CO_2-SPAM into subsurface formations. Firstly, past literature knowledge and organic chemistry principals were used to develop the complete chemical breakdown of CO_2-SPAM gel's synthesis. Secondly, the effect of salt and polyacrylamide (PAM) concentrations on gelation time, gel strength and viscosity were tested through qualitative (Sydansk gel strength coding system) and quantitative methods (rheometer measurement). The results showed that high salinities increase gelation time and decrease gel strength and viscosity, while high PAM concentrations do the opposite. Lastly, the effects on geomechanical stresses caused by CO_2-SPAM injection into the subsurface are also addressed by using the image well method for pore pressure estimation, and frictional faulting theory. The final results determined that the injection of aqueous CO_2-SPAM would induce seismicity in normal faulting zones dipping at a large array of angles in the plane of failure. These findings are significant as they determine the potential of induced seismicity in the area of CCS, which in this case was the Raton basin.

DEDICATION

Insistir, persistir, resistir y nunca desistir.

ACKNOWLEDGEMENTS

First and foremost, I would like thank Dr. Maryam Mirabolghasemi for giving me a once in a lifetime opportunity to be part of something bigger than myself. She has guided me throughout every stage of this research project with her immense knowledge and plentiful experience. I also wish to acknowledge my fellow co-authors, committee members and graduate colleagues for their assistance and insightful feedback throughout the past four years. Lastly, I want to thank my family and friends, especially my mom and dad. Without their tremendous encouragement and unconditional support in the past few years, I would not be where I am today.

TABLE OF CONTENTS

LIST OF TABLES

LIST OF FIGURES

CHAPTER I

INTRODUCTION

Impacts of Global Warming

Global warming and ocean acidification are just a few of various environmental issues humankind has been facing for the past decades due to the continuous increase of greenhouse gases (GHGs) from anthropogenic sources. In 2019, the Environmental Protection Agency (EPA) reported 6,558 million metric tons of carbon dioxide (CO_2) released into the atmosphere which is an increase of 3% since 1990.[1,2] Further reports from EPA indicate that excess of GHGs, such as CO_2, nitrous oxide (NO_2) and fluorinated gases, have increased by 3%, 1%, and 86%, respectively between 1990 and 2019.[1] These gases are presently decreasing the amount of infrared radiation energy escaping the Earth's atmosphere and increasing the accumulation of heat at the Earth's surface causing a more severe greenhouse effect.[3]

Naturally occurring GHGs from plant respiration/decomposition, volcanic activity, and the ocean are crucial to maintain an adequate temperature to sustain life on Earth. The natural greenhouse effect happens when infrared (solar) radiation energy enters the Earth's atmosphere, and a percentage of the energy is reflected to space after the rest is absorbed by Earth's surface.[4] At typical atmospheric levels of GHG, a lesser amount of heat is absorbed by GHGs.[4] However, due to excess GHGs from man-made sources, a significant amount of infrared radiation is accumulating in the lowest layer of the troposphere.[3,4] Heat waves that are redirected back to space are being intercepted by greenhouse molecules.[3,4] When these gas molecules intercept the

heat waves, they “vibrate” and reflect the heat wave back to each other or back to the surface of the Earth.[3] CO_2 is known to be denser than most gases, which means that it is closer to the Earth’s surface; therefore, the constant redirecting of heat waves in the troposphere is causing the Earth’s surface to “warm up”. The continuous increase in temperature causes anthropogenic global warming and climate change. The frequency and severity of some weather events such as droughts, wildfires, heavier rainstorms, and melting of the glaciers are significantly affected by climate change.[3]

In 2002 and 2012, the National Oceanic & Atmospheric Administration (NOAA) recorded CO_2 concentrations of 375.69 ppm and 395.91 ppm respectively for the month of June. The CO_2 concentration has continuously increased up to 420.51 ppm as of June 2022.[5] Excess atmospheric CO_2 also dissolves into the oceans, threatening marine organisms by causing an imbalance in pH and increasing acidity levels.[4] As a result of these problems, many scientists and engineers have developed several methods and technologies to combat these issues and remediate them before it is too late. Carbon capture and storage, also known as carbon sequestration, is a relatively new method used to decrease atmospheric CO_2 levels and prevent future complications.

Carbon Capture and Storage

Carbon capture and storage (CCS) is a technology used to reduce the amount of CO_2 in the atmosphere, and is routinely cited as a feasible tool for climate change mitigation.[6–12] CCS is able to offset industrial CO_2 emissions and is vital for the retention of extracted CO_2 from the points of production.[7] This process involves the capturing of CO_2 from power plants that burn fossil fuels, and many other CO_2-producing sources,[7] followed by the injection of highly pressurized (supercritical) CO_2 into geological formations.[7] To be an effective climate change

mitigation tool, CO_2 must be securely retained for 10,000 years with a leakage rate below 0.01% per year of the total amount of CO_2 injected.[13] Currently, there are limited locations around the globe where CO_2 injection into subsurface storage sites takes place; therefore, the behavior of pressurized CO_2 in confined geological formations is still not completely understood. Broadly studied storage sites include saline aquifers, coal beds, and depleted oil and gas reservoirs.[14] Petroleum engineers and professional geologists have a significant preference for depleted oil and gas reservoirs because they readily provide large storage capacity and strong rock integrity.[7] Additionally, saline aquifers have been often considered a viable option by other authors because of their large storing capacity and broad distribution; however, the risk associated with CO_2 leakage into overlaying resource-bearing strata and CO_2 contamination of soil, ground potable water, and vegetation may outweigh its benefits.[15–20]

As mentioned earlier, depleted oil and gas reservoirs are the most common storage sites for carbon storage due to their relative stability and massive size.[21] These reservoirs are composed of sedimentary rocks with a rock composition that varies between fine to coarse grained permeable rocks (sandstones, carbonates, etc.).[4] Most common oil and gas reservoirs are composed of sandstone with an impermeable shale layer that acts as a seal as seen in Fig. 1.1[22]. Shale is comprised of clay-sized particles and has extremely low porosity and permeability. The cap rock, also known as the trap or seal, prevents the migration of hydrocarbons into the surface and keeps them trapped inside the reservoir rock at high pressures and temperatures.[23] During CCS, CO_2 is injected into the reservoir rock where the hydrocarbons used to be present before extraction. The impermeable shale layer will act as a seal to keep the CO_2 trapped for hundreds of years similar to how it previously functioned for crude oil and natural gas. Engineers rely on

the impermeable properties of the cap rocks to keep the CO_2 stored in the subsurface for a long period of time, but in some cases the cap rock can be compromised.

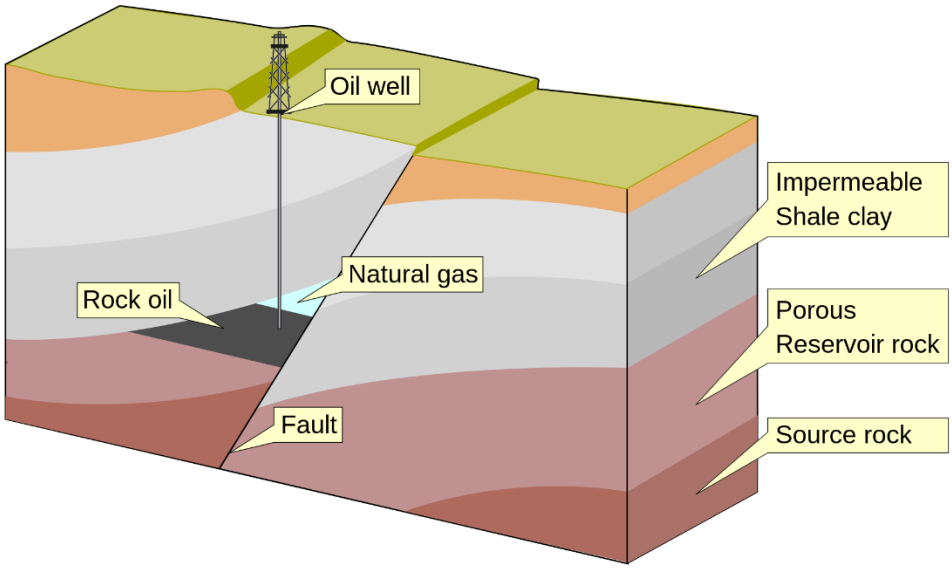

Figure 1.1 Oil and gas trap layers in a faulting zone.

Note. Reprinted with permission from MagentaGreen (2014). Copyright 2014 by Wikimedia Commons CC BY-SA 3.0. No changes or alterations were made to the original work.

As mentioned before, when the recoverable hydrocarbons are extracted and the reservoir is no longer productive, the reservoir can be utilized as a carbon storage site for CCS. During the combined CCS and enhanced oil recovery (EOR) process, high purity CO_2 is injected into the reservoir at high pressures to act as a viscosity reducing agent and provide miscible displacement of the remaining oil from the effective pore space.[24,25] This practice is an example of an enhanced oil recovery technique. EOR is a petroleum recovery process used to extract oil when natural or enhanced pressurized methods are no longer viable.[26] Many oil and gas corporations try to implement CCS during their EOR process as an effort to contribute to air quality improvements and to address environmental concerns.[27–29]

Sustainability of CO_2 Storage

Chemical reactions that take place inside a reservoir may deteriorate and destabilize the structure of the formation by increasing the pore space.[30]For example, silicate minerals that are highly soluble and non-stable (such as plagioclase feldspar, pyroxenes, and amphiboles) may dissolve in the presence of organic acids and increasing burial pressure.[4] The dissolution of grains and cement increases the porosity and permeability of the rock structure. This effect is different from diagenesis as, typically, diagenesis is thought to decrease porosity and permeability through physical and chemical processes where loose sediments progressively compact and lithify to become a cemented rock.[4]

Conditions inside a CO_2 storage reservoir are in favor of dissolution due to the presence of formation fluid and high concentrations of injected CO_2, which in return creates carbonic acid.[4] High temperatures and pressures also play an important role during this chemical reaction. The conditions inside the reservoir can reach levels that may affect the mineralogy of the sandstone or the stability of the reservoir.[14] As mentioned before, it is recommended to understand the effects of storing high concentrations of CO_2 inside reservoirs in order to successfully store it for thousands of years without the potential of leakage. Two main challenges that threaten the sustainability of subsurface CO_2 storage are chemical weathering, and faults and fractures in the geological formation. Both issues are worth mentioning and will be discussed, but the underlying mechanisms of chemical weathering fall outside of the scope of this research.

Chemical Weathering: Simple Solution and Hydrolysis

Chemical weathering is the change of a rock's chemical and mineralogical composition through chemical reactions.[4] Sandstones have silicate minerals that go through a chemical weathering process called simple solution.[4] Simple solution, also known as carbonation, happens

when minerals in sandstones react in an acidic environment and successively break down its content into an aqueous solution with no new minerals being created.[31] This weathering process occurs when minerals go into complete dissolution without the precipitation of other substances. The bonds between mineral ions are broken and as a result, the mineral is destroyed and releases constituent ions into the water solution.[4] As CO_2 is injected to a depleted oil and gas reservoir, it is expected to slowly diffuse in the formation fluid present in the pore space (i.e., brine and crude oil). The following chemical reaction (Eq. 1.1) demonstrates that high concentrations of CO_2 with water will form carbonic acid and subsequently bicarbonate with hydrogen ions H^+.

$$CO_2 + H_2O \leftrightarrow H_2CO_3 \leftrightarrow H^+ + HCO_3^- \quad (1.1)$$

The increasing production of H^+ will contribute to a more acidic setting and will favor a more aggressive dissolution of minerals such as calcite, dolomite, gypsum, halite and even quartz.[4]

Hydrolysis is the most important chemical weathering process where silicate minerals, commonly found in sandstones, mix with organic acids and do not culminate into a complete dissolution.[4] It is the primary process of silicate mineral decomposition during weathering where these minerals break down and release metal cations.[4] These types of incomplete dissolution processes are known as incongruent dissolutions. For example, the presence of a metal in a feldspar-rich sand that is going through incongruent dissolution can form clay minerals as a by-product. High concentrations of CO_2 dissolved in water makes the hydrolysis reaction more aggressive, but it is important to mention that hydrolysis may also occur in environments

containing little to no quantities of CO_2.[4] Moreover, hydrolysis might contribute to reservoir deterioration and may affect preventive remediation techniques for carbon storage sites.[32]

Simple solution and hydrolysis are two main reactions that are most likely to occur in a geological formation meant for carbon storage. These chemical reactions have the potential to affect carbon storage sites by destabilizing the formation's structure and weakening its integrity which can cause consequences such as an exorbitant financial loss for industries funding CCS pilot projects and environmental concerns if collapsing of the subsurface formations occurs.[32] Although these processes are very common in sedimentary rocks, sandstones are more likely to resist these chemical reactions. Sandstones are mostly made of strong and stable mineral quartz. Quartz can be subjected to dissolution, but its properties make it strong enough to survive many transitions through geological time, also known as rock cycles.[4] In contrast, carbonate rocks are significantly less mechanically stable and more susceptible to dissolution.[4] Significant secondary porosity created by dissolution can be beneficial to a certain extent. Secondary porosity is a post-depositional or subsequent process that creates more pore space through physical or chemical processes such as rock fracturing or dissolution of minerals.[33] Through this process, more pore space for CO_2 storage is created, but it may also destabilize reservoir's structure.[34] A continuous increase of void space throughout thousands of years might cause a collapse or subsidence in the reservoir that may lead to faults or fractures. Thinning of the rock structure weakens the overall reservoir and decreases its capacity to support overburden pressures.[35]

Mineral dissolution from carbonic acid plays an important role in structural stability of depleted oil and gas reservoirs used for carbon storage. Although failure might not occur for hundreds of years, it is very important to monitor and continue to study the behavior of reservoirs used for carbon storage. Simple solution and hydrolysis can cause secondary porosity

(i.e., possible faults and fractures can develop through time in the reservoir.). This consequence generates a certain degree of concern among environmentalists, but it is currently safe to preserve CO_2 in these geological formations without any reservations of future repercussions due to sandstone's resistant framework, especially when reservoirs are spatially isolated. It is still believed that CCS is one of the best methods to decrease CO_2 concentrations and slow down the effects of global warming, but most importantly, it is considered the safest way to dispose of and relocate excess CO_2. [6,8,25]

Faults and Fractures

The injection of large amounts of CO_2 in geological formations to offset GHG emissions may potentially induce tectonic movement and can consequently activate underground fractures in the cap rock.[36] The geological formation's integrity is one of the main concerns for a successful CCS process; therefore, the structural condition of the formation's cap rock is a determining factor of whether or not a site is secure for CO_2 storage.[37] In a geological CO_2 storage site, faults and fractures caused by natural or anthropogenic events can create leakage pathways from the reservoir rock layer to the surface, making the efforts of carbon sequestration less effective. Fractures are cracks in the rock which open when stresses are sufficient while faults are fractures with measurable offset. Either structure can be formed or activated by tectonic activity, failure of injection operations, or deep well injections.[38] Faults are comprised by zones of crushed, sheared and fractured rock that have the potential to influence the migration of stored CO_2.[39] Locating pre-existing faults in three-dimensional seismic data can be challenging. Nonetheless, it is safe to assume that all rocks in the upper lithosphere are fractured. Problems arise when these fractures are connected and provide a leakage pathway for CO_2.

Therefore, it is critical for engineers to determine the probability of CO_2 leakage through different methods and strategies.

Several studies have been conducted in the past to estimate the probability of CO_2 leakage through faults and fractures at CO_2 storage sites.[40–43] Quasi-1D single phase flow models, percolations theory, fuzzy rules, and risk assessments are computational simulation methods and hazard identification processes that have been used to estimate the connectivity of existing conduits at a specific site and the probability of CO_2 leakage [41] Conduits refer to the underground channels where CO_2 may escape. Zhang et al. (2009)[41] designed a risk assessment project that could fit into the certification framework, developed by Oldenburg et al. (2009),[40] of a geological CO_2 storage with the objective to develop a detailed foundation for evaluating the risk of leakage in order to approve CCS operations. The certification framework (CF) is a practical risk-based framework used for assessing and approving whether the leakage risk of a potential storage site is below an agreed-upon threshold. It proposes a standardized way to project proponents, regulators, and the public to analyze and understand risks and uncertainties of geological carbon sequestration.[40] Safety and effectiveness are achieved if CO_2 and displaced brine have no significant impact on humans, other living organisms, resources, or the environment. It considers physical and chemical impacts as well as loss of emission-reduction credits due to movements of injected CO_2 and brine.[40] The purpose of the CF is to evaluate the CO_2 leakage risk for each compartment to determine whether the effective trapping threshold will be met for a given storage site.[40] A compartment is defined as a vulnerable entity such as potable groundwater aquifers. Table 1.1 lists the elements of a sample certification framework. These elements are factors that are reviewed, assumed, and taken into consideration when assessing risk of CO_2 and brine leakage. When proposing a preventive permeability reduction

method for leakage pathways, certification framework elements are needed and should be taken into consideration to store CO_2 effectively and safely in geological formations. Fig. 1.2 shows a detailed schematic of the workflow in a CF process.

Table 1.1 Certification framework elements.

Effective trapping	The CF acknowledges that enormous volumes of CO_2 will be injected into the Earth's crust, which is not a leak proof container. The goal of building the CF upon the effective trapping concept is to distinguish benign from harmful migration so that the risk assessment can focus on the likelihood of the latter.
Wells and faults are conduits	The CF assumes that wells and faults are the only potential leakage conduits.
Impact to compartments	The consequences of upward leakage of CO_2 or brine are impact to compartments which are used as collections of related vulnerable entities. ECA: Emission credits and atmosphere HS: Health and safety NSE: Near-surface environment USDW: Underground source of drinking water HMR: Hydrocarbon and mineral resources
Likelihood of impact and risk	Likelihood of intersection of the CO_2 or brine source with a conduit. Likelihood of intersection of the conduit with a compartment. The product of both likelihoods is the probability of the given source-to-compartment leakage scenario.
Plume migration	The source for the leakage scenario is determined by the movement of the CO_2 plume during and after injection, and by the brine movement associated with the CO_2 injection.
Workflow	See Fig. 1.2.

Note. Adapted with permission from the International Journal of Greenhouse Gas Control by Oldenburg et al., 2009, p. 444 - 457. Copyright 2009 by Elsevier.

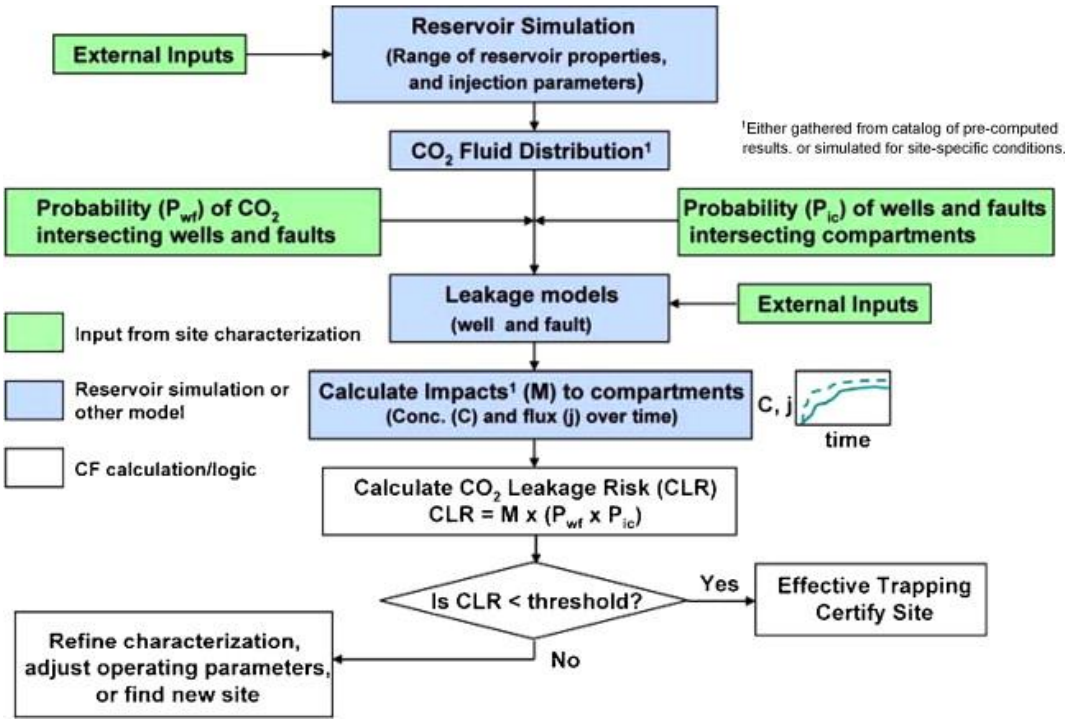

Figure 1.2 Flow chart of the workflow in a CF process where the threshold value is an agreed-upon value provided by external sources such as regulators or carbon credit insurers.

Note. Reprinted with permission from the International Journal of Greenhouse Gas Control by Oldenburg et al., 2009, p. 444 - 457. Copyright 2009 by Elsevier.

It is imperative to take into consideration the regulations under the USEPA Underground Injection Control Class I Program during carbon sequestration to prevent possible migration of CO_2 because this regulation ensures that carbon storage in geological sites do not negatively impact valuable resources and the environment.[41] Unfortunately, because of the large volumes of CO_2 injected, its buoyant nature, and the naturally heavily fractured lithosphere, it is very difficult to meet absolute non-migration-requirements.[41]

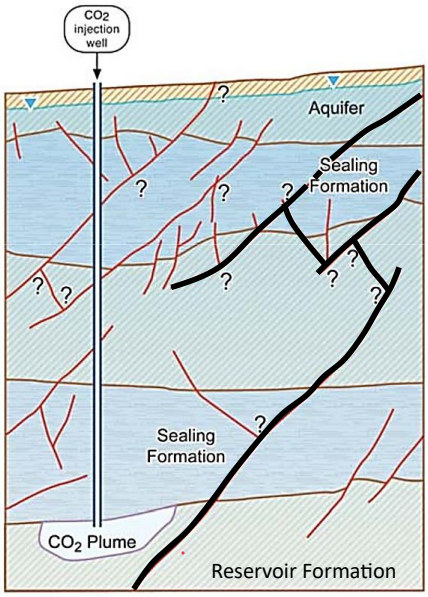

Figure 1.3 Geological cross section demonstrating conductive faults that may or may not intersect as indicated by question marks. Thick black lines depict a connected leakage pathway that extends to the shallow aquifer.

Note. Adapted with permission from Energy Procedia by Y. Zhang et al., 2009, p. 42. Copyright 2009 by Elsevier.

Fig. 1.3 demonstrates the cross-sectional view of a CO_2 injection well, CO_2 plume, reservoir formation, overlaying formations, and potable groundwater aquifer along with conductive faults that have the potential to intersect as indicated with question marks. The probability that the CO_2 plume leaks into a compartment through faults or fractures is related to the geometric characteristics of distribution and connectivity of conduits between the storage reservoir and the compartment, and the size and location of the CO_2 plume.[41] It is challenging to predict whether the conduits are connected and if so, the probability that a CO_2 plume will encounter the connected pathway because there is limited amount of information in regards to the conduit systems.[41] In addition, the location and size of the CO_2 plume is also highly uncertain given the properties of the deep storage reservoir.[41]

A study conducted in 2018 by scientists of the University of Edinburg stated that CO_2 emissions can be captured and securely stored, even if geological faults are present, in a naturally occurring carbon storage site.[13] Researchers from the Universities of Glasgow, Freiburg, Edinburgh, and Heidelberg calculated the natural leakage rates from a 420,000 paleo-record of CO_2 leakage above a naturally occurring, faulted CO_2 reservoir in Arizona, USA.[13] The St. Johns Dome CO_2 reservoir, located on the border of northern Arizona and New Mexico, indicates overall leakage rates of up to 2×10^5 tons per year, which is an order of magnitude lower than annual injection rates at currently operating large-scale carbon storage sites of between 0.7×10^6 and 1.2×10^6 tons per year.[13] It is worth mentioning that faults that provide primary leakage pathways are young and have not yet built up the clay that is naturally produced from weathering fault breccia. This clay built up limits the permeability of the leakage pathway and restricts CO_2 migration.

Sealing CO_2 Escape Routes by In-Situ Polymerization

In-situ remediation processes are necessary for undesired CO_2 migration. A leakage prevention method is recommended in the event of discovering new or undetected leakage pathways in carbon storage sites, specifically depleted oil and gas reservoir for this study. In the past, CO_2 leakage control sealants included cement, geopolymer, foams, biofilm barriers and nanoparticles, but new substances that are CO_2-responsive have grown in popularity.[38] In order to seal the leakage pathways through a fractured cap rock or around wellbores, the usage of CO_2-triggered chemicals have been suggested by several researchers in past literature. These chemical solutions are substances that precipitate or become a gel when they come in contact with high concentrations of CO_2 in reservoir-like conditions.[44] When the chemical seals the leakage pathways in the cap rock, the secondary permeability of this rock layer will decrease

significantly, and the CO_2 will remain contained inside the reservoir. Although various chemical sealing scenarios have been simulated numerically, their effect on reservoir rock for extended periods of time is not well understood yet.

Some of the leakage control sealants mentioned above have been tested for long-term sustainability and performance, but CO_2-sensitive chemicals have the potential to address injectability and mobility issues. Chapter 3 focuses on an in-depth analysis and comparison of a wide range of CO_2-sensitive chemicals that are suitable candidates for in-situ sealing of leakage pathways for CCS applications. It is important that the benefits that come from CCS outweigh potential environmental threats that could harm the ecosystem and human health.[45,46] Thus, when selecting the appropriate CO_2-sensitive chemical for leakage prevention, the influence of temperature, pressure, salinity and pH on its performance needs to be taken into consideration in addition to their chemical properties (i.e., toxicity, injectability, etc.).[38] Previous literatures point out the advantages of CO_2-triggered gel systems over other CO_2-triggered chemicals. CO_2-triggered gel systems are thermally stable, resistant to acidic conditions, highly injectable, widely applied in various industries, commercially available and have shown a significant reduction in permeability in a relatively short amount of time.[14,38,47–56] Limitations of this sealing agent includes a lack of knowledge on long-term gel degradation at reservoir-like conditions and effects of high pressure and salinity on the gel's rheological behavior. Throughout time and with constant high-pressure and elevated temperature conditions, the gel system could potentially reduce its stability and slowly decompose.[38] The following chapters will expand on why CO_2-SPAM is the most suitable candidate for in-situ permeability reduction for CO_2 storage sites by comparing it against other CO_2-triggered systems through a thorough literature review, its

rheological behavior and response to flow and deformation, and its application as a subsurface sealant from a structural geology standpoint.

CHAPTER II

DISSERTATION FOCUS, PURPOSE, AND RESEARCH OBJECTIVES

Issue Statement

Despite extensive research and investigations regarding the possibility of incorporating CO_2-SPAM in CO_2 geological storage operations to prevent CO_2 leakage, the available knowledge on its chemical mechanisms, rheological behavior, and potential to induce seismicity is, to some extent, limited. Firstly, it is important to explore the wide variety of CO_2-triggered chemicals that could be an adequate candidate for in-situ sealing. Hence, a thorough literature review will determine which chemical possesses the required qualities needed for a proper seal and why CO_2-SPAM is ultimately chosen to be further investigated. Secondly, the sequence of reactions that take place in order to synthesize CO_2-SPAM is partially unclear. Therefore, a breakdown of CO_2-SPAM synthesis is done using past findings and organic chemistry principals. Thirdly, previous studies have not established patterns in the rheological behavior of CO_2-SPAM gel as a function of salt concentration in the brine and polyacrylamide (PAM) concentration. Gelation time, gel strength, and viscosity are important rheological properties that affect the stability and feasibility of incorporating CO_2-SPAM in future CCS pilot projects. These factors dictate the gel's mobility across reservoirs, the injection time and injection rate in addition to its plugging performance. Lastly, there is minimal information on how CO_2-SPAM solution injection has the potential to induce seismic activity and what properties of CO_2 storage sites make them prone to induced seismicity. These gaps in previous investigations call for a

comprehensive study of the rheological behavior of CO_2-SPAM and its implementation to prevent CO_2 leakage from storage sites.

Research Objectives

The objective of this study is to form a well-established understanding of the necessary qualities and characteristics a CO_2-sensitive chemical must have to be an ideal sealing agent for in-situ permeability reduction. Also, once the CO_2-sensitive chemical is determined, a series of experiments will determine the material's properties under reservoir-like conditions to predict its behavior once it is injected into a subsurface formation. To do so, this research project focused on:

- Identifying CO_2-SPAM's attributes over other chemicals.
- Developing CO_2-SPAM's sequence of chemical mechanisms.
- Determining patterns in the rheological behavior of CO_2-SPAM as a function of salt and PAM concentration.
- Estimating the potential of induced seismicity as CO_2-SPAM is injected into the subsurface.

Conditions such as temperature, salt concentration, and polymer concentration were taken into consideration to establish a realistic working environment. The experimental study provides a clearer understanding of the phenomenon of what is expected from CO_2-SPAM. This dissertation investigates the following research objectives:

1. **Determine the advantages and disadvantages of CO_2-triggered chemicals.** Through an in-depth literature review, several materials that respond to CO_2 and may be used as in-situ sealing agents were investigated. Chapter 3 is a comprehensive literature review of materials tested and used as sealing agents, such as polymer gels, precipitated minerals, resin systems, etc., in other research projects. This summary provides a synopsis of the benefits and

drawbacks of CO_2-triggered reactions and CO_2-sensitive materials in the context of in-situ sealing of leakage pathways.

2. **Establish the chemical mechanisms of CO_2-SPAM gel's synthesis.** CO_2-SPAM is a resorcinol-methenamine-polyacrylamide gel system that is synthesized in the lab from non-ionic PAM. The chemical mechanism of this synthesis has not been fully described due to various chemical mechanism involved, such as hydrolytic decomposition, neutralization, hydrolysis and polymerization. These complex chemical mechanisms are explained in detail in Chapter 4. The analysis provided in this chapter helps explain the behavior of CO_2-SPAM and how salt and PAM concentration influences its gelation time and gel properties.
3. **Analyze the effects of salt concentration from formation fluid and PAM concentration on CO_2-SPAM gel's gelation time, strength, and viscosity.** Chapter 5 provides a thorough analysis of the effects of salt concentration and PAM concentration on gelation time, and gel strength and viscosity. The salinity levels vary widely among different oil and gas reservoirs. Thus, the effect of these factors on gel behavior must be known for a successful sealing scenario.
4. **Estimate the possibility of induced seismicity through CO_2-SPAM injection for CCS applications.** Induced seismicity is not an uncommon tectonic activity in the oil and gas industry. Wastewater injections and conventional EOR techniques have caused seismicity for half a century. In Chapter 6, the concept of induced seismicity caused by CO_2-SPAM injection is studied based on well data from the Raton basin. The Raton basin is an oil and gas producing depression that has been used as a wastewater disposal structure. Additional scenarios will be taken into consideration to clarify the effect of pore pressure incrementation on fault activation.

Intellectual Merit

Carbon Capture and Storage (CCS) is a GHG technology aimed to mitigate global warming, but it comes with its limitations. The carbon storage phase plays a major role in determining the effectiveness of this method; therefore, approaches to prevent CO_2 leakage is crucial. Studies have been conducted on sealing agents such as cements, foams, geopolymers, resin systems, biofilm barriers and gel systems, but their ability to withstand extreme conditions is questionable. Although the mentioned materials have their advantages, CO_2-SPAM gel's characteristics are better suited for reservoir-like conditions and subsurface injection processes. PAM has been used broadly in water treatment processes as flocculent, in the pulp and paper industry as pulp fiber binder, and in hydrocarbon production as additive for hydraulic fracturing purposes. The testing of PAM's properties, such as its behavior in highly saline solution, will benefit the petroleum and environmental engineering fields and push towards its real-life application. Moreover, there has been a growing interest in CO_2-SPAM gels due to their potential application in CO_2 storage sites as sealing agents and as a result, there has been extensive research done for this specific material. Researchers have studied the effects of metal cross-linkers, temperature, nitrogen, and CO_2 on the strength of the resulting PAM gel system. However, the effects of salinity and PAM concentration on CO_2-sensitive PAM gel's strength and gelation time are not well understood. Additionally, the geomechanics involved in the injection of this polymer solution have not been studied in the past.

Broader Impact

Due to the rising issue of global warming, climate change, ocean acidification, heat waves, and wildfires, researchers have been focusing on methods to reduce the emission of GHGs and develop technologies to store these gases in unproductive geological formations. CCS

is able to safely store excess CO_2 to mitigate global warming. CO_2 storage sites are subsurface geological formations surrounded by impermeable rock formations. However, leakage pathways might exist or develop in this formation's layers posing a threat to this method. To prevent CO_2 escape through these leakage pathways, the usage of CO_2-sensitive PAM gel systems has been proposed. These gel systems change from an aqueous solution to a solid or solid-like state upon contact with CO_2. The procedure blocks the pre-existing escape routes without requiring any prior knowledge about the location of those leaking routes. This research focuses on expanding the limited knowledge in the carbon storage field by evaluating the effectiveness of CO_2-sensitive PAM gel system as a sealing agent under reservoir-like conditions at different salinity levels. This study targets the improvement and optimization of GHG technologies and the overall betterment of the environment.

CHAPTER III

EXPLORATION OF CO_2-SENSITIVE CHEMICALS AS POTENTIAL SEALING AGENTS FOR CO_2 STORAGE SITES

Introduction

Alarming levels of CO_2 have filled the troposphere and is currently threatening life on Earth. Climate change, ocean acidification, heat waves, and wildfires are few examples of consequences humans are facing due to excess CO_2 from anthropogenic sources.[57] As a result, researchers have investigated the possibility of extracting CO_2 from anthropogenic sources and storing it in subsurface geological formations such as depleted oil and gas reservoirs, saline aquifers, and coal beds.[14] This process is referred to as Carbon Capture and Storage (CCS). Unfortunately, the CCS process may be compromised when leakage pathways are present in the storage sites.[7] Leakage pathways include natural or anthropogenic fissures, fractures, and or faults in the cap rock. Leakage pathways can be created through time and tectonic plate's movement or during exploration and drilling phase.[38] In such cases, remediation processes must be implemented to successfully continue the CCS process.[7]

Engineers have faced several challenges in regard to CO_2 leakage mitigation due to limited technologies and access to the leakage pathways. Occasionally, engineers, operators, or geoscientists misinterpret 3D seismic data containing pre-existing faults. Thus, a better approach to ensure CCS sustainability is leakage prevention. Theoretically, sealing all potential leakage pathways before initiating CO_2 injection is the most reliable method to prevent CO_2 escape.

However, locating all leakage pathways in the subsurface is virtually impossible.[41] Numerous studies have been conducted to estimate the probability of CO_2 leakage through faults and fractures at CO_2 storage sites as mentioned in Chapter 1.

Even if locating individual leakage pathways is possible, they are nearly impossible to access in most cases.[41] Sealing subsurface flow paths is commonly carried out by injecting polymer solutions along with a cross-linker. An in-situ polymerization reaction will follow the injection, resulting in the formation of a polymer gel that seals the flow path.[58,59] For an environment saturated with CO_2, however, most of these polymer gels are unstable and they degrade with time, rendering the seal useless.[58,59] Using a polymer that is resistant to CO_2 or a reaction that is triggered by CO_2 may lead to durable sealing.[58,59] When sealing individual leakage pathways is not an option, a more conservative preventive approach might prove practical. This solution consists of creating a sealed layer at the top section of the storage reservoir as demonstrated in Fig. 3.1.

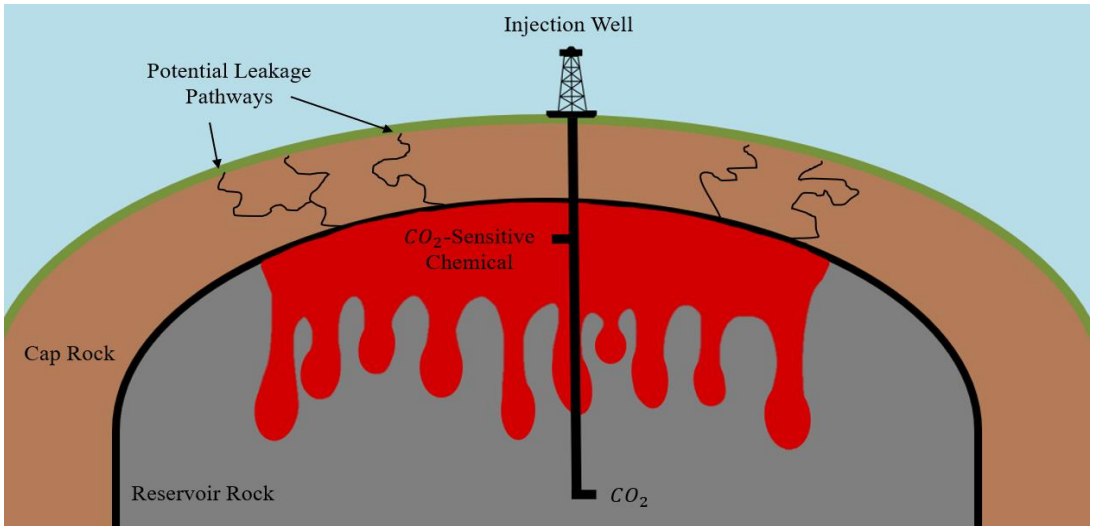

Figure 3.1 Schematic of CO_2-sensitive chemical injection into a depleted oil and gas reservoir for the purpose of preventive in-situ sealing of potential leakage pathways. Ratios do not reflect actual material volume.

In this approach, a CO_2-sensitive chemical, which is in liquid form, is injected at the top section of the reservoir. CO_2-sensitive chemicals are chemical substances such as a polymer, resin, microgel, or mineral solution that, under reservoir conditions, react with CO_2 and form solid or solid-like compounds. Next, CO_2 is injected at the bottom section of the reservoir and diffuses through the reservoir. CO_2 diffusion through porous media is a transport phenomenon worth noting as it provides a clear idea of CO_2 concentration across the reservoir. (Appendix A establishes the governing equations dictating the CO_2 diffusion in porous media and the concentration profile of CO_2 through a CO_2 storage site.) The CO_2-sensitive chemical will travel downwards due to gravity and the CO_2 will travel upwards due to buoyancy. When CO_2 encounters the CO_2-sensitive chemical, a series of reactions take place and a seal forms, which plugs the pore space of the host rock formation. For this specific set up, the relationship between density of the material versus the density of supercritical CO_2 is an important indicator of the feasibility of this application.

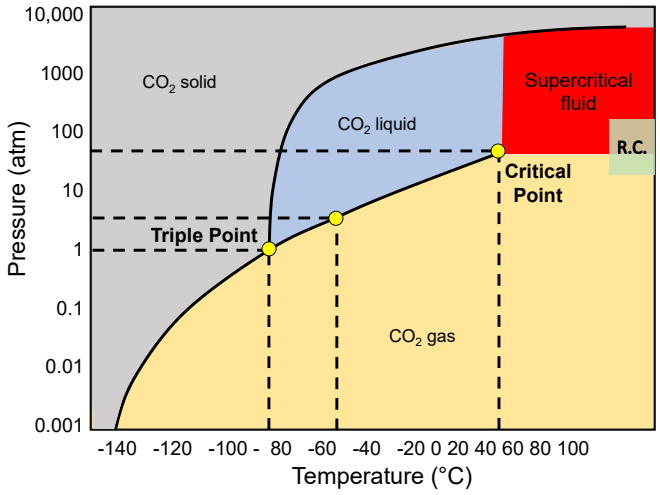

Figure 3.2 Carbon dioxide phase diagram with the typical range of reservoir conditions (green box).

It is expected that the CO_2-SPAM will overcome the injected CO_2's density. To examine the relative densities of injected solution and CO_2, the phase behavior of CO_2 and water at CO_2 storage site pressure and temperatures is studied (Fig. 3.2 and Fig. 3.3). Here, the green box illustrates reservoir conditions (R.C.) which range from 88°C to 175°C and 61 atm to 245 atm. It is clear that under a wide range of pressures and temperatures, water remains in the liquid state and CO_2 is in supercritical or gas phase. As a result, CO_2 will be less dense than the injected solution and they will flow towards each other under the proposed injection scenario.

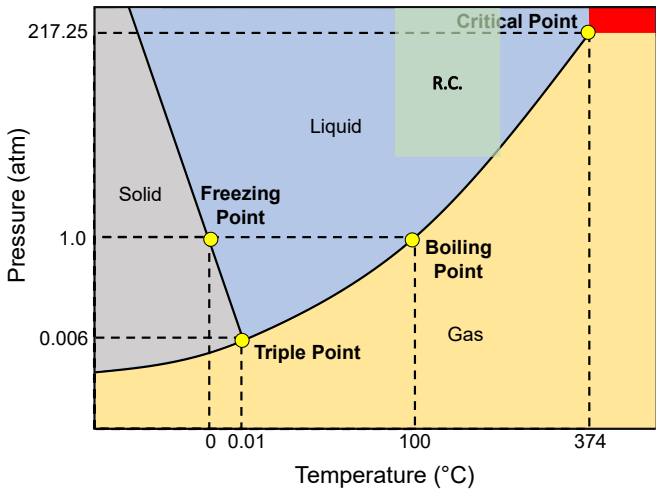

Figure 3.3 Water phase diagram with the typical range of reservoir conditions (green box).

The presence of CO_2 and the CO_2-sensitive chemical either triggers or catalyzes a reaction, which leads to the creation of a solid or solid-like material. A limited number of CO_2-sensitive chemicals have been tested by researchers for the specific purpose of measuring their sealing performance under reservoir conditions.[14,54,60] On the other hand, CO_2 has been used to influence reactions such as polymerization, solidification, precipitation, and gelation for various

industrial and medical applications. Although these applications might not be directly related to CCS, they provide the needed knowledge on which CO_2-sensitive chemicals may potentially be used for preventive sealing of subsurface CO_2 storage reservoirs.

This chapter explores a wide range of reactions that are influenced or triggered by CO_2, leading to the formation of a solid or solid-like material that could potentially seal geological formations. The reactions are categorized as "solid formation" and "particle growth." These are the mechanisms by which a reaction results in the blockage of the flow paths in porous and/or fractured media. Solid formation is the category where chemicals solidify through polymer gelation, mineral precipitation, and resin formation. The particle growth category includes aggregation and swelling. Particle growth mechanisms go through a particularly different chemical reaction were polymer particles' sizes increase. Consequently, these particles block the flow paths in porous media, including fractures and fissures. Ultimately, this study will focus on determining the best suited CO_2-sensitive material for CCS applications.

Solid Formation

Gelation

CO_2 is widely known to be a triggering factor during gelation processes. The mechanisms by which CO_2 triggers or catalyzes gel formation are diverse. For instance, certain substances are influenced by the acidic environment induced by the carbonic acid. As CO_2 dissolves into the solution, hydrogen ions are formed, causing the pH to drop.[14] Other cases are when gelation is triggered by cross-linkers that are responsive to or are activated by high concentrations of CO_2. A cross-linker is a chemical substance that creates a bond or sequence of bonds that link one polymer molecule with another. These mechanisms by which CO_2 induces gelation are discussed in this section.

CO_2 is known to cross-link molecules with amino groups on their side chains.[61] Exploiting this mechanism, Nagai et al. (2011) synthesized a hydrogel by using CO_2 as a gellant. The synthesis of the hydrogel was through a cross-linking process using aqueous solution of polyallylamine (PAA), a base (1,8-diazabicyclo[5,4,0]-undec-7-ene), and CO_2 under high pressure and temperature (2.5 – 5 MPa, 170°C) as seen in Fig. 3.4.[61]

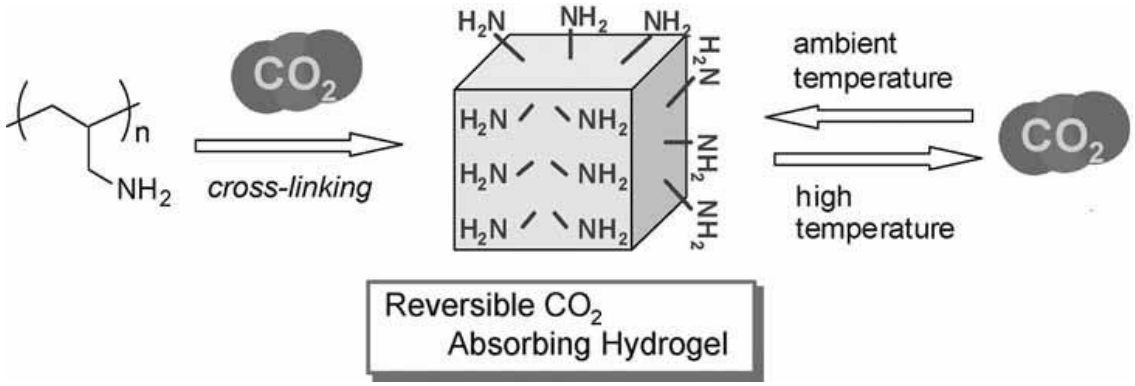

Figure 3.4 Reversible CO_2 absorbing hydrogel.

Note. Reprinted with permission from the Macromolecular Rapid Communications by Nagai et al., 2011. Copyright 2010 by John Wiley and Sons.

This reaction is useful for in-situ sealing because the produced hydrogel not only blocks the leakage pathways, but it is also capable of absorbing high volumes of CO_2.[61] This study also reported that the absorption and desorption of CO_2 does not negatively impact the hydrogel integrity, which is a key property of a potential sealing material. In 2001, another study explored the use of aliphatic amines as latent gelators with CO_2 as a trigger or gelling agent at room temperature.[62] The amine solution starts to gel when it is exposed to CO_2. The presence of CO_2 in the amine solution creates carbamate salts. This gelation process may be reversed by bubbling nitrogen into the heated gel. Additionally, it was found that the ammonium carbamate gelators

are better and more stable (for over 3 months) if the n-alkyl chains of the primary amines are longer.[62] Another amine-CO_2 gelation reaction was introduced by Carretti et al. in 2003 where they used a polyallylamine-alcohol (PAA-alcohol) solution and CO_2 to act as a gellant.[63] Their findings show that when CO_2 is introduced to the PAA-alcohol solution, gelation will take place as carbamate groups are formed.[63] These carbamate groups act as cross-linkers and a gel-sol transition is attained when the temperature is increased enough to release CO_2.[63] In other words, high temperature environments may destabilize the formed gel. Polyethyleneimine (PEI) was also investigated by Carretti et al. (2008) due to its wider commercial availability and greater stability compared to PAA.[64] This compound follows the same mechanism as the PAA reaction with CO_2 where the PEI solution creates a gel when it is exposed to CO_2, due to the carbamate groups.[64] Moreover, the addition of amino groups to polysiloxanes leads to polymers that form a gel when in contact with CO_2. In this process, the cross-links are formed through electrostatic interactions between the CO_2 and the amine groups. The formed gel is stable at room temperature[65,66] and adheres strongly to other surfaces.[67]

Researchers at the University of Kansas developed an in-situ gel system aimed to control the mobility of supercritical CO_2 in heterogeneous reservoirs during CO_2 injection for EOR.[68] This study's experiments were conducted on brine-saturated Berea sandstone cores with initial permeabilities of 70-700 mD, at temperatures between 32.2ºC and 41ºC. This research used the following CO_2-sensitive compounds:

1. KUSP1: This biopolymer is soluble in alkaline solutions above a pH of 10.8 but forms a firm gel when the pH is reduced to 10.8 or below. So, by injecting supercritical CO_2 into the core sample that was saturated with the alkaline polymer solution, they induced gelation, which resulted in over 80% reduction in the permeability of the core sample. This author did not disclose the chemical composition of KUSP1.[68]

2. Sulfomethylated resorcinol and formaldehyde (SMRF): The reaction between these two compounds creates a gel in the presence of brine and supercritical CO_2. This study recorded a permeability reduction of 99% caused by the gelatin reaction at atmospheric pressure and 41°C.[68]

In 2016, a study investigated the use of modified polyacrylamide-methenamine-resorcinol gel system to selectively control CO_2 channeling and reduce its mobility.[48] During this in-situ process, a reaction is triggered by the highly acidic environment brought about by CO_2.[14,48,69] At elevated temperatures and high acidity levels, the methenamine releases formaldehyde which can further produce phenolic resin through polycondensation with resorcinol.[14,48,69] The phenolic resin further reacts with the polyacrylamide and produce strong enough linear polymers that are able to seal channels.[14,48] This gel system's gelation initiates when CO_2 is present; therefore, the aqueous solution will be able to flow for longer distances in the reservoir before it settles and fully gels. This study tested the gel system in two testing tubes for bottle testing under a constant pressure that varied among the experiments between 0.2 and 1 MPa, and a gel solution salinity of 20,000 ppm.[48] This research concluded that increasing pressure decreased the gelation time, although the tested pressures are too low compared to typical subsurface pressures.[48] Additionally, a sand pack experiment was conducted where CO_2-SPAM gel's blocking performance was evaluated. It was concluded that at 80ºC the gel solution has good CO_2 sensitivity and becomes very strong.[48] Their findings also indicate that the gelation time decreases as temperature increases.[48] Furthermore, as the concentration of polyacrylamide increases, gel strength increases but its viscosity decreases, however, the viscosity drop can be modified by increasing the temperature.[48] Finally, this study reported up to 99% of permeability reduction in their low-permeability samples, whereas the permeability of the high-permeability sand packs decreased by 90%.

Poly(ionic liquids) (PILs) are another class of CO_2-sensitive chemicals that form a gel upon contact with CO_2. A recent study developed a PIL through the copolymerization of an imidazolium-type ionic liquid monomer at 25ºC and 1200 psi.[70] The CO_2 was bubbled into the PIL solution and changed its rheology, converting it into a stable gel. This PIL gel reverses its state back into an aqueous solution when nitrogen is bubbled into it.[70]

Han et al. (2012) synthesized a CO_2-senstivive hydrogel by incorporating a weak acid comonomer into a thermosensitive polymer block.[71] After dissolving the synthesized polymer in water, the authors bubbled CO_2 through the solution and observed a sol-gel transition. They stated that the acid comonomer responds to the CO_2 and renders the polymer less soluble in water. The acid comonomers that were tested were acrylic acid, methacrylic acid, and ethyl acrylic acid, which they incorporated into $PMEO_2MA$, a thermosensitive polymer.[71]

Electrostatic interactions induced by CO_2 is another mechanism by which CO_2 may trigger gelation. These interactions take place in aqueous solutions of triblock copolymers. One study tested an ABA-type triblock copolymer which consisted of a middle block (B), which is hydrophilic, and two end blocks (A), which are CO_2-responsive.[66] Their method consisted on mixing two ABA triblock copolymers with the same B block but different A blocks (First triblock copolymer was a negatively charged polyelectrolyte and the second one was turned a positively charged polyelectrolyte under CO_2 conditions).

Triblock copolymer 1: $PMAA^-$-b-PEO-b-$PMAA^-$

Triblock copolymer 2: $PDMAEMA^+$-b-PEO-b-$PDMAEMA^+$

Gel-sol transition was observed when two ABA triblock copolymer solutions were mixed, and CO_2 was bubbled through the mixture. The transition to gel is a result of electrostatic interaction between the oppositely charged A blocks on the two copolymers.[66] CO_2 brings about

this electrostatic interaction by protonating the A blocks on the CO_2-responsive copolymer.[66] This research focused on achieving CO_2-induced gelation of polymer aqueous solutions at very low polymer concentrations.[66] The authors reported that the gel strength is tunable in this gelation method, and the gelation reaction is stable within wider temperature ranges compared to other methods.[66]

Some advantages that gels have are their ability to withstand high temperatures, CO_2 resistance, and the ability to be reversed into an aqueous solution. The reversibility of gel-sol conversion has potential applications in EOR and conformance control. In addition, gel solutions are ideal for injection processes where the solution needs to be low viscosity.[38] Certain disadvantages regarding gels include the lack of available information regarding their rheology at high pressures and salinity levels.

Precipitation

Mineral precipitation is another mechanism that results in solid formation. Mineral carbonation is a mechanism by which insoluble salt precipitation is triggered by CO_2.[72,73] For example, precipitation of calcium carbonate ($CaCO_3$) by bubbling CO_2 in an aqueous solution of calcium hydroxide ($Ca(OH_2)$) with ammonium hydroxide (NH_4OH) acting as a catalyst is a significantly fast reaction at room temperature and ambient pressure.[74]

Calcium carbonate precipitation for CCS has been proposed as a viable method due to the marketability of the final product (e.g., calcite) and the low cost of feed materials that are commonly obtained from recycled industrial waste, such as coal fly ash. Studies have shown that the process of calcite precipitation may be tuned to control the morphological structure of the precipitate.[73] Chemical additives, pH, temperature, and the method of introducing CO_2 to the

aqueous $Ca(OH_2)$ solution influence the morphology of the formed crystals (Fig. 3.5).[75–77] For example, sulphate and magnesium ions are known to inhibit $CaCO_3$ precipitation.[78]

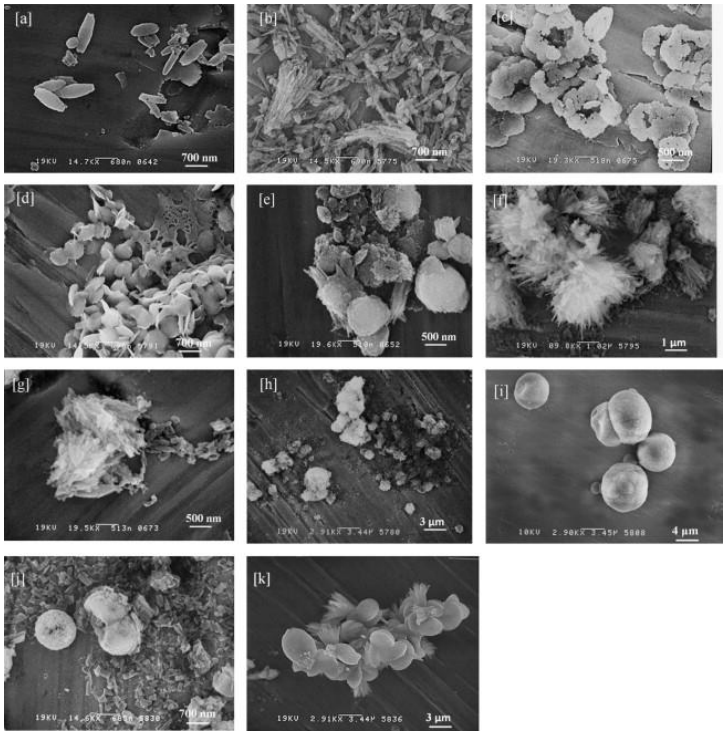

Figure 3.5 SEM imaging of precipitated powder filtrated from aqueous suspensions. Samples were precipitated (a) without organic additive, with (b) butylamine, (c) hexylamine, (d) octylamine, (e) 1,2-diaminoethane, (f) 1,4-diaminobutane, (g) 1.6-diaminohexane, (h) 1,8-diaminooctane, (i) glycine, (j) 4-aminobutyric acid and (k) 6-aminohexanoic acid.

Note. Reprinted with permission from the Journal of Crystal Growth by Chuajiw et al., 2014. Copyright 2014 by Elsevier.

In addition to calcium carbonate, barium carbonate ($BaCO_3$) and magnesium carbonate ($MgCO_3$) are salt precipitates that may be generated by using CO_2. A study by Shen et al. (2012) focuses on the production of $BaCO_3$ crystal sheaves with carboxymethyl cellulose through a carbonation process.[79] CO_2 aids the crystallization process while the concentration of

carboxymethyl cellulose defines the structure of the $BaCO_3$ crystals. This reaction's pressure was at 3.5 MPa and its temperature was at 25ºC.[79]

CO_2 storage reservoirs' pressures and temperatures are often favorable for carbonation reactions that lead to the formation of magnesite, a mineral that does not form under ambient conditions.[80] Furthermore, the feed for these reactions ($Mg(OH_2)$) (slurry) may be sourced from industrial waste.[81] Montes-Hernandez et al. (2012) studied the synthesis of magnesite crystals through two sequential reactions. In the first reaction, the authors used CO_2 in a very alkaline medium to develop the aqueous carbonation of brucite at ambient temperature (20ºC).[80] This process led to the precipitation of dypingite aggregates $(Mg(CO_3))_4 * 5\ H_2O$ after 24 hours of reaction.[80] This reaction was followed by the transformation of dypingite to magnetite through heat aging (going from 20ºC to 90ºC).[80] Throughout this process, sodium hydroxide (NaOH) was used as a catalyst to accelerate the brucite carbonation reaction, decreasing the reaction time from days to hours.[80] The increase of carbonate ions caused by sodium hydroxide promotes the formation of magnesite in the heat aging process.[80]

Employing mineral salt precipitation as a preventive sealing measure leaves the final precipitate in the pore space of the subsurface carbon storage formation. The accumulation of the precipitated salt in the pore space creates a flow barrier. It is crucial to quantify the alteration of formation porosity and permeability due to salt precipitation, under reservoir conditions. In other words, engineering the precipitation process enables the prediction of fluid mobility in porous and fractured media.[82] Porosity change due to precipitation is readily predictable through the precipitation reaction kinetics and the density of the precipitate; however, estimating the permeability alteration is more involved.[82] Permeability alteration is controlled by the location at which mineral precipitation takes place at the microscopic level.[83,84] Nonetheless, the

permeability decrease due to precipitation is commonly estimated by general empirical porosity-permeability correlations such as Verma-Pruess or Kozeny-Carmen equations, which might not yield the most accurate estimates.[82,83] Fig. 3.6 shows the results of a pore-scale study in which the size of random throat sizes in a pore-network model was altered and was used to calculate the permeability of the network.

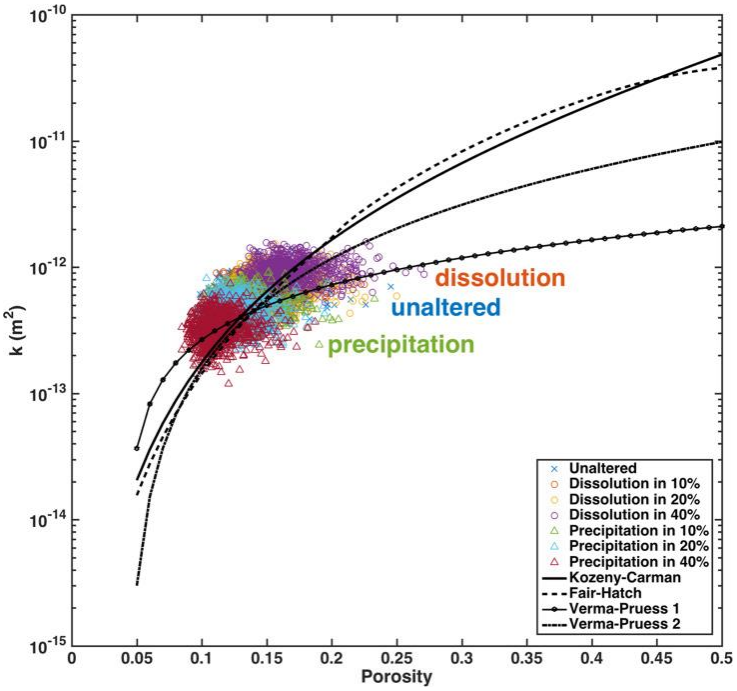

Figure 3.6 Changes in the permeability and porosity of a pore network model. Pore size of this model were changed to simulate dissolution and precipitation.

Note. Reprinted with permission from the Water Resources Research by Beckingham et al., 2017. Copyright 2017 by John Wiley and Sons.

The plot also shows the predicted permeability values by various empirical porosity-permeability correlations. It is clear that the predicted values show large errors for the majority of the simulated cases in this study. Precipitation of minerals have the great advantage of being

environmentally friendly, has a low cost associated with it, significantly reduces permeability and is a long-term application. Carbonation can easily occur in a reservoir and mineral structures can tolerate extreme conditions in comparison to gels. The limitations of this method are that mineral precipitation has a very slow chemical process and is highly affected by bacteria, temperature, and pH .[38]

Resin Systems

Resins are compounds that are derived from natural or synthetic polymers and form complex networks. Synthetic resins such as epoxies, polyurethanes, and phenol formaldehyde are thermosets that become cured or rigid upon application of heat. Their remarkable characteristic is their ability to change from a viscous liquid to a solid when cured and become less temperature sensitive because they form a cross-linked networks structure through chemical bonds.[85] Resins are particle-free fluids that exhibit low mobility and when cured, they become rigid impermeable materials.[86] Furan, epoxy, and phenolic resin have been traditionally used as oil field resins to as sealing agents for leakage mitigation in the near-wellbore and wellbore regions as it cannot travel through farther out due to its low injectability.[86] Even though most of them are thermally activated, certain resin systems create cross-linked networks under the presence of high concentrations of CO_2. For example, a study by Li et al. (2014) researched the use of CO_2-cured resol phenol formaldehyde. This resin undergoes a neutralization process and hydrolysis to solidify into a resin under the influence of high concentrations of CO_2.[14] The application of the resulting resol phenol formaldehyde resin to block CO_2 leakage pathways was studied to test its blocking performance in a sand pack flooding experimental set up.[14] Resin synthesis and sand pack flooding took place at 100°C. The results showed that the compressive strength of resin was

satisfactory with a maximum plugging rate of approximately 100% due to high bonding strength and thermal stability after the resin cured.[14,38,86]

Resin systems are known to be chemically resistant, thermally stable, resistant to low pH and high salinities, impermeable when cured, and have a high bonding strength.[86] They can endure extreme temperatures and have a long-life durability. However, resins are relatively expensive, brittle (low strain-at-break), toxic, difficult to prepare, and have low injectability (same mobility as cement).[38,86] It is required to use an economically feasible material that can travel long distances through pore space and be non-toxic, therefore resins are not an adequate candidate for in-situ CO_2 sealing.

Particle Growth

Aggregation

CO_2 has been used to change the rheology of some polymer solutions for various applications. A novel study used CO_2 to alter the viscosity of water-soluble polymers.[87] Lu et al. (2014) synthesized PDAMCn (poly(acrylamide)-*co*-poly(*N*,*N*-dimethylaminoethylmethacrylate)-*co*-poly(*N*-cetyl DMAEMA)), with different monomer ratios of acrylamide, N,N-dimethylaminoethyl methacrylate (DMAEMA), and hydrophobic monomer N-cetyl DMAEMA.[87] The synthesis of PDAMCn included CO_2 bubbling for 10 minutes and was left to polymerize under CO_2 atmosphere at 45°C for 8 hours. The resulting copolymer demonstrated a significant viscosity-response to CO_2. It is known that amidine and tertiary amine switchable surfactants can bicarbonate when they encounter CO_2. PDAMCn could be forming hydrophilic ammonium bicarbonate because its tertiary amine groups are being protonated by purging CO_2. The protonation of the hydrophobic tertiary amide groups causes an increase in electrostatic repulsion in the polymer chain's backbone causing a molecular microstructure change. Their

experiments demonstrated that CO_2 increased the viscosity of several polymer solutions up to two orders of magnitude (Fig. 3.7).

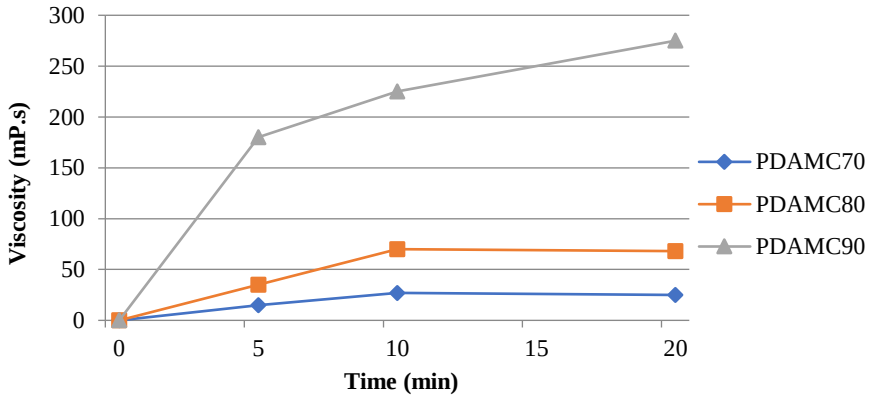

Figure 3.7 The aqueous solutions contain 10mg mL-1of PDAMCn (PDAMC70, PDAMC80, and PDAMC90). Viscosity of these solutions increased by bubbling CO_2 at 25ºC.

Note. Adapted with permission from the Journal of Applied Polymer Science by Lu et al., 2014. Copyright 2014 by John Wiley and Sons.

Further polymer size analysis showed that CO_2 treatment changed PDAMCn diameters. At first glance, PDAMCn does not seem to be a viable candidate for in-situ sealing of CO_2 reservoirs because an increase in polymer solution viscosity does not prevent CO_2 escape.[87] However, the increase in polymer chain size may lead to the blockage of the pore space.[87]

Table 3.1 Effective diameters of PDAMC70, PDAMC90, PDAM60, and PDAM70 before and after contacting with CO_2.

		PDAMC70	**PDAMC90**	**PDAM60**	**PDAM70**
Effective Diameter (microns)	**Original**	1.203	1.068	0.74	0.798
	After CO_2 addition	3.189	2.763	7.543	7.816

Note. Reprinted with permission from the Journal of Applied Polymer Science by Lu et al., 2014. Copyright 2014 by John Wiley and Sons.

Table 3.1 lists the original and altered diameters of various PDAMCn and PDAM. Note that the initial and final size of the polymer particles determine the type of rock formation that could be treated by this polymer solution.[87] For instance, to continuously inject a polymer solution of 1-micron particles into a formation, the mean pore size of the formation must be larger than 3 microns. If after contact with CO_2, aggregates of 3-micron dimeter form, then these aggregates could block pores that are smaller than 9 microns in diameter (according to the 1/3 – 1/7 rule of thumb).[88] Hence, this polymer solution is suitable for treating a formation with a mean pore size of 3 microns and a maximum pore size of 9 microns. If injected into a formation with smaller mean pore size, permeability will rapidly decline and consequently, the formed seal layer will only cover a limited area near the injection well.

Swelling

A new study tested the response of P(NIPAM-co-DMAEMA) (N-isopropylacrylamide copolymerized with dimethylaminoethyl methacrylate), which is a bulk hydrogel, to CO_2.[89] They found that at 37°C, the hydrogel swelled by absorbing 4 times more water.[89] They suggested that the reaction between CO_2 and DMAEMA, which is an amine-containing unit, causes the swelling.[89] Based on this interpretation, they proposed the incorporation of amine-containing units into ordinary polymers to synthesize CO_2-responsive polymers.[89]

A novel research on CO_2-triggered liquid-solid switching of a microgel suspension (poly(N,N-dimethylaminoethyl methacrylate) was performed in water through a jamming mechanism.[90] During this process, the PDMAEMA microgel's amine groups become protonated under acidic conditions and as a result, the microgel swells. As the microgel swells, it occupies more effective volume fraction which can surpass a critical point for jamming transition. Consequently, the microgel will transition from liquid to solid.[90] The microgel's hydrodynamic

radius increases abruptly when the solution reaches a pH level of 5. The radius changes from 480nm at a pH of 6.8 to 1250 nm when the pH decreases to 5. The microgel suspension is able to change its physical state from liquid into solid as CO_2 is bubbled into it, but it returns to liquid after the CO_2 is blown away with nitrogen.[90]

Recently, water-swelling microgels have been used as a mobility control technique for water flooding operations.[91] Mobility control is a process through which highly permeable flow paths (e.g., fractures) are blocked to increase the hydrocarbon recovery during water, gas, or CO_2 injection.[92] The main drawback of water-swelling gels is that they shrink under high temperatures. An alternative to water-swelling microgels for high-temperature environments is double swelling smart polymer microgels (SPMs).[93] Swelling of SPMs is triggered by the presence of CO_2 and heat. Temperatures higher than 65ºC cause the SPM to swell, which counters the shrinking effects of heat-induced dehydration.[93] Upon testing the SPM in sand packs, a 97% permeability drop under 5 MPa pressure was reported.[93]

Evaluation of Potential Sealing Agent

Researchers have developed several chemical reactions that are triggered or catalyzed by CO_2. Certain gel polymers, mineral solutions, microgels, and resins demonstrate a change of physical properties upon interacting with CO_2. Those reactions that lead to a change on their physical state (from a liquid to a semi-solid or solid), are particularly useful for preventive sealing of subsurface CO_2 storage reservoirs. For this purpose, it is important that the ultimate sealing material is stable at high temperatures, pressures, acidity levels, and salinity. In addition, the long-term stability, cost, injectability, and toxicity of the chemicals are important factors that contribute to the appropriate selection of a CO_2-triggered chemical for leakage prevention. Table 3.2 and 3.3 summarize the advantages and drawbacks of each chemical mechanism investigated

in Chapter 3 to determine the ideal system which will be further investigated. The ideal compound should be cost effective, have a minimal environmental impact, and not require a long complex synthesis or slow chemical reaction. The cost of materials cannot be discussed until a future study reveals the amount of material that must be injected into the reservoir. However, a general chemical cost comparison reveals that mineral precipitation is one of the most economical options for preventive sealing of subsurface CO_2 storage sites.

Table 3.2 Summary of advantages and disadvantages for systems undergoing solid formation.

Gel Systems		**Mineral Precipitation**		**Resin Systems**	
Pros	*Cons*	*Pros*	*Cons*	*Pros*	*Cons*
✓ High permeability. reduction ✓ Resistant to acidic environment ✓ Adjustable and versatile ✓ Highly injectable ✓ High thermal stability	✖ Limited knowledge on long-term plugging performance ✖ Gel degradation under high pressures	✓ Non-toxic ✓ Low cost ✓ High permeability reduction. ✓ Long term application.	✖ Influenced by pH ✖ Secondary reactions can increase permeability ✖ Slow chemical mechanism	✓ High bonding strength. ✓ High thermal stability. ✓ Adjustable viscosity. ✓ Long term application.	✖ Expensive ✖ Complex preparation ✖ Low injectability ✖ Brittle ✖ Toxic

Table 3.3 Summary of advantages and disadvantages for systems undergoing particle growth.

Aggregation		**Swelling**	
Pros	*Cons*	*Pros*	*Cons*
✓ High permeability reduction. ✓ Resistant to acidic environment. ✓ Highly injectable.	✖ Limited knowledge on long-term plugging performance. ✖ Gel degradation under high pressures. ✖ Not resistant to salt.	✓ Reversable reaction. ✓ High permeability reduction.	✖ Shrink under high temperatures. ✖ Plugging success is highly dependent on gel particle size. ✖ Influenced by acidity.

Finally, field-scale simulation studies are necessary to determine the feasibility of the proposed preventive treatment using various CO_2-sensitive chemicals and under various injection conditions. Furthermore, CO_2-triggered reactions need to be tested at a wider range of pressures and temperatures representative of reservoir-like conditions. A typical oil and gas reservoir has a temperature gradient ranging between 0.6°F to 1.6°F per 100 ft of depth and a pressure gradient ranging from 0.43 psi/ft to 0.47 psi/ft. Exploratory and production well's depth can range from a couple hundred feet to 20,000 ft, but typically they average between 2,000 ft to 8,000ft.[94,95] Oil producing reservoirs with a depth between 2,000 ft and 8,000 ft have a temperatures ranging from 88°C to 175°C and pressures ranging between 900 psi to 3600 psi (61 atm to 245 atm, although much higher pressures are possible).[96] Moreover, if an aquifer is considered for CO_2 storage, it is important to note that aquifers have salinities ranging from 7,000 ppm to 340,000 ppm.[97] Fig. 3.8 puts into perspective the range of pressures and temperatures of a typical subsurface CO_2 storage reservoir contrasted with the pressure and temperature ranges of the tested materials mentioned in this chapter. Table 3.4 lists the references and data from previous studies used to create Fig 3.8.

Studies conducted in gelation, precipitation, resin, aggregation, and swelling are coded as a green diamond, brown square, red triangle, orange square with asterisk, and blue circle, respectively. It is clear from this graph that most of the studied CO_2-triggered reactions have not been tested in a range of typical reservoir conditions in terms of pressure and temperature.

Table 3.4 References and parameters from previous studies on CO_2-triggered chemicals.

	Reference	Temperature (°C)	Pressure (atm)
Gelation	Li et al. (2014)[14]	90	14.8
	Zhang et al. (2016)[70]	25	81.7
	Nagai et al. (2011)[61]	170	49.3
	Han et al. (2012)[71]	37	1

Table 3.4 (continued)

	Reference	Temperature (°C)	Pressure (atm)
Precipitation	Shen et al. (2012)[79]	25	34.5
	Montes-Hernandez et al. (2012)[80]	60	39
	Chuajiw et al. (2013)[98]	30	1
	Domingo et al. (2004)[75]	25	197.4
	Prigiobbe et al. (2009)[32]	150	98.7
Resin System	Li et al. (2014)[14]	100	1
Aggregation	Lu et al. (2015)[87]	25	1
Swelling	Zhao et al. (2013)[90]	65	1
	Han et al. (2012)[89]	37	1
	Tian et al. (2019)[93]	40	1

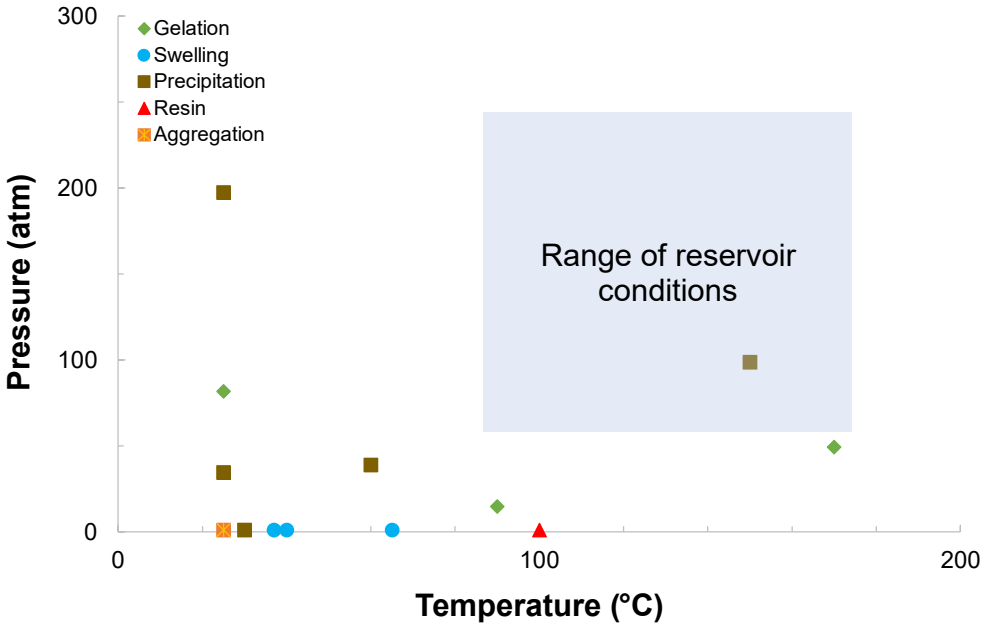

Figure 3.8 Studies performed on CO_2-sensitive chemicals as a function of pressure and temperature. Typical range of storage reservoirs' temperature and pressure is shown in the blue box.

Precipitated minerals and gel systems are the only mechanisms that have been studied closer to reservoir-like conditions and demonstrated positive outcomes. Both mechanisms exhibited high permeability reduction percentages and appropriate thermal stability. Gel system, unlike mineral precipitant, are resistant to low pH levels, have been widely employed in various industrial processes, have a faster reaction time, and can travel across the reservoir to address a specific target zone. CO_2-SPAM proved to be the most suitable candidate for in-situ sealing due to its high permeability reduction properties, commercial availability, simple synthesis, high resistance to acids, and its less-toxic derivatives. It has been recorded that CO_2-SPAM has reduced permeability by 92% in core samples with a permeability of 59.6 mD at 80°C while being highly injectable.[14] Finally, its properties such as viscosity can be easily modified by changing the gel's polymer concentration, cross-linker concentration or by increasing temperatures.

Conclusions and Direction of Future Research

The sealing materials evaluated and discussed previously have proven to satisfy several ideal properties an in-situ sealant is required to have. Mineral precipitants are environmentally friendly, non-toxic, stable for long term applications and have shown to reduced permeability significantly. Resin systems have demonstrated to have high thermal stability, high bonding strength and be ideal for long term applications. Systems undergoing particle growth through both swelling and aggregation processes are highly injectable, resistant to acid, and reduced permeability in porous media. Nevertheless, all these systems have impactful drawbacks that prevent them from being an ideal candidate for in-situ sealing. Mineral precipitants are highly influenced by pH levels and have a slow chemical reaction mechanism while resin systems are

expensive, toxic and difficult to inject. Systems undergoing particle growth are influenced by temperature, particle size and salinity.

In conclusion, CO_2-SPAM has proven to be an exceptional material for in-situ sealing purposes due to its versatility, high injectability, thermal stability, resistance to acids, commercial availability, and high permeability reduction properties. As a result, future studies in this dissertation points to expanding on CO_2-SPAM's synthesis (Chapter 4) and how its composition correlates to its behavior under high salinities (Chapter 5) while exploring the impact on the geological stresses caused by its injections into the subsurface (Chapter 6).

CHAPTER IV

DEVELOPMENT OF CO_2-SENSITIVE POLYACRYLAMIDE GEL: CHEMICAL MECHANISM

Introduction

CO_2-sensitive polyacrylamide (CO_2-SPAM) is a polymer that changes its physical structure from aqueous to semi-solid gel under the presence of CO_2.[99,100] In the past decade, CO_2-triggered gelation of CO_2-SPAM has been studied by a number of research teams but, nevertheless, there is not a clear path of the sequence of chemical mechanisms that occur throughout its synthesis.[67,100–102] CO_2-SPAM gel is prepared by using polyacrylamide (PAM), methenamine, and resorcinol. PAM $[C_3H_5NO]_n$ is a water-soluble polymer that is widely used in various industrial applications and can be found as nonionic (Fig. 4.1a) and hydrolyzed (4.1b). PAM is used in various applications such as a drilling fluid viscosifier,[103] water treatment flocculant,[104–106] and pulp fiber binder,[107–110] to name a few.

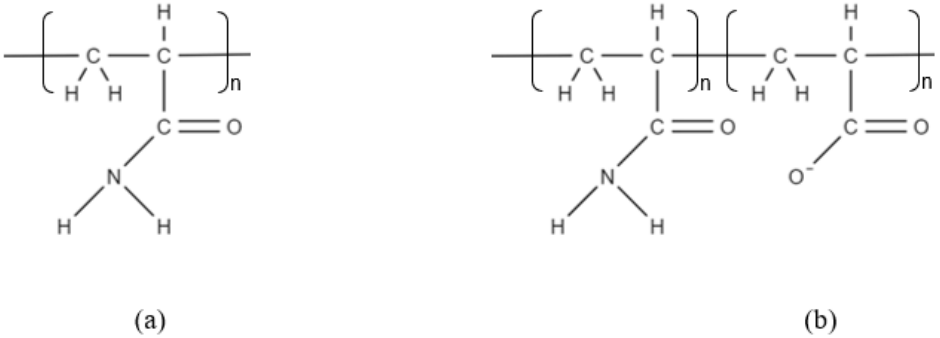

(a) (b)

Figure 4.1 (a) Non-ionic polyacrylamide and (b) hydrolyzed polyacrylamide.

Polyacrylamide gels and polymers are generally cross-linked with a metal agent[111] (e.g., Al^{3+}, Cr^{3+}, Ti^{4+} and Zr^{4+}) or an organic cross-linker (e.g., phenol formaldehyde,[112,113] terephthalaldehyde, hydroquinone-hexamethylenetetramine,[114] and polyethyleneimine (PEI)[115]). A cross-linked polymer refers to a polymer network in which adjacent polymer chains are linked through covalent bonds (joining molecules by sharing two or more pairs of electrons between atoms).[116] Different forms of polyacrylamide (e.g., hydrolyzed polyacrylamide,[54,111,117] partially hydrolyzed polyacrylamide,[114,117–121] acrylamide-based copolymer,[53,122] and PAM-based materials[123,124]) are used to produce soft materials such as gels. Methenamine [$C_6H_{12}N_4$] is a heterocyclic organic compound with a cage-like structure that is water soluble and releases formaldehyde under acidic conditions (Fig. 4.2).[125] Methenamine's structure comprises of a carbon ring with three nitrogen atoms, hence, its classification as a heterocyclic compound.[126] This compound can be found in two additional forms: methenamine hippurate (which contains hippuric acid) and methenamine mandelate (which contain mandelic acid).[127] Resorcinol [$C_6H_4(OH)_2$] is a crystalline solid organic compound and one of three different isomeric benzenediols, specifically the 1,3 isomer (Fig. 4.3).[127] This phenol compound is water soluble and is used in the manufacturing of resins, plastics, medicine, etc.[127]

Methenamine Hydrolytic Decomposition

Oil and gas reservoirs, where CO_2 is used for EOR or stored, are naturally under high temperature (>88°C), high pressures (>900 psi) and high salinity brine saturation (>20,000 ppm). Injection of CO_2 under these conditions provides ideal conditions for an acidic environment.[128–130] CO_2 dissolves into the formation water and produces carbonic acid.[100]

Acidic environments formed by carbonic or acetic acid have been shown to induce polymerization in polyacrylamide-resorcinol-methenamine system, which is the CO_2-SPAM

under study.[131] Polymerization is the process where smaller molecules, such as monomers, dimer, and oligomers, are covalently bonded to create longer and larger molecule known as polymers. In reservoir-like conditions, high temperatures and low pH levels are expected. These conditions are favorable to the breakdown of methenamine into formaldehyde and ammonia as seen in Fig. 4.2

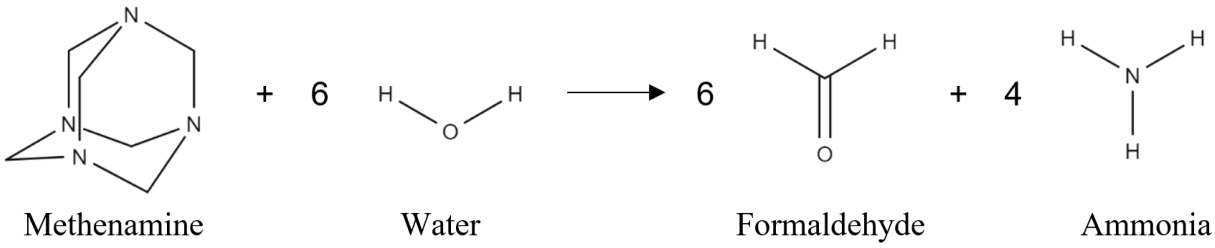

Figure 4.2 Hydrolytic decomposition of methenamine into formaldehyde and ammonia.

This process, known as methenamine's hydrolytic decomposition, is also described as methenamines' hydrolysis.[14] Here, methenamine (the reactant) is hydrolyzed and water breaks its chemical bonds. This chemical process is well known as it used for several manufacturing products such as adhesives, coatings, sealants, rubber, etc.

Resorcinol and Formaldehyde Addition and Polycondensation

The released formaldehyde from methenamine's hydrolytic decomposition reacts with resorcinol to form simply, doubly or triply hydroxymethyl derivatives ($–CH_2OH$) by connecting in the meta position through an addition reaction that can happen without a catalyst or any substance that can accelerate the chemical reaction at ambient conditions as seen in Fig. 4.3.[132–134] Addition reaction is defined as the chemical reaction where two different molecules combine to form one (i.e., A + B = C)

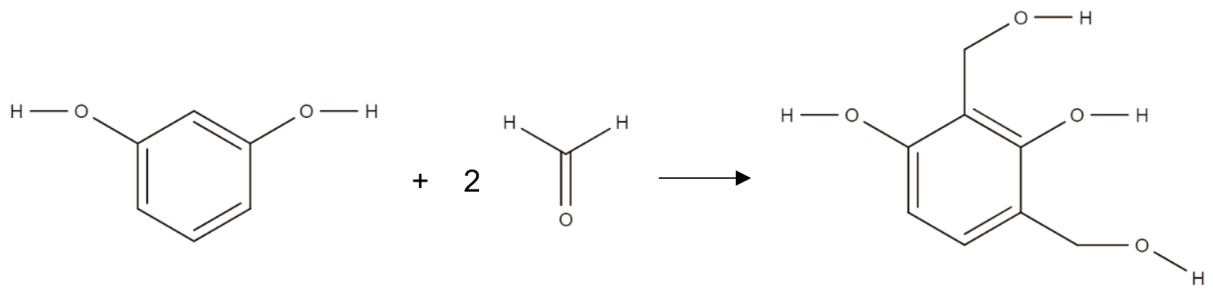

Resorcinol Formaldehyde Hydroxymethyl-Resorcinol

Figure 4.3 Addition reaction of resorcinol and formaldehyde.

The hydroxymethyl-resorcinol is a monomer that can be covalently bonded to an identical molecule to create a macromolecule. In this case, hydroxymethyl-resorcinol may also ultimately generate phenol formaldehyde resin network, also known as phenolic resin, through polymerization.[134] It is conventionally believed this process is the result of polycondensation of hydroxymethyl derivatives, but other authors established that the resorcinol-formaldehyde's synthesis consist of a subtle interplay between chemical and physical processes.[135] Through liquid-phase nuclear magnetic resonance (NMR), they determined that no condensation products were produced and that nanoscale clusters assemble.[135] NMR is a spectroscopy tool used to identify the content or molecular structure in a sample through the use of radiofrequency electromagnetic radiations with the nuclei of the molecules in a strong magnetic field.[136] The polymerization reaction between hydroxymethyl-resorcinol molecules can be acid (carbonic acid produced from CO_2 and water) or base catalyzed and can lead to the formation of a larger more complex structure. The hydroxymethyl groups will release H_2O as they create of ether bridges (–CH_2–O–CH_2–) or methylene bridges (–CH_2–) by reacting with a unsubstituted resorcinol site until a three-dimensional cross-linked polymer is formed as seen in Fig. 4.4.[132,137] Note that the

squiggly lines attached to the ends of the resorcinol-formaldehyde depict the accessible sites for further polymer expansion.

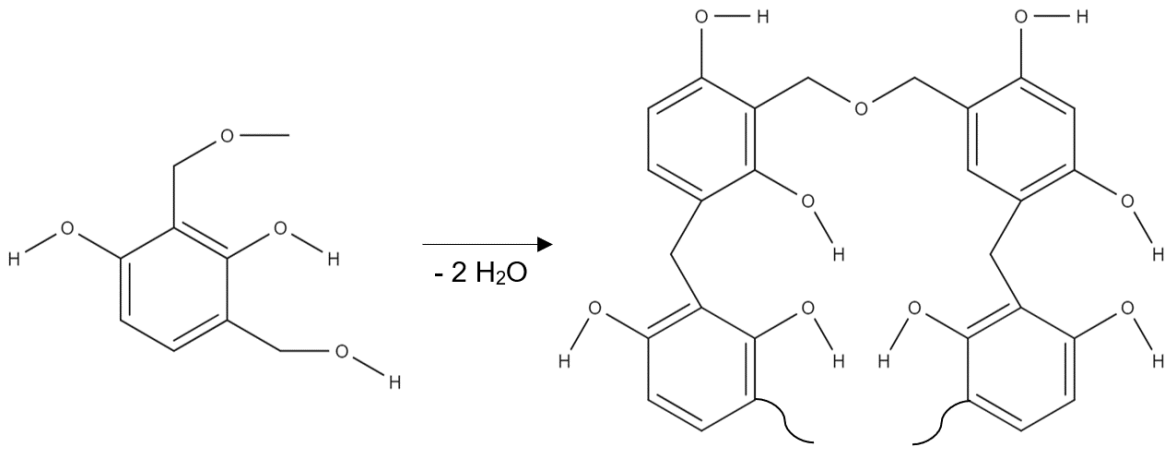

Figure 4.4 Resorcinol-formaldehyde polymerization leading to phenolic resin formation.

Hydrolysis of Polyacrylamide and Deprotonation Process

Polyacrylamide should undergo hydrolysis under acidic conditions as it is known to hydrolyze through N-protonation (proton attacking amide group) or O-protonation (proton attacking the carbonyl oxygen).[138] O-protonation is more energetically favorable than N-protonation.[138] Hydrolyzed polyacrylamide contains chains with carboxylic acid groups (R-COOH) (Fig. 4.5).[139]

The carboxylic acid has a hydroxyl group (-OH) attached to the carbonyl carbon (C=O) and due to oxygen's electronegativity, the carboxyl group undergoes ionization and discharges a proton. The deprotonation process creates a carboxylate ion which is stable under the presence of the two oxygen atoms as seen in Fig. 4.5.[139]

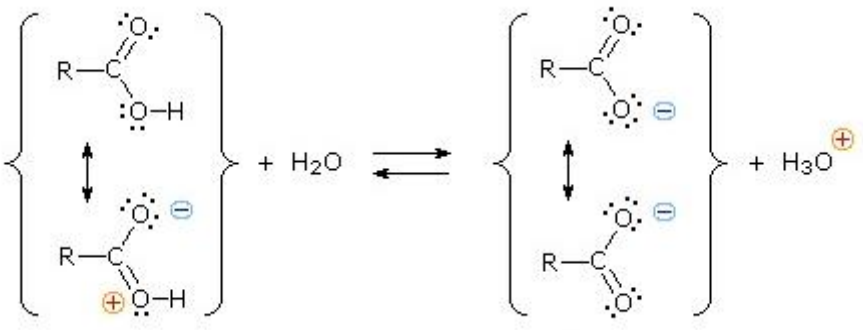

Figure 4.5 Conjugation and deprotonation of carboxylic acid into carboxylate ions.

Note. Reprinted with permission from LibreTexts by Kennepohl et al., 2014. Images in Acidity of Carboxylic Acid is shared under a not declared license and was authored, remixed, and/or curated by LibreTexts.

Hydrolyzed Polyacrylamide and Hydroxymethyl-Resorcinol Three-Dimensional Network.

Hydrolyzed PAM's amide groups further react with formaldehyde to create long polymer chains as seen in Fig. 4.6. Furthermore, hydroxymethyl-resorcinol goes through a polycondensation process with PAM's accessible amide groups, which creates a 3-dimensional gel structure (Fig. 4.7).[131] The covalent bonds created by these organic cross-linkers are more stable than ionic bonds formed by cross-linking HPAM with metal agents.[140] The covalent bonds also provide better thermal stability to the gel.[56,141,142]

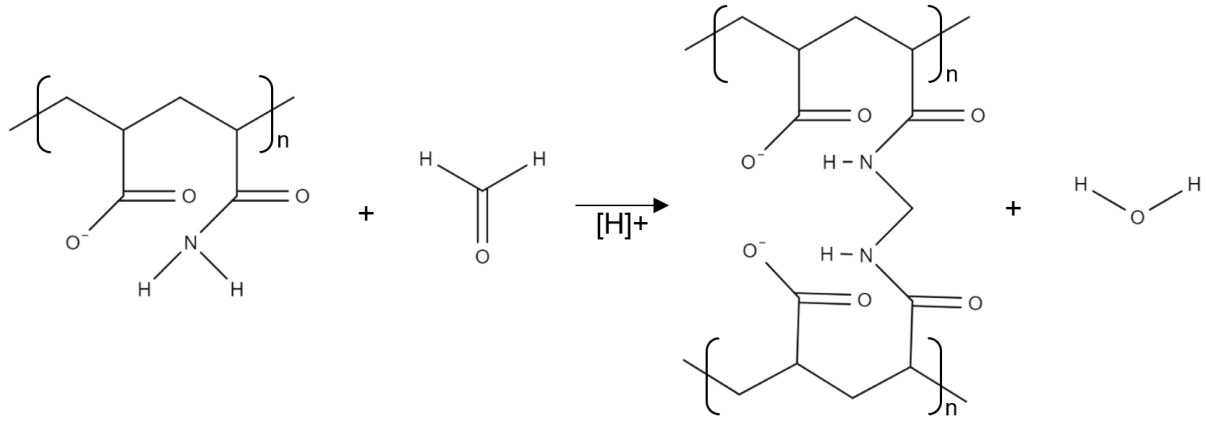

Figure 4.6 PAM and formaldehyde reaction.

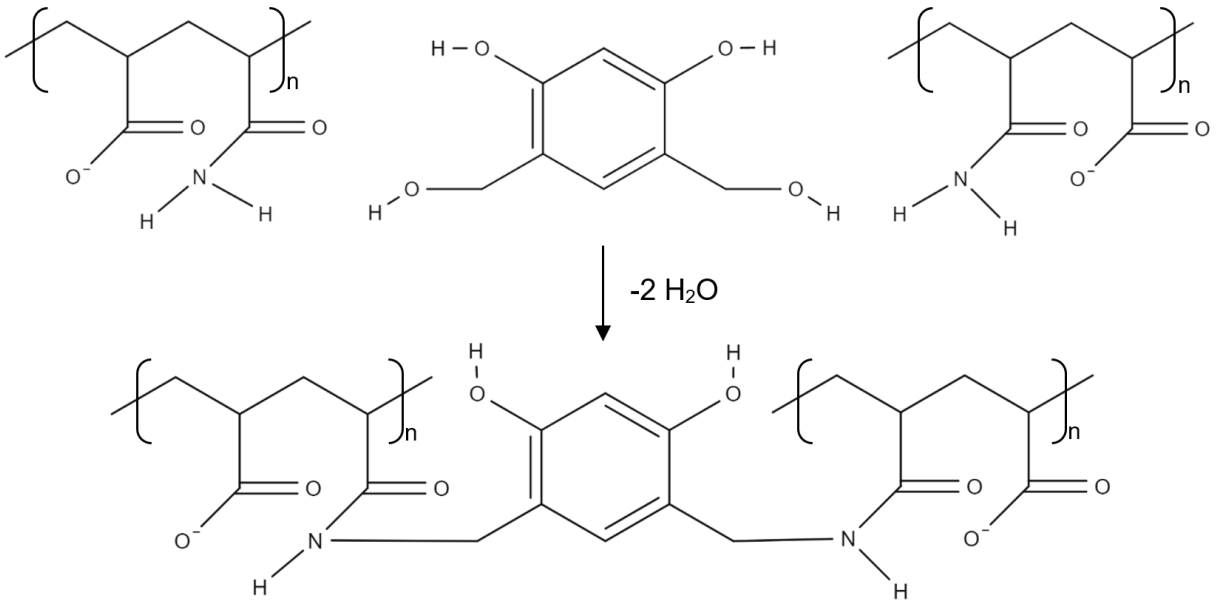

Figure 4.7 Polymerization reaction of PAM and hydroxymethyl-resorcinol.

Network Structure

Based on past literature and organic chemistry principles, it is believed that the final CO_2-SPAM includes three different polymer structures: resorcinol-formaldehyde resin, PAM-formaldehyde, and PAM-hydroxymethyl-resorcinol. However, it is unclear whether these polymer structures copolymerize or form some type of interpenetrating network. If the former, then CO_2-SPAM would be a single cross-linked network. If the latter, multiple polymer structures will be present and interpenetrating each other.

An interpenetrating polymer network (IPN) is a polymer system that is comprised of two or more cross-linked polymer networks being partially intertwined or entangled but not cross-linked or covalently bonded with one another.[143] Similar to an IPN, a semi-interpenetrated polymer network (SIPN) is a polymer system that is comprised of a cross-linked polymer network and a linear or branched polymer.[144] In this study, phenolic resin, PAM-formaldehyde and PAM-hydroxymethyl resorcinol are expected to create polymer networks. Each of these polymers could potentially play a role in the final gel structure; however, it is not clear whether one or more of these polymers play the main role in forming the gel structure. To understand this behavior, the following experiment was conducted to interpret the gelation process of each polymer chain.

Methodology and Experimental Procedure

Materials

The materials included methenamine (molecular weight: 140.19 g/mol, grade: USP, purity: 99-100.5%, Spectrum Chemical MFG CORP), resorcinol (molecular weight: 110.112 g/mol, grade: USP, purity: 99-100.5%, Spectrum Chemical MFG COPR), PAM (average M_W: 5,000,000 to 6,000,000, monomer molecular weight: 71.08 g/mol, Thermo Fisher Scientific),

sodium chloride (molecular weight: 58.44 g/mol, grade: reagent, Thermo Fischer Scientific), distilled water (molecular weight: 18.015, grade: extra pure, Thermo Fisher Scientific) and carbon dioxide (Industrial grade gas, Airgas). A mixture was prepared of distilled water and sodium chloride with a concentration of 20,000 ppm. PAM, methenamine, and resorcinol's chemical structures can be seen in Fig. 4.1, 4.2 and 4.3.

Mixture Preparation

Solution #1 was prepared in a brine solution at 20,000 ppm. The solution contained 0.4 wt% of methenamine and 0.1 wt% of resorcinol. Firstly, the brine solution was heated and maintained at 90°C in a ceramic stirring hotplate in addition to being continuously bubbled with CO_2 in an Erlenmeyer flask. Methenamine was first added to the brine and stirred (550 rpm) for 15 minutes until fully dissolved. Resorcinol was successively added to the mixture and reached full dissolution after 15 minutes. Fifty milliliters of the dissolved solution were placed in a test tube and placed in a water bath at 90°C and under CO_2 conditions (CO_2 bubbling). The dissolved mixture was exposed to CO_2 for an additional 30 minutes while visual changes in the sample were recorded.

Secondly, Solution #2 was prepared in a brine solution at 20,000ppm with 0.4 wt% of methenamine and 1.0 wt% of PAM. Similar to Solution #1, the brine reached 90°C and was subjected to CO_2 bubbling before introducing methenamine into the mixture. PAM was added into the mixture following methenamine's dissolution. After complete dissolution of the reactants, 50 mL of the mixture was placed into a test tube. The test tube was then placed in a water bath at 90°C and subjected to CO_2 bubbling for 30 minutes as visual changes were noted.

Lastly, Solution #3 was prepared in a brine solution at 20,000ppm with 0.4 wt% of methenamine, 0.1 wt% of resorcinol and 1.0 wt% of PAM. Solution #3 had the exact same

preparation process as Solution #1 with the addition of 1.0 wt% of PAM after resorcinol's complete dissolution. After the complete dissolution of PAM, 50 mL of the mixture was placed in a test tube and subjected to 90°C in a water bath and CO_2 bubbling for 30 minutes while visual changes in the sample were recorded.

Results and Discussions

The methenamine and resorcinol mixture ultimately changed from a clear, colorless liquid to an opaque, rust-colored liquid (Fig 4.8), indicating that a chemical reaction had occurred. The solution appeared to be homogeneous with no solid precipitates, and no visible changes in viscosity were noted (compared to the initial aqueous solution) that would indicate formation of a network structure.

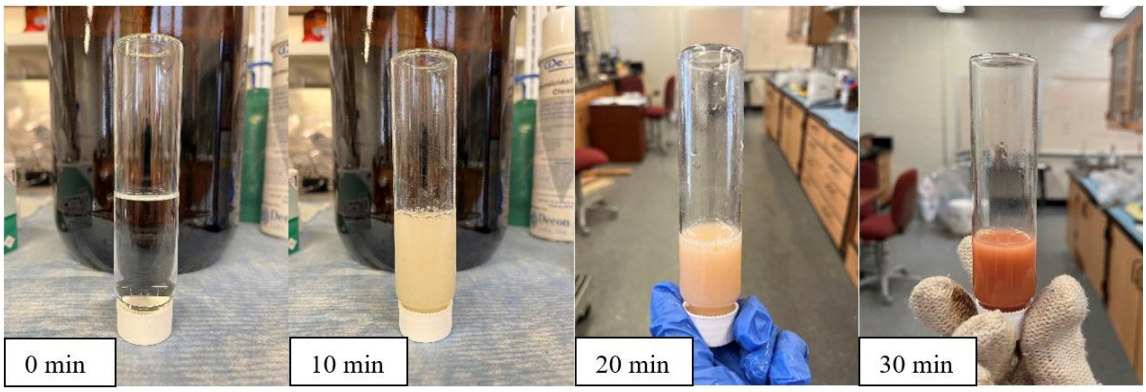

Figure 4.8 Methenamine and resorcinol mixture under CO_2 conditions at 0 minutes, 10 minutes, 20 minutes, and 30 minutes.

Throughout the entirety of the experiment, Solution #1 remained a flowing liquid, which showed that the formation of resorcinol-formaldehyde resin may not contribute to the formation of the gel structure due to the absence of rheological changes in the mixture. It is possible that only oligomers could be forming in Solution #1. An explanation as to why the phenolic network

structure did not form could be attributed to a low fractional monomer conversion. In a step polymerization, low monomer conversion results in low degrees of polymerization (molecular weight), since only dimers, trimers, etc. are being formed early in the reaction.[145] The critical conversion for phenolic resin to gel was estimated to be 0.7071 from the following equation (Eq. 4.1):[146]

$$critical\ conversion = \frac{1}{\sqrt{r + r(f-2)rr}} \tag{4.1}$$

Here, it was assumed that the feed ratio (r) of resorcinol and formaldehyde is equal to 1, the branching ratio (rr) of the hydroxyl groups is equal to 1, and the functionality of hydroxymethyl-resorcinol is 3. This result means that, when the system achieves a critical conversion of 0.7071, the crosslinked network is expected to form. Additional experiments would be necessary to measure the concentration and conversion of hydroxymethyl-resorcinol through NMR spectroscopy and/or the molecular weight of phenolic resin through static light scattering or mass spectroscopy.

Secondly, Solution #2 reflected the formation of PAM-formaldehyde chains from methenamine and PAM. This mixture appeared to be homogeneous as well with no solid precipitates and did experience an increase in viscosity unlike Solution #1. The majority of the viscous fluid flows to bottom of the test tube by gravity upon inversion, and the viscosity increased compared to the initial aqueous solution as seen in Fig. 4.9.

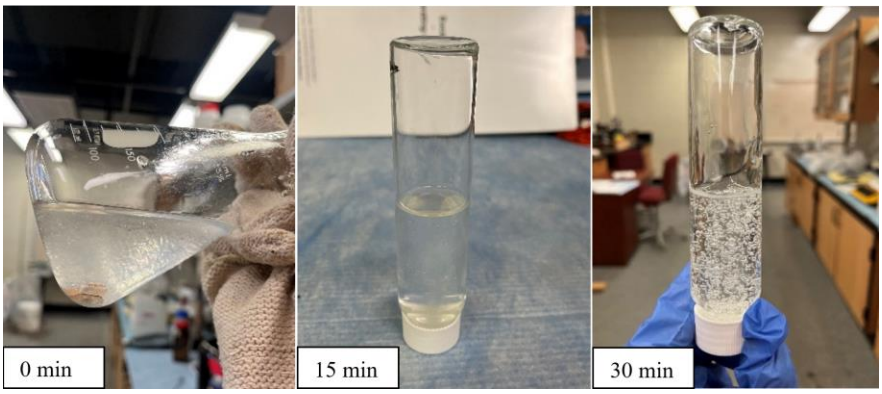

Figure 4.9 PAM-formaldehyde synthesis from methenamine and PAM in brine at 20,000 ppm under CO_2 conditions at 0 minutes, 15 minutes, and 30 minutes.

This rheological response suggests that PAM-formaldehyde chains alone do not contribute to the formation of a strong gel network, and the increase of viscosity suggests that linear chains may be dissolved in the brine. Thus, on average, one formaldehyde appears to be reacting per pair of PAM chains, which would account for the linear structure and not a crosslinked network. This scenario is likely to occur with low concentrations of formaldehyde, so additional experiments are recommended to measure the concentration of formaldehyde in the solution through titration or infrared spectroscopy.

Finally, Solution #3 demonstrated a drastic increase in viscosity. Upon inversion of the test tube after 30 minutes of reaction time, the system appeared to be a slightly deformable, non-flowing gel with a Sydansk gel strength code of H^{147} (Fig. 4.10). Since the mixture is no longer a solution and only contain 5.0 wt% monomeric starting material, it is probable that a cross-linked network has been formed and is swollen with the brine solution.

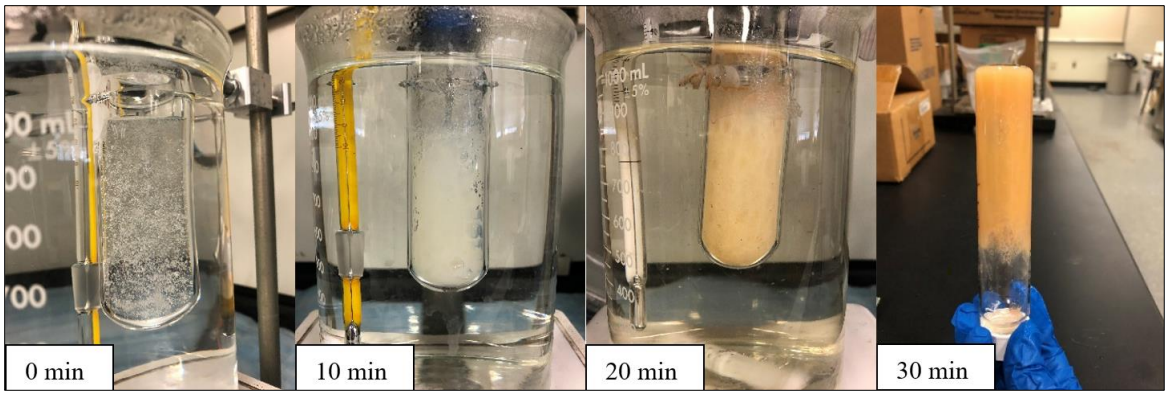

Figure 4.10 CO_2-SPAM gel synthesis from PAM, resorcinol and methenamine.

Based on these results, it is believed that the polymer created by the formation of repeated PAM-hydroxymethyl-resorcinol is the main contributor to the formation of CO_2-SPAM and responsible for its positive attributes as a sealing agent. From these series of experiments, Solutions #1 and #2 demonstrated to be homogeneous solutions with no solid precipitates. Solution #1 is believed to have formed oligomers due to low conversion while Solution #2 was able to form linear polymer structures soluble in the brine solution. Solution #3 demonstrated to be a swollen polymer by increasing its viscosity and expanding its volume through hydrophilic interactions between the polymer network and the solvent (brine). The presence of oligomers, linear polymers and a cross-linked network suggests that the CO_2-SPAM may be semi-interpenetrated network. Chapter VII explores future work and recommendations on how to properly identify a semi-interpenetrated system using Soxhlet extraction and spectroscopy tools.

Conclusions

CO_2-SPAM is a novel polymer gel system that has demonstrated exceptional in-situ sealing capabilities for CCS applications. However, limited knowledge was available on the chemical mechanisms that involved its synthesis. The suggested chemical mechanisms that

methenamine, resorcinol, and PAM undergo to form the CO_2-SPAM were examined. Methenamine releases formaldehyde through hydrolytic decomposition, which is further used to create resorcinol-formaldehyde, PAM-formaldehyde, and hydroxymethyl-resorcinol-PAM chains. Resorcinol and formaldehyde go through a two-step process to create resorcinol-formaldehyde resin: addition reaction between resorcinol and formaldehyde to create hydroxymethyl-resorcinol and polymerization of the hydroxymethyl derivatives to form resorcinol-formaldehyde resin. Lastly, PAM's amide groups react with both unreacted formaldehyde and hydroxyl-resorcinol to create a three-dimensional structure. It was found that the CO_2-SPAM includes the mentioned polymer chains, but it was not clear whether these chains were covalently bonded or interpenetrated with each other. A qualitative test was performed to form resorcinol-formaldehyde resin, PAM-formaldehyde and CO_2-SPAM gel, and identify visual changes in their flow characteristics. The methenamine and resorcinol solution reacted (as demonstrated by a color change from colorless to red) to for resorcinol-formaldehyde but with no change in viscosity. The PAM and methenamine solution reacted to form PAM-formaldehyde polymers that resulted in a slight change in viscosity but not enough to be a non-flowing rigid gel for sealing purposes. However, a mixture of all three components (methenamine, resorcinol, and PAM) in the brine solution exhibited a drastic change from a liquid to a non-flowing gel. Thus, all three components of CO_2-SPAM play a significant role in the creation of the 3D swollen, cross-linked network structure.

CHAPTER V

INFLUENCE OF NACL BRINE CONCENTRATIONS ON CO_2-SENSITIVE POLYACRYLAMIDE GEL

Introduction

CO_2 is known to be a triggering factor for certain gelation processes. These gelation mechanisms have applications in EOR to control the mobility of CO_2[68] and in subsurface CO_2 storage to prevent leakage from injection-induced fractures.[99] For in-situ sealing of leakage pathways, the sealing agent must be able to travel through the leakage pathways and create an impermeable seal once it encounters CO_2. To this end, a CO_2-triggered gelation reaction may serve as a desired solution. Table 5.1 lists some common CO_2-triggered gelation reactions reported in the literature, which are also included in Chapter 3.

Table 5.1 CO_2-triggered gelation reactions.

Wu et al. (2018)[148]	Silica aerogel formation with CO_2 gas
Floren et al. (2012)[149]	Silk fibroin hydrogel formation with high pressure CO_2
Gurikov and Smirnova (2018)[150]	Alginate-lignin aerogels gelation with CO_2
Li et al. (2019)[69]	CO_2-triggered gelation of polyacrylamide-based solution
Yu et al. (2017)[66]	CO_2-triggered gelation of triblock copolymers
Tian et al. (2019)[93]	CO_2-triggered microgels
Carretti et al. (2003)[63]	Polyallylamine gelation with CO_2
Nguele et al. (2021)[151]	Evaluation of CO_2-triggered silica gel polymer
Lin and Theato (2013)[67]	CO_2-responsive poly(allylamine)

Li et al.[14,69] studied the influence of temperature and concentration on a polyacrylamide-hexamethylenetetramine-resorcinol solution's gelation time and its blocking performance. This

study used Sydansk[147] gel strength code on all samples exposed to nitrogen and CO_2 to determine the gel strength. They reported a strength code of H for gels exposed to 50°C, 60°C, 70°C, and 80°C. It was also noted that gelation time decreases as temperature increases but increases as polymer concentration increases. Finally, the blocking performance was measured in a sand pack and found PAM at 1 wt% to exhibit great sealing capabilities with a plugging rate of 92% and higher. This study investigated the effect of high temperature, which is one of the characteristics of deep formations. The other common attribute of subsurface CO_2 storage, and hydrocarbon reservoirs is the presence of high salinity brine. For instance, saline aquifers or salt domes, which contain high salt concentrations, can potentially be used to store CO_2; therefore, the effects of high salt content from the formation fluid on the gel's sealing properties need to be investigated. (Salt domes are impermeable geological structures made out of salt including halite and evaporites that intrude and eventually break through overlaying rock reaching towards the surface due their greater buoyancy.[152]) In situations where the cap rock is a salt dome, gel and CO_2 injection is best done through a directional well (non-vertical well angled towards a specific target zone) to avoid the technical drilling challenges that arise from drilling through the salt dome, such as a poor cement job, drilling mud losses and wellbore washout.[153] Salt domes are not likely to be easily fractured due to their ductility and integrity,[154] but CO_2-SPAM can be injected close to the target leakage pathways located between the salt dome and the reservoir rock. Geological CO_2-storage sites vary in salt content, therefore, the influence of salt on gel formation and its sealing performance is crucial. PAM gelation time, its pre-gel solution viscosity, and PAM gels mechanical properties are known to be affected by the salt content of the solution.

Jia et al.[55] summarized the results of 11 studies on the effect of salinity on the gelation times of various PAM-based gels. According to these studies, gelation time may decrease or increase as a result of increased salinity. Table 5.2 lists those studies as well as more recent studies that used NaCl as the salt.

Table 5.2 Studies of salinity effects on PAM-based gels.

PAM-based Gel	Temperature	Salt	Salinity	Gelation Time	Reference
HPAM/Cr^{3+}-methanal	25-32°C	NaCl and synthetic brine	5000 to 100,000mg/L	Decrease and then increase	[120,155]
HPAM/$ZrOCl_2$	28°C	NaCl,$CaCl_2$, $MgCl_2$	492 to 13,838 mg/L	Decrease	[156]
HPAM/PEI	40°C -65°C	NaCl	5,000 to 100,000 mg/L	Increase	[119,157]
PAtBA/PEI	120-150°C	NaCl, KCl, $CaCl_2$	1186 to 58348 mg/L	Increase	[50,51,118,158,159]
HPAM/Resorcinol /Phenol-formaldehyde	65°C	NaCl	10,000 to 30,000 mg/L	Decrease	[112]
HPAM/Resorcinol /Formaldehyde /NH4Cl	30°C	NaCl	10,000 to 100,000 mg/L	Increase	[113]
PHPA/Hexamine/ Hydroquinone	80°C -120°C	NaCl	1 to 4 wt%	Increase	[114]
PAM/Cr^{3+}	24°C	NaCl, KCl, $CaCl_2$, $MgCl_2$	Na+, K+, Ca+2 and Mg+2 mass ratio 14:1:3:1	Increase	[160]

Several of the listed studies show that when hydrolyzed polyacrylamide (HPAM) or partially hydrolyzed polyacrylamide (PHPA) is cross-linked with an organic cross-linker, gelation time tends to elongate as the solution increases its salinity. Furthermore, the effect of monovalent and divalent ions from salts on the elastic properties of the formed gel is undesired

as it decreases the gel's structural stability .[114,159,161,162] Monovalent cations are positively charged ions with a single charge from the loss of electrons such as Na^{+1} and K^{+1}. Divalent cations, also known as bivalent cations, are also positively charged ions with a valence of 2+ such as Ca^{+2} and Mg^{+2}. Reservoir formation water, has an abundance of cations (Na^{+1}, K^{+1}, Ca^{+2}, and Mg^{+1}) present as well as anions (Cl^{-1}, HCO_3^{-1}, and SO_4^{-1}).[163] The presence of various salt ions have the potential to interfere with gel formations. Jia et al. studied the influence of monovalent (NaCl and KCl) and divalent (Ca_2Cl) salts in a PAM gel's gelation time. Their study reported that monovalent cations have a retardant effect on gelation time.[55] The gelation time increase as Na^{+1} and K^{+1} concentration increased from 1 to 5 wt% in their respective PAM solution, but Na^{+1} increased gelation time more than K^{+1} because of sodium's higher charge density.[55] Divalent cations on the other hand showed to delay gelation time even more. Ca^{+2} showed a higher effect on gelation time than Na^{+1} and K^{+1} and it is attributed to its higher ionic charge number.[55]

Most of the studies reviewed above, focused on the effects of salinity on the gelation of HPAM-based solutions *via* organic or metal cross-linkers. Polyacrylamide has been studied thoroughly as it is a highly versatile polymer used widely across many industries, but knowledge of its application as a CO_2-triggered sealant and its rheological behavior under reservoir like condition is still limited. This study targeted the behavior of CO_2-SPAM under conditions that are expected in depleted oil and gas reservoir and have not been addressed by other studies as seen in Fig. 5.1.[14,32,61,70,71,75,79,80,87,90,93,98]

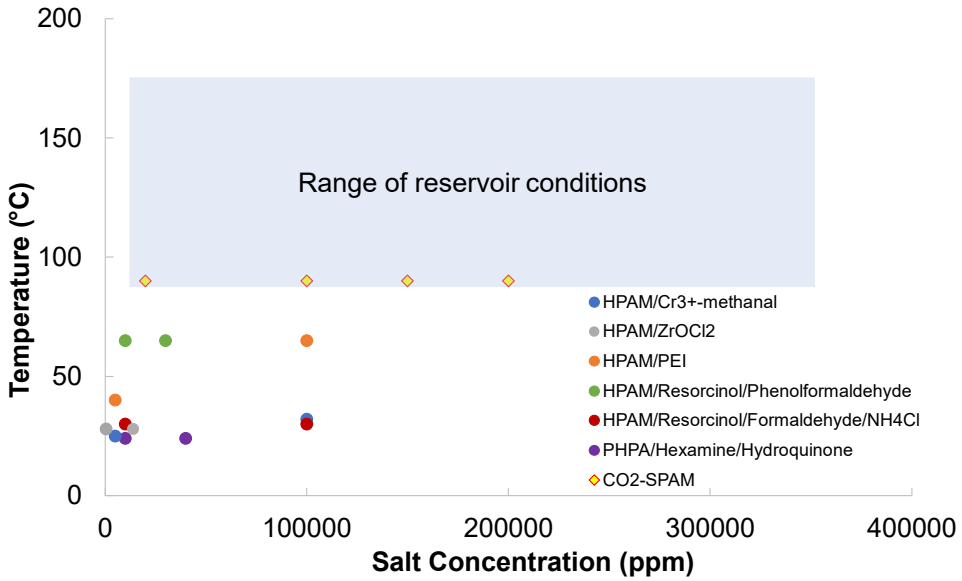

Figure 5.1 Studies performed on PAM-based polymers as a function of temperature and salinity.

Research on the effect of high salinity on CO_2-triggered gelation of PAM-based solutions is lacking. The present work addresses the effect of salinity on the gelation time of CO_2-sensitive polyacrylamide gel. Furthermore, it outlines the results of rheological tests on CO_2-SPAM solutions and gels under various NaCl and polyacrylamide concentrations.

Methodology

Materials

Poly(acrylamide) (average M_W: 5,000,000 to 6,000,000, monomer molecular weight: 71.08 g/mol, Thermo Fisher Scientific); methenamine (molecular weight: 140.19 g/mol, grade: USP, purity: 99-100.5%, Spectrum Chemical MFG CORP); resorcinol (molecular weight: 110.112 g/mol, grade: USP, purity: 99-100.5%, Spectrum Chemical MFG COPR); sodium chloride (molecular weight: 58.44 g/mol, grade: reagent, Thermo Fischer Scientific); water

(molecular weight: 18.015, grade: extra pure, Thermo Fisher Scientific); carbon dioxide (Industrial grade gas, Airgas).

Gel Preparation

Aqueous CO_2-SPAM gel solution consists of 0.4 wt% methenamine, 0.1 wt% resorcinol, PAM at different concentrations (0.5 wt%, 1.0 wt%, 1.5 wt%, 2.0 wt% and 3.0 wt%) and brine at different salt concentrations. Methenamine and resorcinol's weight percentage remained constant throughout all gel samples while PAM wt% and salinity concentrations were varied as shown in Table 5.3.

Table 5.3 CO_2-SPAM samples with constant 0.4 wt% of methenamine and 0.1 wt% of resorcinol.

Sample #	PAM wt%	Brine (ppm)		Sample #	PAM wt%	Brine (ppm)
1	PAM 0.5 wt%	20,000		9	PAM 1.5 wt%	20,000
2		100,000		10		100,000
3		150,000		11		150,000
4		200,000		12		200,000
5	PAM 1.0 wt%	20,000		13	PAM 2.0 wt%	20,000
6		100,000		14		100,000
7		150,000		15		150,000
8		200,000		16		200,000

CO_2-SPAM gel samples were prepared using a brine solution as the solvent with a salinity level comparable to that of formation water in a depleted oil and gas reservoir.[164] Brines with salt concentrations of 20,000ppm, 100,000ppm, 150,000ppm and 200,000ppm were tested and compared. First, 100mL of brine was heated to 90°C in a conical flask and stirred with a magnetic stirrer at 550 rpm at ambient pressure. After it reached the desired temperature, 0.4 wt% of methenamine was added to the heated brine solution and stirred until fully dissolved (~15 minutes). Resorcinol was consecutively added to the mixture and stirred for an additional

15 minutes until it fully dissolved. Finally, polyacrylamide was added to the solution, and the mixture was agitated for 1 hour to achieve complete dissolution. A sample of approximately 50 mL from the mixture was transferred to a test tube and placed in a hot water bath at 90°C. After the sample reached the set temperature, gaseous CO_2 was bubbled into the mixture by inserting a silicone tube connected to the CO_2 supply as seen in Fig. 5.2.

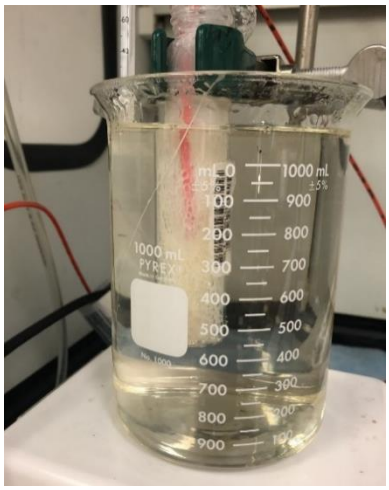

Figure 5.2 CO_2 bubbling into test tube in a hot water bath.

CO_2 was bubbled into the sample for 30 minutes. Afterwards, the CO_2 supply was shut off, and the test tube was closed immediately. This technique allowed CO_2 gas to remain inside the test tube. The solution was left to gel under CO_2 condition and at 90°C in the water bath. Note that CO_2 bubbling is not an accurate representation of the exact CO_2 diffusion mechanism happening in porous media, but is the standard operating procedure reported in other studies to introduce CO_2 into samples.[100,165,166] In the reservoir, the CO_2 will encounter the CO_2-SPAM layer as a front traveling upwards as mentioned in Chapter 1. A more precise representation of CO_2 encountering CO_2-SPAM will be through a core flooding experiment as seen in Fig. 5.3.

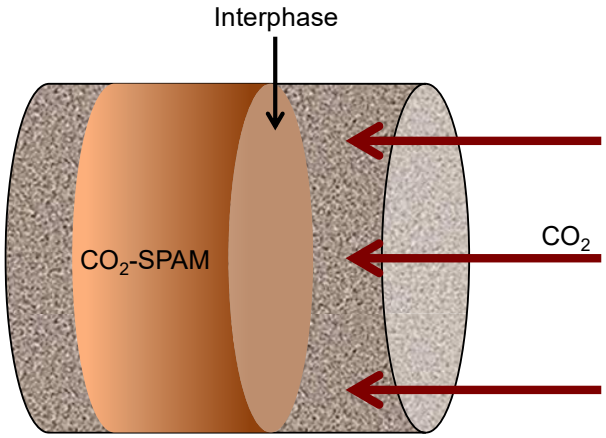

Figure 5.3 Schematic of CO_2 diffusion through porous media with CO_2-SPAM seal.

In this setup, CO_2-SPAM is injected into the core followed by the injection of CO_2. The core will then be sealed off to let the CO_2 diffuse into the CO_2-SPAM saturated area, react with it, and form a gel. This experimental set up would be a better representation of CO_2 diffusion and gel formation in porous media. Two main drawbacks from this method are: 1) the gelation will take longer because CO_2 will slowly diffuse into the solution and 2) the formed gel will not be retrievable for rheological testing.

Gelation Time Measurement, t_{gel}

Gelation time (t_{gel}) is the time required for the aqueous CO_2-SPAM solution to change its physical properties and become non-flowing/rigid. For this study, the Sydansk gel strength coding system[147] was used to categorize and describe gel's physical characteristics as seen in Table 5.4. This coding system has been widely used to characterize gels for oilfields wellbore operations and for permeability reduction of subterranean hydrocarbon-bearing formations such as CO_2 storage sites in addition to being convenient and inexpensive.[101,131,167–169] Other studies have quantified the gelation time by determining the gel's inflection point on the viscosity vs.

time curve as seen in Fig. 5.4 using a viscometer.[55,56,131,170] The inflection point is defined as the onset of gel formation. The initial and final gelation times are also used as an indicator of gelation. The initial gelation time is considered the time needed to see a sudden increase in viscosity while the final gelation time is the time needed to achieve a steady viscosity.[131] Quantitative determination of gelation time requires continuous viscosity measurement as the solution turns into a gel. A dynamic viscosity measurement was not possible at our facility because it was not possible to provide a CO_2 atmosphere around the rheometer. Thus, we decided to use the qualitative Syndask method similar to other studies that have investigated CO_2-triggered gelation.

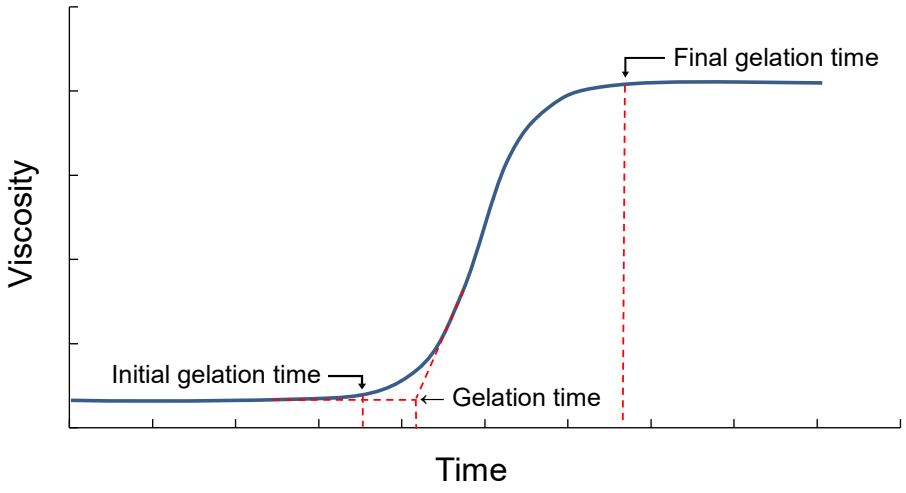

Figure 5.4 Gelation time's inflection point in a viscosity vs. time plot.

The gel strength descriptions from Table 5.4 are illustrated in Fig. 5.5. The figure depicts the gel's flowing capabilities corresponding to each gel strength code when tested by inverting the testing tube containing the gel.

Table 5.4 Sydansk gel strength code.

Gel Strength Code	Gel Description
A	*No detectable gel*: No visible change on the gel's viscosity compared to the initial aqueous solution.
B	*Highly flowing gel*: Slight visible change on the gel's viscosity compared to the initial aqueous solution.
C	*Flowing gel*: Majority of the gel flows to bottom of the testing tube by gravity upon inversion
D	*Moderately flowing gel*: Only a small portion (5-10%) of the gel does not flow to the bottom of the testing tube by gravity upon inversion.
E	*Barely flowing gel*: The gel can barely flow and/or a significant portion (>15%) of the gel does not flow by gravity upon inversion.
F	*Highly deformable non-flowing gel*: The gel does not flow to the bottle cap by gravity upon inversion.
G	*Moderately deformable non-flowing gel*: The gel deforms about halfway down the testing tube by gravity upon inversion.
H	*Slightly deformable non-flowing gel*: Only the gel surface slightly deforms by gravity upon inversion.
I	*Rigid gel*: There is no gel surface deformation by gravity upon inversion.

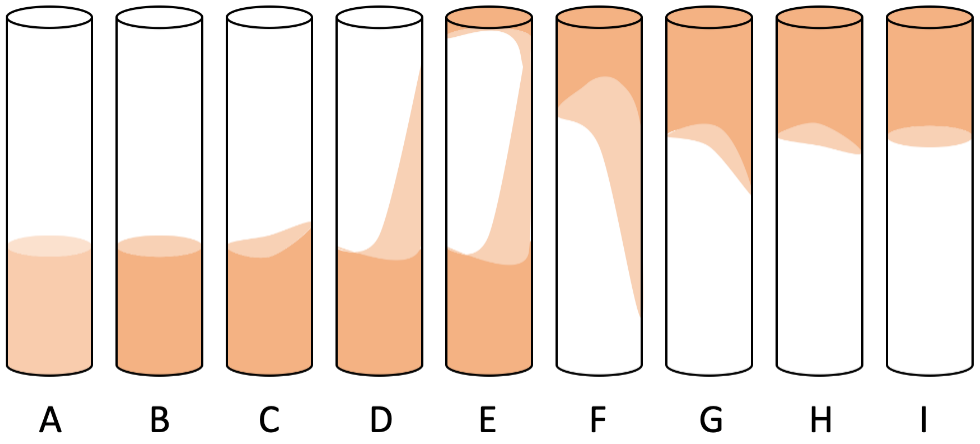

Figure 5.5 Sydansk gel strength code visualization.

Recording the gelation time was started with the introduction of CO_2 into the CO_2-SPAM aqueous solution (Fig. 5.6a). As CO_2 was continuously bubbled into the sample, visual changes

were recorded every five minutes to document all aspects of the evolution of the CO_2-SPAM. Fig. 5.6b shows a CO_2-SPAM gel after CO_2 shut-off with a gel strength code F, and Fig. 5.6c depicts a gel with a gelation time longer than one hour with a gel strength code H.

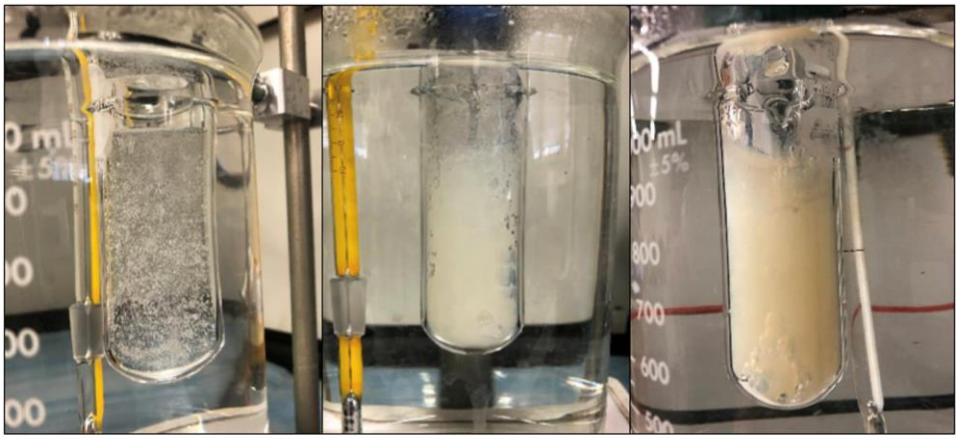

Figure 5.6 (a) PAM aqueous solution at t = 0. (b) PAM gel solution at t = 40 minutes. (c) PAM gel solution at t > 1 hour.

Qualitative characteristics of the gel, such as cloudiness, color, apparent flow behavior, bubble's consistency and size, etc., were documented and used to determine the code based on Sydansk's gel strength code.[121,128,147,171] Samples were considered fully gelled when their Sydansk's gel code reached G (moderately deformable non-flowing gel). When the gel reached a gel strength code of G, time recording was stopped, and the sample's t_{gel} was logged with its respective PAM concentration and salinity. All samples need to be replicated a minimum of three times and demonstrate similar results with minimal variation to validate the results.

Rheology Study

The gel was characterized by utilizing an angular oscillatory rheometer (Discovery Hybrid Rheometer) with a stainless-steel parallel Peltier plate. This instrument's function is to apply shear stress and characterize the elastic properties of soft materials such as CO_2-SPAM gel.[172] The rheometer uses a 20mm parallel plate geometry as seen in Fig. 5.7. The gel was characterized after gelation time was completed at ambient pressure and 30°C to prevent noise interfering with the data collection (the rheometer shows inconsistent and noisy readings at high temperatures). Note that the sample is removed from the water bath at 90°C when placed immediately in the rheometer for testing.

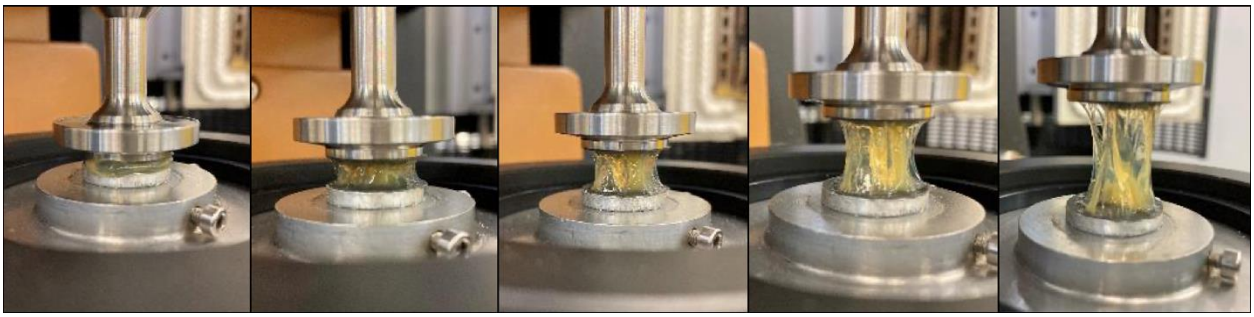

Figure 5.7 Visualization of upper plate retraction from loaded gel sample on oscillation rheometer after testing.

Amplitude sweep. An oscillation amplitude sweep is an oscillatory assay that uses an increase in energy input (amplitude) to probe soft materials' rheological and mechanical stability. In this test, the rheometer is set to a loading gap of 45,000 microns and the gel sample is placed on the lower plate. The upper plate is lowered to a gap of 800 microns ensuring not sample spills over the lower plate. After the sample is loaded to the rheometer, the amplitude sweep test is selected in the TRIOS software and initiated with the following parameter:

- Environmental Control
    - Soak time: 60 seconds
- Test Parameters
    - Angular frequency: 1 rad/sec
    - Strain %: 0.1% to 10.0%
    - Points per decade: 10

The apparatus exerts oscillating angular strain on the gel between the two plates and measures the stress. This test determines the material's ratio of elastic stress to strain at a constant frequency with increasing oscillation strain percentage. In other words, the strength of the gel is quantified by its ability to withstand stresses before inelastic deformation occurs (storage modulus). This measurements are important because they determine the strength of the gel which subsequently relates to the gel's sealing/blocking performance. A high storage modulus indicates that the material tested demonstrates more solid-like characteristics and is able to withstand higher stresses (higher pressures) before inelastic deformation (seal rupture). The amplitude sweep was performed at a constant frequency on gel samples (PAM at 1.0 wt%, 2.0 wt%, 3.0 wt%) in brine solutions of 20,000ppm and 200,000ppm to identify the change in storage modulus (G') and loss modulus (G'') as a function of oscillation strain percentage.

The storage modulus, also known as the elastic modulus, represents the elastic strength of a material but in terms of shear deformation, while the loss modulus is the viscous response of a material and also a measurement of dissipated energy from shear deformation.[173] This analysis also determined the linear viscoelastic (LVE) region of the gel and the strain percentage at which the frequency sweep was performed. The viscoelastic region is equilibrium state of a material's structure where the ratio between the applied stress and strain percentage is linear. At a constant

frequency and temperature, a linear relationship between moduli and strain percentage can be measured which results in what is called the LVE region. The viscoelastic properties (i.e., storage and loss modulus) are independent of strain within the linear region. At the end of the linear region (at the critical strain), the storage modulus becomes strain dependent. It is important to note that the material's temperature can affect the critical strain.[174] Temperature's effect on a material's modulus can be typically classified in four regions of viscoelasticity: glassy region, transition region, rubbery plateau region and terminal region (Fig 5.8).[174]

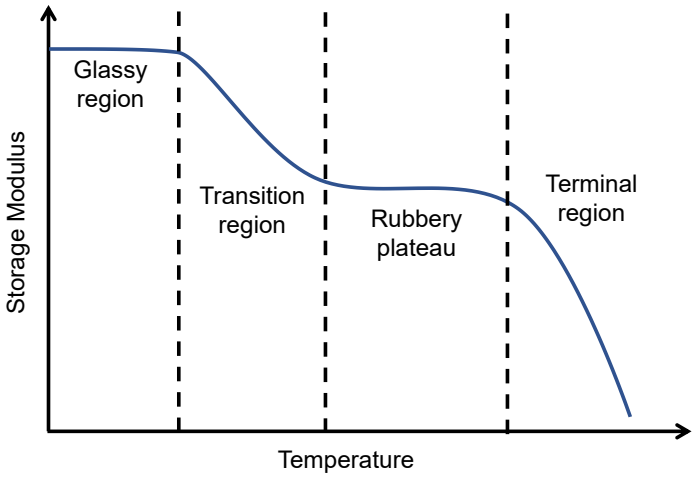

Figure 5.8 Viscoelastic regions based on storage modulus as a function of temperature.

Note. Adapted with permission from Acta Astronautica by Kawak et al., 2017. Copyright 2017 by Elsevier.

These regions can be identified using a temperature ramp test or a frequency sweep. The glassy state is often characterized by a high plateau in the storage modulus at lower temperatures.[174] As the material is heated, the glassy state shifts to the transition region where the storage modulus decreases.[174] Continuous exposure to higher temperatures leads the material

to the rubbery plateau and finally the terminal region also known as the liquid flow region. The rubbery plateau in a modulus-temperature plot indicates the presence of entanglement of cross-links in the sample and is also inversely proportional to the molecular weight between two successive entanglements.[175] Amplitude sweep's strain (displacement) or stress (torque) amplitude can be varied linearly or logarithmically while data are recorded by the rheometer.

Flow sweep. A flow sweep illustrates the change in viscosity (Pa.s) as a function of shear rate (sec^{-1}). Similar to the amplitude sweep, the gel sample is loaded into the rheometer and the Flow Sweep test is selected in the TRIOS software and initiated with the following parameters:

- Environmental Control
    - Soak time: 60 seconds
- Test Parameters
    - Shear rate 1.0 sec^{-1} to 10.0 sec^{-1}
    - Points per decade: 10

The flow sweep gathers a series of single viscosity data points at each logarithmic stress steps when steady state is reached. The resulting data is a viscosity vs. shear rate plot of the material's rheological behavior when subjected to sinusoidal deformation. This viscosity vs. shear rate study was conducted on the CO_2-SPAM gel sample after CO_2 exposure. The flow sweep aims to determine the viscosity of the non-flowing gels to identify the effects of PAM concentration and salinity. Both flow sweep and amplitude sweep tests are required to be replicated on each sample a minimum of four times with minimal variation to corroborate the data.

Results and Discussions

Salt Concentration vs. Gelation Time

Visual changes in the gel demonstrated that gelation time increased as salinity levels increased but decreased as PAM concentration increased. During the 60 minutes after CO_2 was first introduced to the solution, PAM solution at 0.5 wt% did not achieve gel strength beyond "F", which is not sufficient to block subsurface fractures or interstitial pores. As mentioned before, the weight percentage of resorcinol and methenamine were kept constant as PAM's weight percentage was varied. This low polymer concentration allowed more brine into the sample, which led to the unsuccessful formation of the gel. Also, lower polymer concentration (i.e., less polymer chains within the solution) results in low viscosities and low gel strength.[176,177] The rest of the samples did achieve a gel strength of G or higher, which indicates that the PAM concentration significantly affects the viscosity of the gel. All CO_2-SPAM samples (except for the 0.5 wt%) at 20,000ppm became highly deformable non-flowing gels after 35 minutes of CO_2 exposure and achieved a gel strength code I at approximately 45-50 minutes after exposure. Samples in a brine solution of 200,000ppm experienced a gelation time longer than 1 hour. Most samples achieved a grade D and E after 1 hour of CO_2 flooding and achieved a grade G and H after ~2 hours.

The mechanism of gelation retardation at high salinity is explained as follows:

1. Under acidic and high temperature conditions, PAM undergoes hydrolysis and becomes a polyelectrolyte with negative charged carboxylate groups on its backbone along the chain.[138,178,179].

2. When salt is added to the mixture, salt cations interact with the carboxylate groups. As salt's cations neutralize negative charges on the molecular chain, the repulsion force in the chain lessens and the molecular chain contracts (Fig. 5.7.[180]).[122,123]

3. Coiled polymer chains have a lower probability of reacting with other[51,161] chains and forming a gel.

4. Sodium cations shield amide groups and block potential cross-linking sites.[114] These processes slow down the gelation and diminish the mechanical strength of the gel.[161]

For instance, in distilled water, the polymer chain are able to extend due to the electrostatic repulsion of the carboxylate ions as seen in Fig. 5.9.[180] In the presence of NaCl ions, the polymer chain curls and shrinks because of electrostatic shielding.[117,122,170,180,181] Additionally, the shielding effect of the monovalent cations can cause an increase in the molecule's flexibility but a decrease in hydrodynamic volume and number of accessible sites.[182]

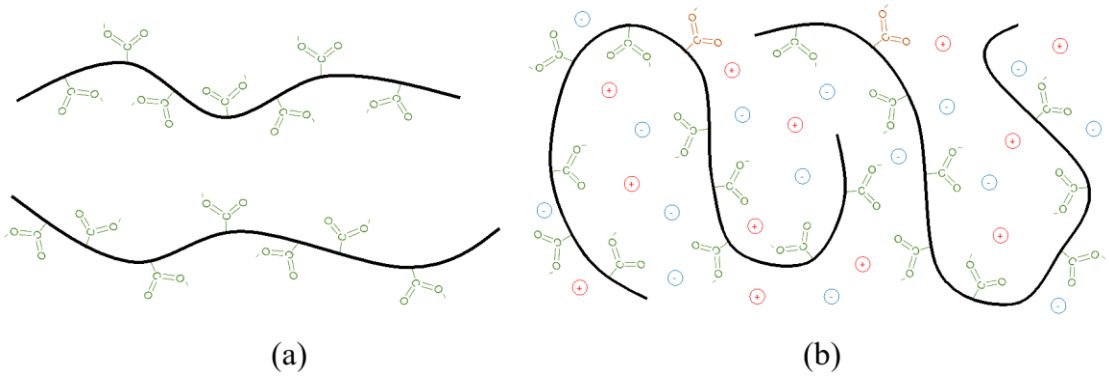

Figure 5.9 (a) Electrostatic repulsion of carboxylate ions in PAM chain in distilled water. (b) Electrostatic shielding of PAM chain in brine solution.

The qualitative results from the gelation measurements are shown in Fig. 5.10. PAM at 0.5 wt% (Fig. 5.10a) did not fully gel after 1 hours of CO_2 exposure. In addition to that, the qualitative gel strength dipped at 35 minutes. The sudden decrease in gel strength can be explained by the constant inversion of the test tube. This particular sample was highly deformable and highly flowing; therefore, the constant and repeated inversion of the test tube

and force of gravity kept the gel from adhering to the test tube walls and staying in place. PAM at 1.0 wt%, 1.5 wt%, and 2.0 wt% (Fig. 5.10b, 5.10c, and 5.10d, respectively) achieved a gel strength code of G at a brine concentration of 20,000 ppm within the first hour of CO_2 exposure, while samples at higher salinity concentrations experienced an elongation in gelation time. As mentioned above, this increase in gelation time is caused by the excess amount of charged ions interacting with the polyelectrolyte and curling of the polymer backbone that limits access to the cross-linking sites. The plateaus areas or step changes depicted in Fig. 5.10 are the result of the qualitative and subjective nature of the coding system as well as the lack of resolution in the code itself. It also shows how the gel continues to polymerize, and highlighted changes in viscosity and gel flow are more visible in intervals.

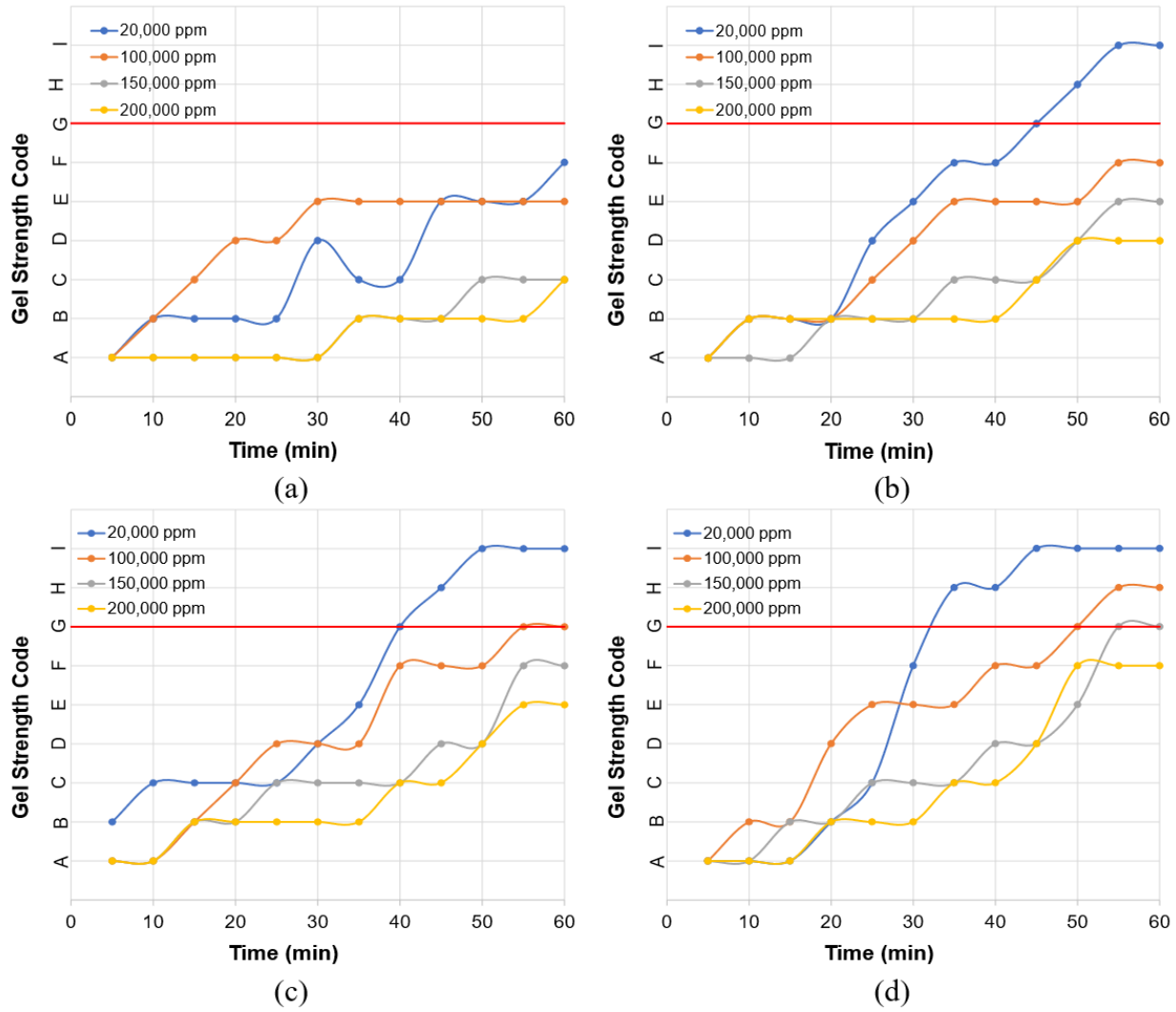

Figure 5.10 Effects of salinity in gelation time for (a) PAM at 0.5 wt%, (b) PAM at 1.0 wt%, (c) PAM at 1.5 wt%, and (d) PAM at 2.0 wt%. The red line shows the gel's threshold code (G).

PAM concentration, on the other hand, has the opposite effect on gelation time. Fig. 5.11 shows how, as PAM concentration increases, gelation time decreases for PAM at 1.0 wt%, 1.5 wt%, and 2.0 wt%. The effect of increasing salinity on gelation time can also be observed at longer times, but it is evident that samples at higher polymer concentration gel faster. Gelation time decreases because the increase of polymer concentration increases the amount of accessible

cross-linking sites and the likelihood that hydroxymethyl-resorcinol (i.e., the cross-linking molecule) will encounter PAM. Hence, the probability of cross-linking reaction increases and accelerates the formation of the gel.

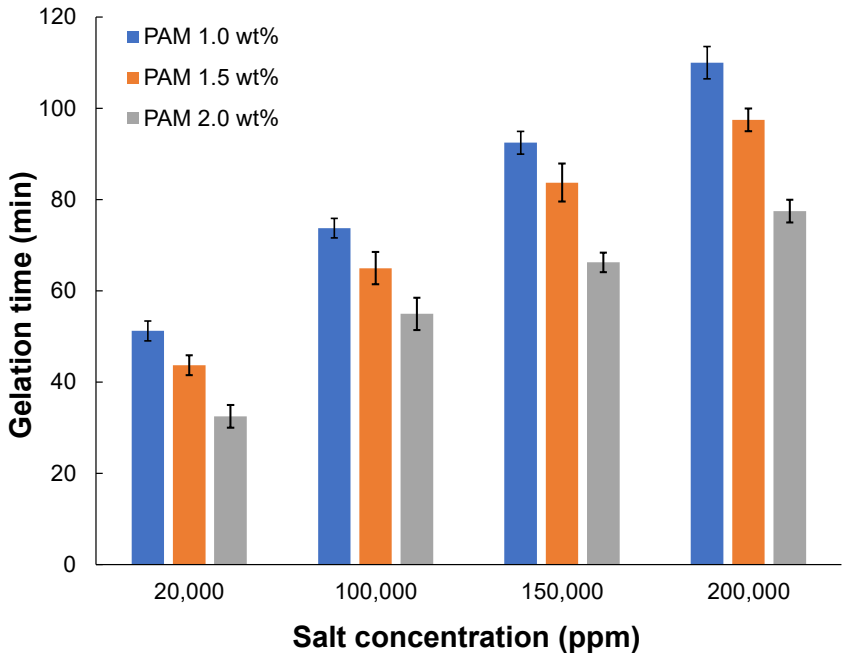

Figure 5.11 Gelation time as a function of salinity for PAM at 1.0 wt%, 1.5 wt%, and 2.0 wt%. Each sample was replicated a minimum of four times with minimal variation.

Amplitude Sweep

All samples were replicated a minimum of four times and the average values were used to further assess the fluid's properties and salinity effects. The trials are shown in Fig. 5.12, 5.13 and 5.14 where error bars show the small variances between samples. The results of the multiple tests produced CO_2-SPAM's linear viscoelastic region (LVE) and demonstrated the difference in storage moduli between samples at different salinities. The difference in storage moduli shows the effect of salinity on gel strength, which correlates to the gel's sealing capabilities.

CO_2-SPAM, at different PAM and salt concentrations, demonstrates a LVE region ranging from strain of 0.5% to ~20% (highlighted in red bars). The end of the LVE was calculated by finding the amplitude at which the initial value of the storage modulus changes by 5%.[183] After 20% strain, the gel becomes strain dependent, and further strain will destroy the structure of the sample.

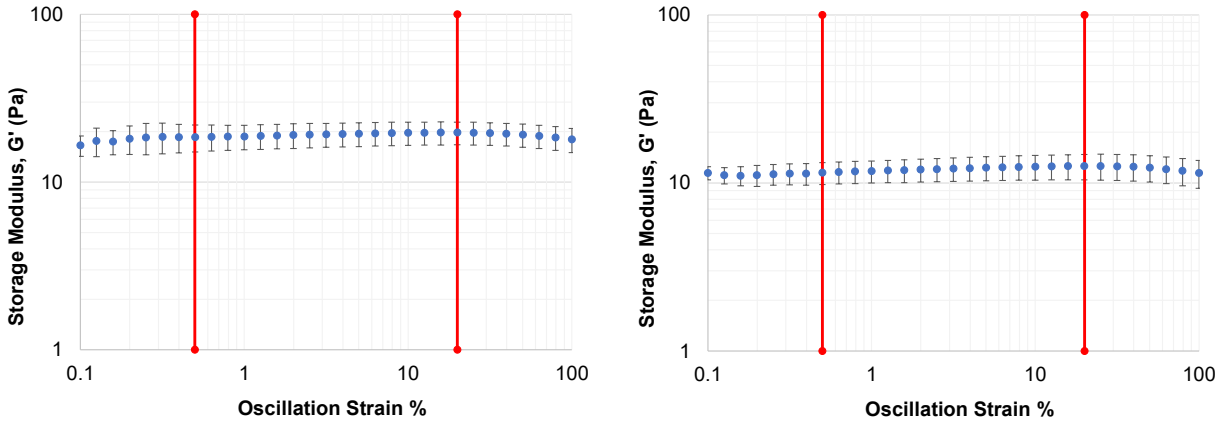

Figure 5.12 Determination of the LVE region and comparison of storage moduli of samples with 1.0 wt% PAM at salinity of (a) 20,000ppm and (b) 200,000ppm.

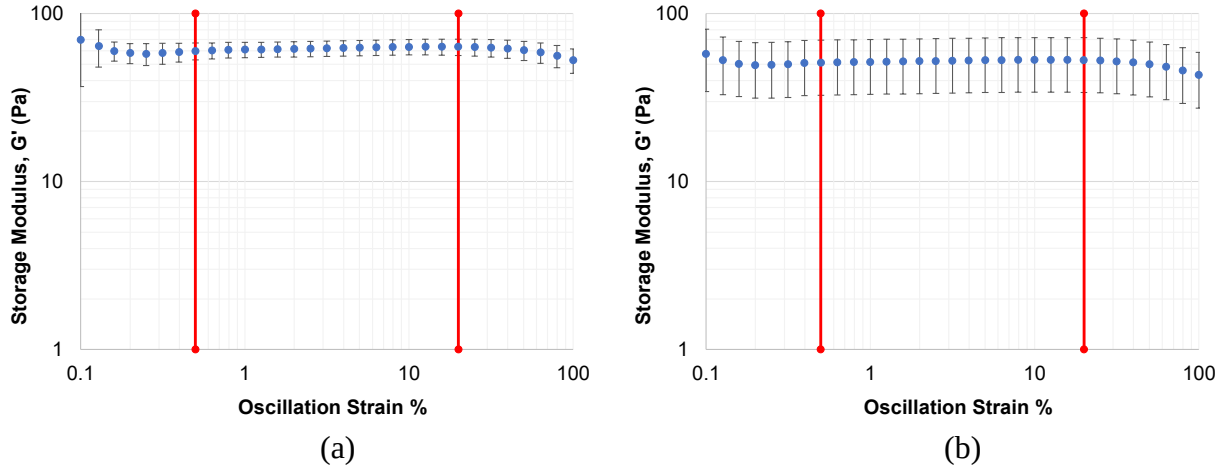

Figure 5.13 Determination of the LVE region and comparison of storage moduli of samples with 2.0 wt% PAM at salinity of (a) 20,000ppm and (b) 200,000ppm.

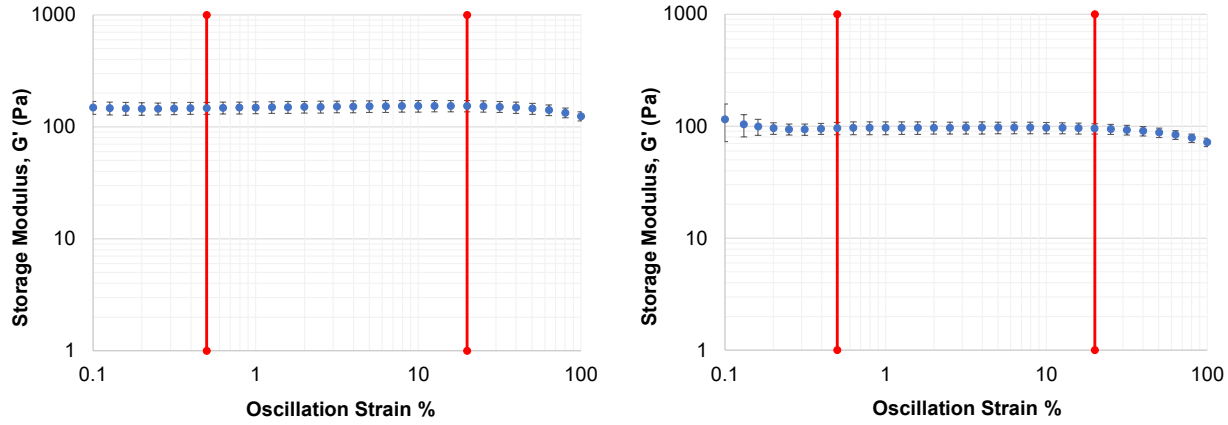

Figure 5.14 Determination of the LVE region and comparison of storage moduli of 3.0 wt% PAM at salinity of (a) 20,000ppm and (b) 200,000ppm.

The loss modulus was significantly lower than the storage modulus (G' > G'') for all samples, which indicates that the CO_2-SPAM gel demonstrates more solid-like characteristics than fluids and can be termed as a viscoelastic solid material (see Fig. 5.15). The effect of salinity on the loss and storage moduli does not remain consistent as PAM concentration increases. Finally, the linear viscoelastic region (LVE) was determined to be in between 0.5% and 20% oscillation strain. After 20% strain, the sample demonstrates non-linear elastic deformation and the breakdown of the superstructure.

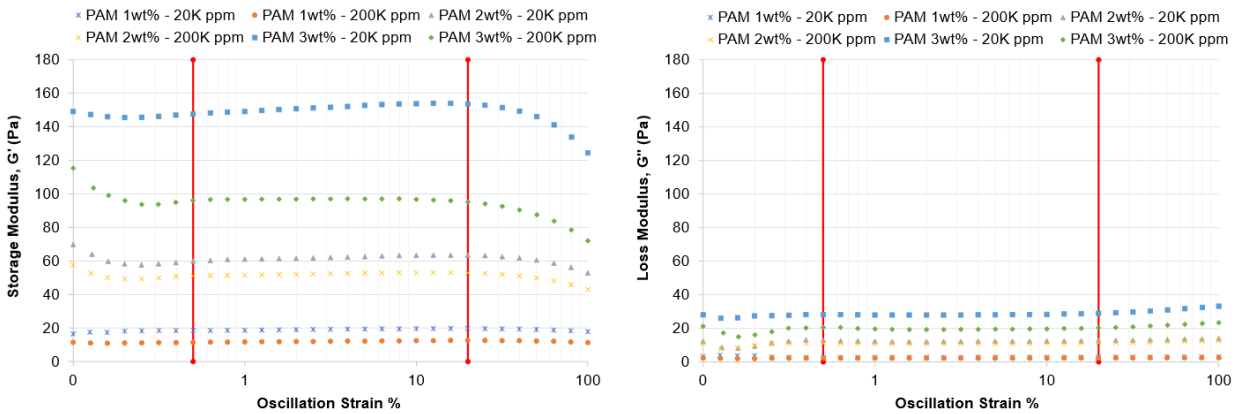

(a) (b)

Figure 5.15 Compilation of PAM and salt concentration effects on (a) storage modulus and (b) loss modulus at oscillation strain ranging from 0.1% to 100%.

As PAM concentration increases, the storage modulus increases. The increase in G' is attributed to the increase in cross-linking reactions and cross-linking density when PAM concentration is increased. Unlike PAM concentration, salinity decreases the gel's storage modulus. The average percent decrease in storage modulus caused by an increase in salinity for PAM at 1.0 wt%, 2.0 wt%, and 3.0 wt% was 35%, 13%, and 38%, respectively at an oscillation strain of 5% (see Fig 5.15a). The average percent decrease in loss modulus as a result of increasing salt concentration for PAM at 1.0 wt%, 2.0 wt%, and 3.0 wt% was 8%, 18%, and 27%, respectively (Fig 5.15b). It is evident that salinity diminishes the gel's strength as salt ions hinder the accessibility of cross-linking sites and inhibit the formation of a complete three-dimensional structure.

Fig. 5.16 illustrates the effect of increasing PAM concentration on both the storage (G') and loss modulus (G'') as a function of salt concentration to explore the appropriate PAM concentration for a certain storage site at a specific salinity.

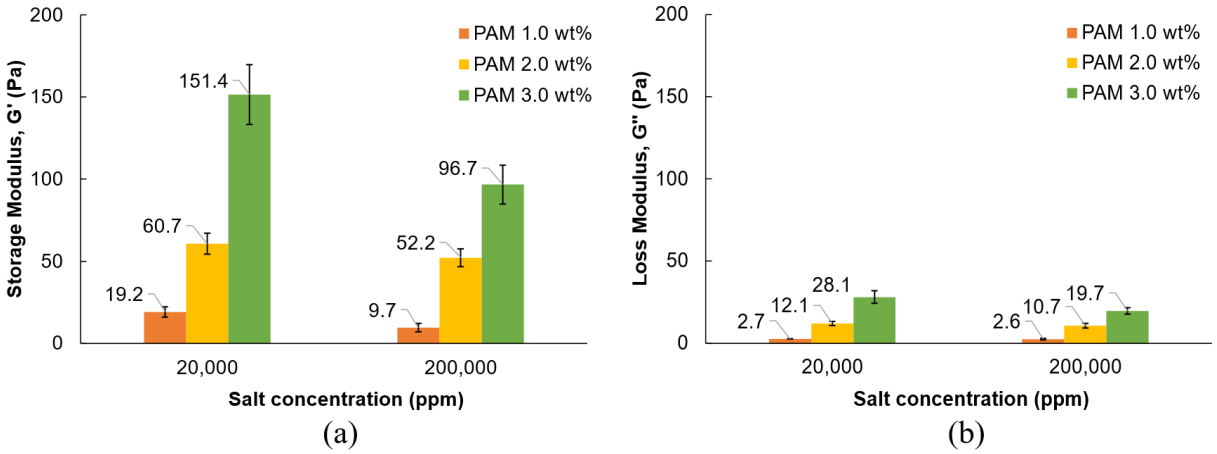

Figure 5.16 Effects of PAM and salt concentration on (a) storage modulus and (a) loss modulus in the LVE region. Values are based on the average storage modulus value between an oscillation strain percent of 0.5% and 20%.

Since the average value of the linear viscoelastic region of each sample was used, the results in Fig. 5.16 only reflect the gel being strained 0.5% to 20%. Storage sites with high salinity are able to benefit from higher PAM concentrations. Fig. 5.16a shows that a higher polymer concentration leads to a higher gel strength (higher G') and consequently a higher sealing performance. Fig. 5.16b puts into perspective low G'' is compared to G' and how there is a minimal difference between salinities. The slight differences in G'' between 20,000 ppm and 200,000 ppm are because the gel exhibits more of an elastic response and can store much more energy when subjected to oscillating loads than just dissipating it.

Flow Sweep

The flow sweep test was utilized to identify the behavior of the fluid's viscosity as a function of shear rate. The results from this study revealed that the CO_2-SPAM gel demonstrated pseudoplastic behavior. In other words, the gel exhibits both plastic and Newtonian flow behaviors due to its low viscosity at high shear rates and high viscosity at low shear rates. Note

that all samples were replicated a minimum of four times with minimal variation and the average values were used to compare the samples. Fig. 5.17, 5.18, and 5.19 show the shear-dependent viscosity equation of all PAM samples at 20,000 ppm compared 200,000 ppm. Here, the power law can be obtained from empirical data and is able to predict fluid behavior as a function of shear rate. Typically, non-Newtonian fluid behavior can be modeled using the power law model (Eq. 5.1):

$$\mu = K\gamma^{n-1} \tag{5.1}$$

Where μ is the viscosity, K is the flow consistency index, and n is the power law constant. Table 5.5 lists the power law constants values from the power law equations obtained from empirical data. The approximate percent decrease in flow consistency index for PAM at 1.0 wt% between 20,000 ppm and 200,000 ppm is 35.8%. A similar behavior was found for PAM at 2.0 wt%, and 3.0 wt%. The percent decrease in flow consistency index between PAM at 2.0 wt% in a brine solution of 20,000 ppm and 200,000ppm is 20.1%, whilst for PAM at 3.0 wt% saw a difference of 12.2%. The percentage decrease indicated that excess salt in the solution leads to lower viscosity. As PAM concentration increases, the flow consistency index increases, which directly impacts the increase in viscosity as seen in Eq. 5.1. Also, the flow consistency index is a numerical indicator of shear strength at a shear rate of 1.0 sec^{-1} and can be used to compare and quantify how salinity increases or decreases viscosity as seen in Table 5.5.

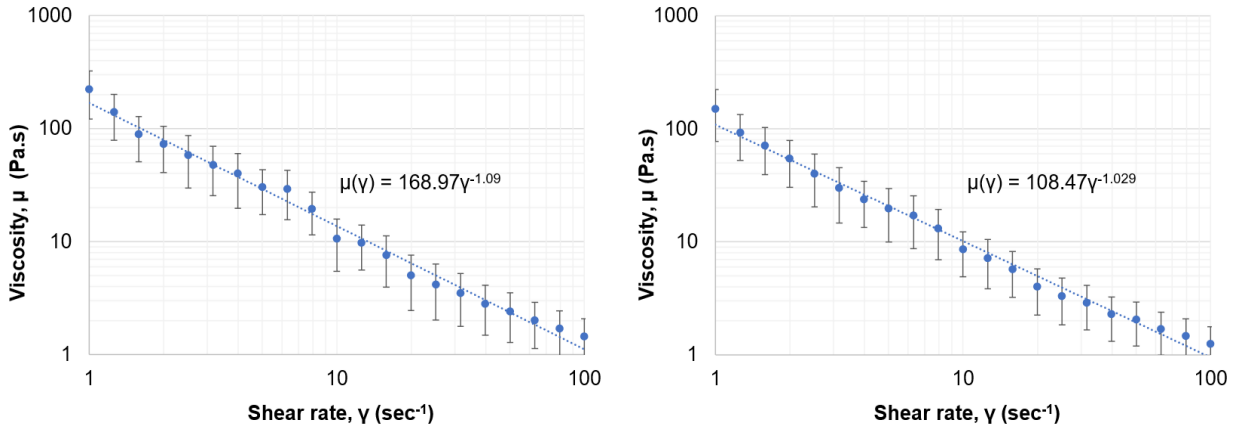

Figure 5.17 Determination of power law model for solutions with 1.0 wt% PAM at salinity of 20,000 ppm and (b) 200,000ppm. Regression coefficients are 0.9656 and 0.971 for 20,000 ppm and 200,000 ppm, respectively.

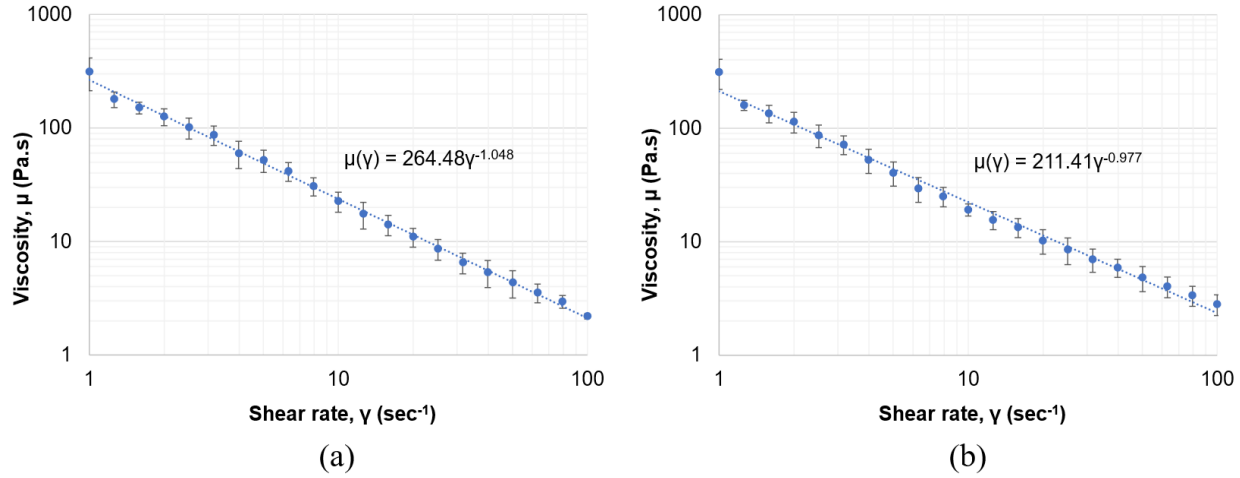

Figure 5.18 Determination of power law model for solutions with 2.0 wt% PAM at salinity of 20,000 ppm and (b) 200,000ppm. Regression coefficients are 0.9744 and 0.9438 for 20,000 ppm and 200,000 ppm, respectively.

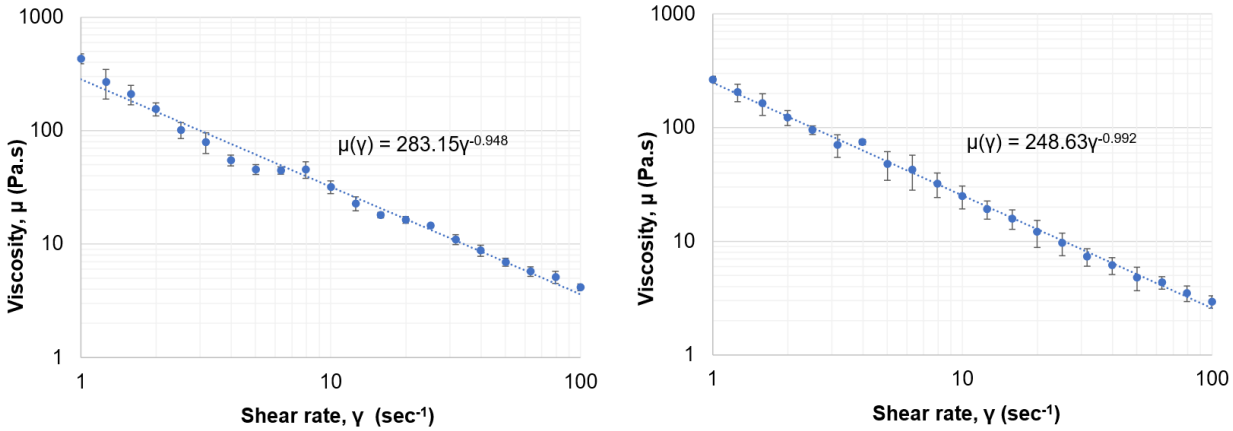

(a) (b)

Figure 5.19 Determination of power law model for solutions with 3.0 wt% PAM at salinity of 20,000 ppm and (b) 200,000ppm. Regression coefficients are 0.9498 and 0.9964 for 20,000 ppm and 200,000 ppm, respectively.

Table 5.5 Power law constants for samples with various PAM concentrations, obtained empirically from rheological experiments, demonstrate shear-thinning behavior (n < 1).

	Flow consistency index (K)		Power law constant (n)	
PAM (wt%)	20,000 ppm	200,000 ppm	20,000 ppm	200,000ppm
1	168.97	108.47	-0.09	-0.029
2	264.48	211.41	-0.048	+0.023
3	283.15	248.63	+0.052	+0.008

For all six samples, viscosity decreases as shear rate increases. Soft materials with this rheological characteristic have an apparent viscosity that decreases with increasing shear rate, due to the polymer molecules' ability to align themselves with the shear field to reduce internal friction.[179] As expected, PAM concentration and salinity levels have a marked effect on the gel's viscosity. As PAM concentration increases from 1.0 wt% to 3.0 wt%, the viscosity increases. The increase in viscosity is attributed to the increase in large molecules interacting with each other and exerting drag forces.[184] Salinity on the other hand, has the opposite effect on viscosity. As salt concentration increases, the viscosity decreases. This behavior is not as noticeable at higher PAM concentrations because the increasing amount of polymer chains interacting with

each other does not provide sufficient space to flow and salt effects are inconspicuous. Most water soluble polymers demonstrate an extreme loss in intrinsic viscosity as salt concentration increases in the brine solution.[185,186]

The reasoning behind this effect is the decrease of the dielectric constant as salt concentration is increased.[185] The decrease in the dielectric constant causes the reduction in energy of the hydrogen bonds and solvent-power.[185,186] Thus, as salt concentration increases the viscosity steadily declines because the polymer chain is not as extended in a high-salinity solution as in a low-salinity solution. In other word, it is believed that when salt is introduced into the solution, the polymer chain coils and the free volume increases as it is occupied by the brine, hence viscosity decreases.

Finally, some of the limitations of this study are as follows:

1. Study of the effects of high temperatures and high pressures, as well as gel degradation are also necessary for a well-rounded evaluation of the performance of CO_2-SPAM under reservoir-like conditions. These factors were not, however, studied due to the lack of adequate equipment. It is recommended that for future work, a core flooding experiment is performed to address the effects of high pressure and high temperatures on the gel's sealing performance.

2. Due to the nature of the gel formation, a dynamic rheological study was not possible because CO_2 flooding was not viable based on the rheometer's set up. A glovebox or a similar sealed vessel can be attached to the rheometer's measuring assembly (upper and lower plates) and connected to a CO_2 supply to perform a dynamic rheological study of gel formation under CO_2 atmosphere.

3. Formation water comprises of a mixture of various salts with different ionic charge numbers (monovalent or divalent ions). However, the present work only addresses the effect of sodium chloride in order to isolate its influence and systematically analyze the response of CO_2-SPAM to NaCl as the most abundant salt in formation water.[187]

4. CO_2 bubbling as well as complete saturation of CO_2 in porous media not realistic. Appendix A explores how CO_2 diffuses in porous media and even at time = infinity, CO_2 concentration will not reach 100%. Also, Fig 5.3 demonstrates how CO_2 does not bubble through the seal but encounters the seal as a front.

5. The core flooding experiment needs to address residual oil and gas saturations.

Conclusions

In conclusion, the effect of salinity and PAM concentration on the polyacrylamide-methenamine-resorcinol gel strength and viscosity was evident in this study. An increase in PAM concentration decreased gelation time and increased the viscosity of the gel as well as its strength. The decrease in gelation time and increase in gel strength and viscosity, as a result of increasing PAM concentration, is due to the excess amount of long polymer chains interacting with each other, increasing cross-linking density and exerting drag. Most of the solutions with various levels of salinity and PAM concentrations gelled within an hour of encountering CO_2. The solution at 0.5 wt% PAM did not achieve the desired gel strength code of H for the duration of the experiment (120 min); therefore, it was no longer considered a viable sample. Higher salt concentration increased gelation time and decreased gel strength and viscosity. Gelation time was elongated because salt ions interact with the polyelectrolyte and hinders its ability to cross-link by blocking the accessible cross-linking sites. Gel strength and viscosity decrease due to the salt ions shielding effects. This shielding effect decreases the electrostatic repulsion that allows the polymer chain to expand. Consequently, the polyacrylamide chain shrinks and curls, allowing the free volume to be occupied by brine. Note that when selecting an appropriate PAM concentration for a specific site, it is important to consider not only the salinity in the formation but also the required gel viscosity (for mobility purposes). High salinities have a negatively impact on the gel's sealing performance as it decreases the gel's strength, but it also benefits gel mobility across a reservoir because it reduces its viscosity and elongates gelation time. A longer

gelation time and a lower viscosity allow the gel to travel farther distances before becoming a non-flowing gel and reaching the desired target zone.

Now that a clear understanding of the salinity effects on CO_2-SPAM have been established, a proper assessment on CO_2-SPAM injection into subsurface geological formations for sealing purposes can be achieved. As concluded, high salinities lead to an increase in gelation time and low viscosity and gel strength. Depending on the injection scenario, the high salinities can be beneficial or unfavorable. Leakage pathways that are located kilometers away from the injection zone require low viscosity polymer gels with longer gelation time because the gel needs to travel through the reservoir's pore space to reach the target zone. Low-viscosity fluids can travel more easily through interstitial pores in comparison to high viscous fluids. On the other hand, fractures located close to the wellbore or leakage pathways with high permeability can be sealed by gel systems with high viscosity and high gel strength. Because injection scenarios vary quite often, PAM at 1.0 wt% and PAM at 1.5 wt% are recommended for injection scenarios. Both PAM concentrations gelled and reached a minimum Sydansk gel strength code of G at 20,000ppm, which is the commonly cited oil and gas reservoir salinity. Additionally, their lower viscosities, compared to PAM at 2.0 wt% and 3.0 wt%, allows them to move across a reservoir without much effort. As a result, these concentrations were selected to further study their potential to induce seismicity in the next chapter

CHAPTER VI

INDUCED SEISMICITY BY CO_2-SENSITIVE POLYACRYLAMIDE SOLUTION INJECTION FOR CCS APPLICATIONS.[1]

Introduction

As global warming remains a constant issue, environmental remediation technologies are continuously developed to meet the standards and goals set by the environmental agencies to contain the damaging effects of climate change.[188,189] Excess GHGs and aerosols in the atmosphere cause an imbalance in the Earth's natural infrared radiation cycle.[190] These gases, especially CO_2, are presently decreasing the amount of infrared radiation energy departing the Earth and increasing the accumulation of heat in the Earth's surface causing a severe greenhouse effect.[4] As a result, new technologies have been developed to curb CO_2 emission into the atmosphere. One of these technologies is Carbon Capture and Storage (CCS), in which CO_2 is captured at its source (e.g. power plant) and is injected into subsurface geological formations.[191] CCS is considered a safe solution to dispose of excess CO_2 from anthropogenic sources for long periods of time. CO_2 is captured from CO_2-emitting sources and refined into pure supercritical CO_2. Highly pressurized CO_2 is then injected into the storage site (e.g., saline aquifers, unminable coal seams, and depleted oil and gas reservoirs) and is projected to remain permanently stored for thousands of years. Despite this technology's promising solution to

[1]Article in press.
Quan, L., K. Crane, and M. Mirabolghasemi, 2022, Induced seismicity by CO_2–sensitive polyacrylamide solution injection for CCS applications: SAGE Record, v. 1, 2022–049, in press.

dispose CO_2, it comes with its own limitations. Leakage pathways are escape routes that have the potential to compromise the CCS process by allowing CO_2 to migrate back into the atmosphere.[192–194] These leakage pathways could be nearby faults or fractures created through naturally occurring processes or during well drilling.[192–194] Similar to any leakage problem, sealing appears to be a potential solution to CO_2 leakage from subsurface storage sites. One chemical that has been studied as a sealing agent is CO_2-sensitive polyacrylamide (CO_2-SPAM) gel.[100] CO_2-SPAM undergoes gelation when in contact with high concentrations of CO_2 in reservoir-like conditions. To create an in-situ seal in a CO_2 storage reservoir, CO_2-SPAM is injected into the upper section of the reservoir rock, followed by the injection of CO_2 into the lower section as seen in Fig. 6.1. The injected aqueous CO_2-SPAM as well as CO_2 will flow towards the least resistant pathways first, such as zones of high permeability and fractures. When they meet inside these leakage pathways, the gel forms and seals the pathway.

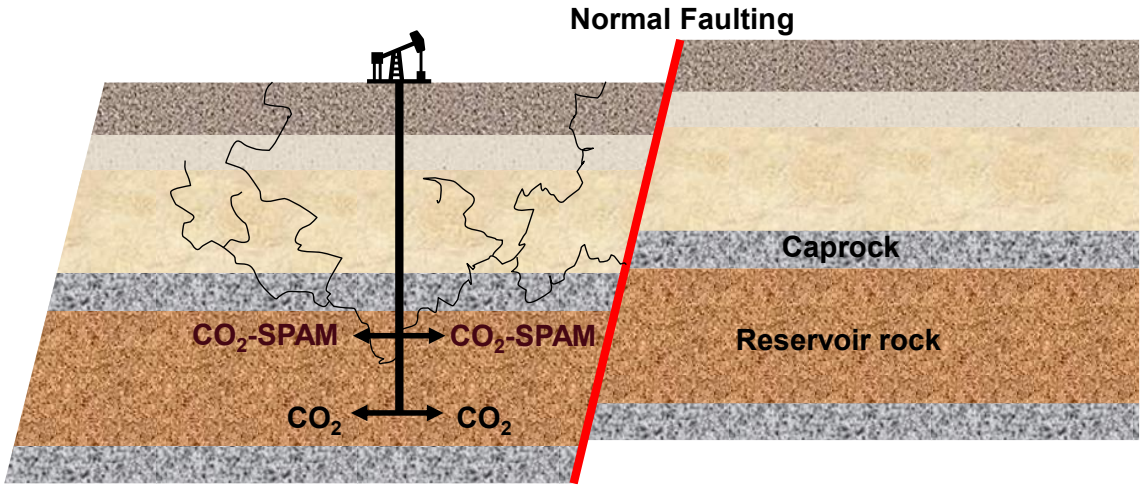

Figure 6.1 CO_2-SPAM injection sequence in depleted oil and gas reservoir.

Outside of the leakage pathway and in the intact formation, CO_2 travels upwards while the solution flows downward. Eventually the two fronts meet and upon contact, the CO_2-SPAM

solution gels, and seals off the area above it. Consequently, some storage pore space is lost due to the seal forming lower than the cap rock interface. It is recognized that this technique causes a loss of storage space above the seal but the tradeoff of having a reliable seal to prevent future leakage is paramount. A way to address and minimize this problem is by using numerical multiphase flow simulations in the reservoir to determine an optimum sequence of injections.

Despite the promising potential of the in-situ sealing approach, concerns arise when the pore pressure near a fault zone increases due to the injection of highly viscous gel solution. This increased pore pressure changes the effective geomechanical stresses in the fault zone, which leads to induced seismicity[195,196]. In this study, the severity of induced seismicity as a result of CO_2-SPAM injection into the Raton Basin is investigated. Initially, the geological structure of the Raton Basin is examined to select a candidate injection well that is in close proximity to a fault. Subsequently, the necessary geological and well data are collected to estimate the pore pressure at the nearby fault. Rheological tests were conducted to identify CO_2-SPAM's response to shear rate. Finally, the calculated pore pressures are used to determine the variety of angles at which fault planes can be reactivated while also deriving a criterion that will indicate the pore pressure necessary to induce seismicity in an intact rock mass.

The Raton Basin

The Raton Basin is a geological depression or dip with an area of about 4000 mi^2 located in northern New Mexico and southern Colorado and is known for its gas production (coal-bed methane deposits) in the Upper Cretaceous Trinidad Sandstone and Vermejo formation and Upper Cretaceous and Paleocene Raton formation.[197] Although lithologic ages within the basin range from Pennsylvanian to Tertiary (volcanics), the basin deepened during the Cretaceous when Laramide compression took place.[198,199] Faulting in the basin is characterized by steep,

branching thrusts (likely Laramide faulting) and normal to strike-slip faults that align with and extend from more recent volcanic dike systems.[198] The juxtaposition and opposite senses of stress required by these younger structures suggests that the Raton Basin is also at the crossing of two significant stress fields, a North-South vertically compressive stress field producing normal faults and a horizontally compressive stress field producing East-West strike-slip faults.[199,200]

This basin, which experienced minimal seismic activity two decades ago, is now known for the high earthquake activity that occurred between 2008 and 2010 that is linked to wastewater injection and disposal.[201–203] Modern seismic activity in the basin dates back to 1966, but a drastic increase of earthquakes in 2001 was correlated to oil and gas wastewater injection[203] and as a result, this area has become of great interest to further study induced seismicity.[201,204] In 2016, a study by Glasgow et al.[195] was initiated and four years of continuous seismic data were collected. Local arrays detected approximately 38,000 earthquakes located between 2.5 km and 6 km below sea level with ranges of Richter local magnitude (M_L) < -1 to 4.2 between 2016 and 2020.[195] The majority of the earthquakes originated from zones containing short faults (< 3 km) with variable orientations.[195] The Raton Basin has proven to be a productive region and an area where oilfield wastewater is disposed, and therefore, it is possible to utilize this area as a CO_2 storage site.

In this study, the Dakota formation is the reservoir layer of interest due to its history of gas production. In the selected scenario, CO_2-SPAM is injected into an existing well near a normal faulting zone. The well selected for this study is Dike Mountain Unit #7-7, which is currently plugged and abandoned in Huerfano, Colorado. Dike Mountain Unit #7-7 is a natural gas producing well, which was operated by Arco Permian (Atlantic Richfield Company) in 1977 and is located approximately 80 meters from the North Abeyta Creek fault. The solution's

injection zone is within the well's perforation zone (~6645 ft to 7550 ft) and closest to the top of the Dakota formation (~6604 ft).

Geological data from Dike Mountain Unit #7-7 were retrieved from a conventional core analysis, performed by Core Laboratories Inc., of the Dakota formation. A significant deviation in permeability values helped determine a possible damaged zone. The suspected damaged zone is a small layer of high permeability from 6783 ft to 6787 ft. This damage zone which consists of fractured host rock, non-foliated cataclasite and foliated cataclasite is evidence of the damage from the seismic activity in the North Abeyta Creek fault. Fig. 6.2a shows the wellbore diagram[205] and Fig. 6.2b the bulk density log[206] at a depth of 6700 ft to 6800 ft. The red arrow on Fig. 6.2b signals the abrupt change in bulk density which is evidence of damage caused by the nearby fault.

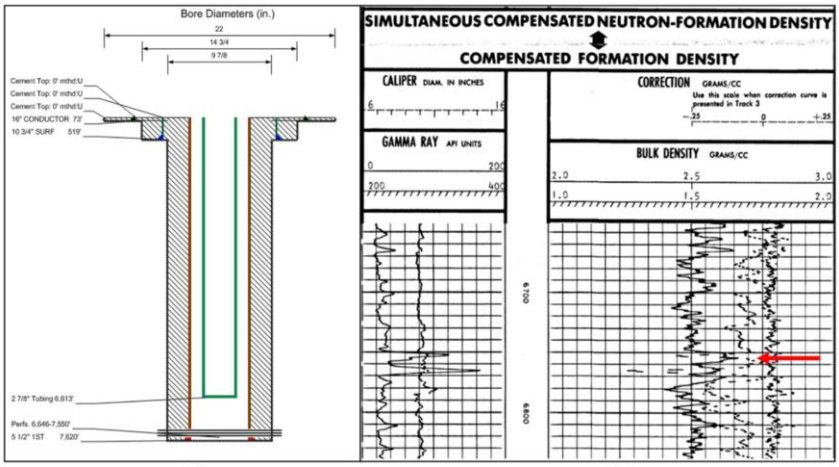

Figure 6.2 (a) Well completion diagram, from Dike Mountain Unit #7-7.[2] (rb) Simultaneous compensated neutron-formation density log at 6700 feet depth.[3]

Fig. 6.3a illustrates the U.S. Geological Survey (USGS) 250K geologic map[207] and Fig. 6.3b shows much higher resolution geologic map (48K)[208] of the same area.

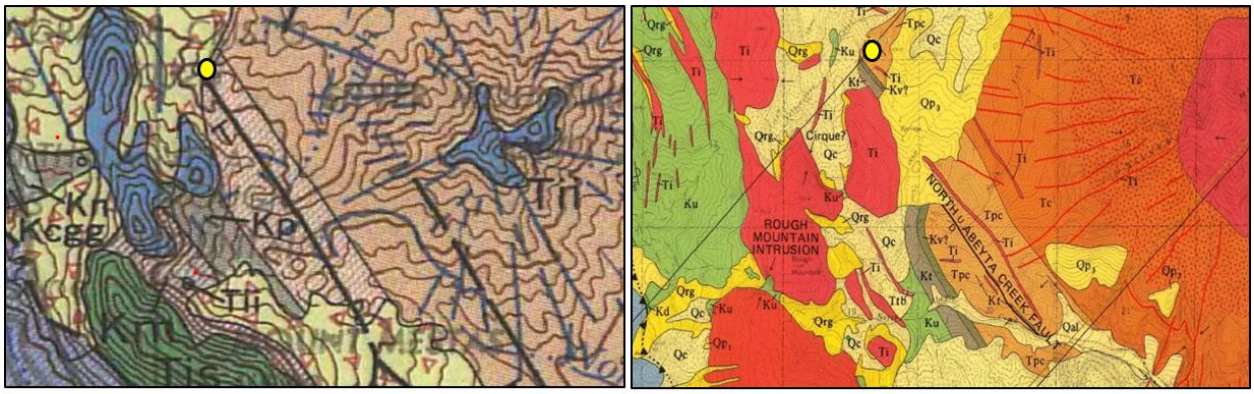

Figure 6.3 (a) Geologic map from the USGS (1969) with yellow well markers as geographically referenced by the Colorado Oil & Gas Information System

Public records.

[2] Colorado Oil and Gas Information System. (1996). Well Information [Wellbore Completion Diagram]. Retrieved from https://cogcc.state.co.us/cogisdb/Facility/FacilityDetail?api=0550604.

[3] Colorado Oil and Gas Information System. (1996). Well Information [Neutron Log]. Retrieved from https://cogcc.state.co.us/cogisdb/Facility/FacilityDetail?api=0550604.

(COGIS). [4](b) Higher resolution geology map of the Raton Basin (USGS, 1974). [5]Thick black lines in both maps show the North Abeyta Creek fault. Well location shown as yellow dot.

Using these geologic maps and a 1/3 arc second digital elevation model, a three-dimensional model was produced to demonstrate the exact location of the well and adjacent formation layers. This 3D model was developed by utilizing georeferenced geological maps with cross section lines and digitized well logs, strikes and dips through a geological modelling software, MOVE[209]. Dike Mountain Unit #7-3 was plotted by several well information from Table 6.1 and the well plotting feature in MOVE™. Fig. 6.4 shows the Dike Mountain Unit #7-7 depth and the drilled-through horizons.

Public records.

[4] United States Geological Survey. *Geologic map of the Trinidad quadrangle, south-central Colorado* [map]. Miscellaneous Investigations Series Map I-558. Reston, Va: U.S. Department of the Interior, 1969.

[5] United States Geological Survey. *Geologic map and cross sections of the La Veta Pass, La Veta, and Ritter Arroyo quadrangles, Huerfano and Costilla Counties, Colorado* [map]. Miscellaneous Investigations Series Map I-833. Reston, Va: U.S. Department of the Interior, 1974.

Table 6.1 Three-dimensional basin model inputs and parameters.

Well Information	Well data
Location	SWSE 7 28S69W 6
Elevation	8710 ft
Latitude	37.622
Longitude	-105.149
Perforation range	6646 ft – 7550 ft
Formation	**Log top**
Niobrara	5202 ft
Fort Hays	6058 ft
Codell	6118 ft
Greenhorn	6329 ft
Graneros	6493 ft
Dakota	6604 ft
Morrison	6852 ft
Entrada	7395 ft

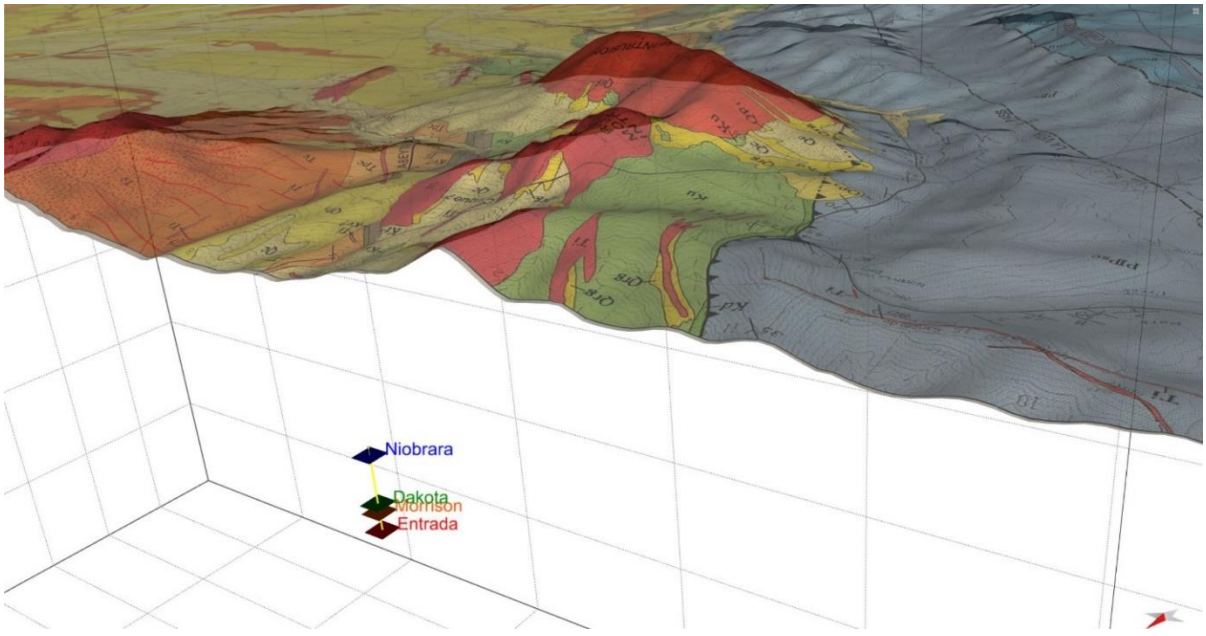

Figure 6.4 Three-dimensional model of well location in the Raton Basin.

Experimental Procedure and Methodology

The probability of inducing seismicity at the Raton Basin though gel injections is very high due to it being already an active faulting zone and its decades-long history of wastewater

injection. Ultimately, it is not a matter of if induced seismicity will occur but at what range of the angles of frictional sliding will failure happen. First, the viscosity of the CO_2-SPAM was measured through a series of rheological tests. Secondly, the pore pressure at the fault was calculated based on the measured viscosities and transient solution for radial flow near a sealing fault. Additionally, geological reports, core analyses and well data were used to calculate the overburden stress (S_v) while the least principal stress was calculated based on the frictional faulting criterion. This stress study was then used to plot the Mohr circles and Frictional Failure Envelopes and calculate the range of angles at which fault activation and reactivation may occur.

Materials

The materials needed to create the CO_2-SPAM are polyacrylamide (Nonionic water-soluble polymer, MW $5x10^6$ – $6x10^6$) provided by Sigma-Aldrich, methenamine (USP, 99-100.5%, MW 140.19), resorcinol (Crystalline powder, USP, 99-100.5%, MW 110.11), sodium chloride (MW 58.44) supplied by Spectrum™, and water (Deionized, extra pure, MW 18.015) supplied by Thermo Scientific™.

Instrumentation

The Discovery Hybrid Rheometer (Discovery HR-2) with a stainless steel 20mm parallel plate geometry (Peltier plate) was utilized to perform a flow sweep on the gel solution to determine its viscosity in an aqueous solution.

CO_2-SPAM's Aqueous Solution Preparation

Two 100 mL solutions were prepared by mixing NaCl brine solution at 150,000 ppm with 0.1 wt% of resorcinol and 0.4 wt% of methenamine, and 1.0 wt% and 1.5 wt% of polyacrylamide as seen on Table 6.2.

Table 6.2 CO_2-SPAM sample composition.

Sample #	Methenamine wt%	Resorcinol wt%	PAM wt%	Salt concentration (ppm)
1	0.4	0.1	1.0	150,000
2	0.4	0.1	1.5	150,000

Firstly, 100 mL of brine was poured into a conical flask and heated to 90°C in a magnetic stirring hotplate. After the desired temperature was reached, methenamine was added into the solution and stirred at 550 rpm until complete dissolution. Resorcinol was later added to the mixture and stirred until fully dissolved. Lastly, polyacrylamide was mixed into the solution following resorcinol's dissolution and stirred for one hour at ambient pressure. After an hour, the solution was fully dissolved and ready for testing as seen in Fig. 6.5.

Figure 6.5 CO_2-SPAM solution at 1.5 wt% PAM concentration.

CO_2-SPAM Solution Rheological Study

Rheological studies are often used to characterize fluids or soft materials and their response to an applied force. A viscosity vs. shear rate study, also known as flow sweep, is performed on two samples of CO_2-SPAM using an oscillatory rheometer. The influence of shear

rate is investigated on the solution's viscosity at rates ranging from 0.01 sec^{-1} to 2500 sec^{-1} through a flow sweep procedure.

It is known that polyacrylamide exhibits non-Newtonian (shear thinning) properties[210–212] at high shear rates and as a result, a shear rate representative of normal reservoir conditions will be selected based on an effective shear rate model developed by Eberhard et al. (2019). During subsurface injection processes, the solution travels through the pore space in the rock formation at a specified flow rate, therefore; the shear rate is highly dependent on the volume of the targeted area, rock porosity and rock permeability.

Pore Pressure Calculation

It is assumed that the North Abeyta Creek fault is a sealing fault, i.e., it does not allow hydraulic communication through and across it. This assumption leads to a higher estimate for pore pressure at the fault, which results in a conservative recommendation for the allowable injection rate. In a homogeneous system, pore pressure at a sealing fault may be determined by the line source solution for radial transient flow and the principle of superposition in space. In this method, a sealing fault may be represented by an image well. The image well is the mirror image of the main well (i.e., same production rate, same well characteristics, and same distance from the fault). For the resulting two-well system in an infinite-acting reservoir an analytical solution exists that expresses the pore pressure at the fault as a function of other system properties (Eq. 6.1).

$$P_f = P_i - 2\left(70.6\frac{\mu B}{kh}qE_i\left(-948\frac{\varphi\mu c_t r_f^2}{kt}\right)\right) \tag{6.1}$$

P_f is the pore pressure at the fault (psia), P_i is the initial pore pressure (psia), ϕ is the rock porosity, μ is the viscosity of injected fluid (cP), B is the fluid's formation volume factor in reservoir barrels per standard barrels (RB/STB), k is the rock's permeability in millidarcies (mD), h is the thickness of the reservoir layer (ft), q is the fluid's injection rate (STB/day), E_i is the exponential integral function, c_t is the total compressibility (psi^{-1}), r_f is the distance between the well and the fault (ft), r_w is the wellbore radius, is the and t is time (hr). The fluid's injection rate is calculated based on the volume of the targeted zone, the rock's porosity, oil saturation, and time of injection.

$$q = \frac{4.274(\pi r_s^2 h)\varphi(1 - S_o)}{t} \tag{6.2}$$

Where r_s is the radius of the intended sealed. Substitution of Eq. 6.1 into Eq. 6.2, results in:

$$P_f = P_i - 2\left(301.8\frac{\mu B\pi r_s^2 \varphi(1 - S_o)}{kt}E_i\left(-948\frac{\varphi\mu c_t r_f^2}{kt}\right)\right) \tag{6.3}$$

E_i is the exponential integral function defined as:

$$Ei(-x) = -\int_x^{\infty} \frac{e^{-y}}{y}dy \tag{6.4}$$

In this study, an approximation of the exponential integral function from Kizilkan and Dincer[213] is used to simplify the calculations for the special analytical function on the complex plane.[214,215]

For $0 < x < 1$

$$Ei(x) = ln\,(x) + 0.57721566 - 0.99999193x + 0.24991055x^2 - 0.05519968x^3 + 0.00976004x^4 - 0.00107857x^5 \tag{6.5}$$

For x > 1

$$Ei(x) = -\frac{A}{Bxexp(x)} \tag{6.6}$$

Where,

$$A = x^4 + 8.5733287x^3 + 18.059017x^2 + 8.637609x + 0.2677737 \tag{6.7}$$

and,

$$B = x^4 + 9.5733223x^3 + 25.6329561x^2 + 21.0996531x + 3.9684969 \tag{6.8}$$

According to our findings and other reports[216–218], the CO_2-SPAM solution is a non-Newtonian (shear-thinning) fluid. However, for calculating the possible maximum pore pressure at the fault, Newtonian behavior is assumed. In this approach, the range of viscosities is first calculated for the range of shear rates encountered between r = r_w and r = r_f. Next, Eq. (6.3) is used for each viscosity in this range and the corresponding pore pressure at the fault is calculated. Consequently, a range of pore pressures at the fault is obtained to find the lower and upper limits of pore pressure at the fault without finding the exact amount of pore pressure at the fault (as it entails complicated numerical solution to the non-Newtonian flow equations). This approach provides the maximum pore pressure at the fault which is a conservative estimate for investigating the worst-case scenario in terms of fault activation.

First, the power law correlation between the viscosity and shear rate is observed (Eq. 6.9):

$$\mu(\dot{\gamma}) = K\dot{\gamma}^{n-1} \tag{6.9}$$

Where μ is the fluid's viscosity as a function of shear rate (Pa.s), $\dot{\gamma}$ is the shear rate (sec^{-1}), K is the viscosity at $\dot{\gamma} = 1\ sec^{-1}$ and n is the power-law index.[218] This expression is obtained empirically from the flow sweep test.

Based on Cannella et al.'s findings[219], effective shear rate in porous media is expressed as:

$$\dot{\gamma}_{eff} = C\left(\frac{3n+1}{4n}\right)^{\frac{n}{n-1}} \frac{4v}{\sqrt{8\kappa\varphi}} \tag{6.10}$$

Where v is Darcy velocity (m/s), and κ is rock permeability (m^2). Cannella et al.[218,219] discovered the constant C = 6 to be able to describe a great variety of flows in different settings.

At a constant injection rate, Darcy velocity (m/s), and consequently, effective shear rate become functions of the distance to the wellbore (r):

$$v = (1.978 * 10^{-5})\frac{q}{2\pi r h} \tag{6.11}$$

$$\dot{\gamma}_{eff} = C\left(\frac{3n+1}{4n}\right)^{\frac{n}{n-1}} \frac{(7.91 * 10^{-5})q}{\pi r h\sqrt{8\kappa\varphi}} \tag{6.12}$$

Hence, the viscosity varies with the distance to the wellbore and minimum viscosity occurs at the wellbore sand face. The range of viscosity variation for the injection rate is obtained and the resulting range of pore pressures at the fault is calculated using Eq. (6.3) and parameters listed in Table 6.3. The maximum pressure at the fault is selected from this range for the fault activation study.

Table 6.3 Parameters at Dike Mountain Unit #7-7.

Distance from wellbore to fault	80 meters
Radius of the sealed zone	262.47 ft
Thickness of gel layer	5 ft
Formation volume factor	1.0 RB/STB
Injection time	30 days
Rock porosity	0.0867
Rock Permeability	0.04 mD
Oil Saturation	0.204
Total Compressibility	6.39×10^{-6} $psia^{-1}$

Stress Calculations

In normal faulting regimes, the vertical stress, Sv, is the maximum principal stress while S_{hmin} is the least horizontal principal stress. The vertical stress is determined by either integrating the rock densities ρ(z) from the surface to depth, or the mean overburden density $\bar{\rho}$.

$$S_v = \int_0^z \rho(z) g dz \approx \bar{\rho} g z \tag{6.13}$$

Where ρ is rock density (kg/m3), g is standard acceleration of gravity (m/s^2), and z is thickness of rock layer (m). The density log, obtained from the Colorado Oil and Gas Information System's (COGIS) database, provides continuous record of the rock formation's bulk density along the length of the borehole, which is used to calculate the overburden stress as a function of depth. S_{hmin} is calculated using the Frictional Faulting Theory for a normal faulting zone described in Eq. 6.15.

Frictional Faulting Theory

The Earth's crust exists at failure equilibrium or a constant state of being just on the edge of failure, which indicates that any sudden change or perturbation in the stress regime or pore pressure can activate quiescent faults[220]. Seismic activity is caused by the sudden movement or

rupture along a fault plane and raising pore pressure tends to de-stabilize faults and encourage slip.[220] This phenomenon is explained by the Frictional Failure Criterion (FFC). FFC, is commonly used to determine fault sliding:

$$\tau = \hat{\mu}\sigma_n \tag{6.14}$$

Where $\hat{\mu}$ is the coefficient of sliding friction, and τ and σ_n are the shear and normal stresses necessary to cause fault slip. Fault activation in existing faults is normally caused by frictional sliding along the plane of failure. Frictional sliding is controlled by the shear and normal stress on the fault plane. In other words, fault sliding happens when the ratio between shear stress and normal stress is equal or greater than the coefficient of sliding friction. Therefore, under high shear stress and low normal stress, fault sliding is expected.

In practice, effective normal stress (σ_n) is the result of the normal stress minus the pore pressure. By allowing a fluid in the faulting plane, the fluid will exert a force against the normal stress and decrease the effective stress (the stress pinning the fault closed). Correspondingly, the injection of CO_2-SPAM into the Raton Basin near a fault increases the pore pressure at the fault and may lead to fault slip. A coefficient of sliding friction, $\hat{\mu}$, equal to 0.6 was used to analyze fault slip due to the injection of CO_2-SPAM[221]. A choice of $\hat{\mu}$ = 0.6 is a conservative estimate based on Byerlee's and Townsend and Zoback's maximum friction studies[221,222]. The frictional faulting criterion will be used to determine S_{hmin}. For a normal faulting zone, the frictional faulting theory is a follow:

$$\frac{\sigma_1}{\sigma_2} = \frac{S_v - P_f}{S_{hmin} - P_f} = [\sqrt{\hat{\mu}^2 + 1} + \hat{\mu}]^2 \qquad where\ \hat{\mu} = 0.6 \tag{6.15}$$

By plotting Mohr circles based on the FFC, it is assumed that faulting is happening at some angle. Alpha (α) is the angle between the plane of failure and the maximum principal stress while the angle of frictional sliding (dipping plane) is denoted as Beta (β). These angles are highly dependent on the orientation of the planes and the principal stress as seen in Fig. 6.6. In the final stress studies, two Mohr circles are plotted where one diagram does not consider the effects of pore pressure and the other one subtracts pore pressure from the principal stresses. These scenarios depict how the Mohr circle will shift to the left and cross the Frictional Failure Envelope. As pore pressure increases and the Mohr circle crosses the failure envelope, a range of angles will demonstrate the variety of orientations a plane of failure has to be to become activated and slip.

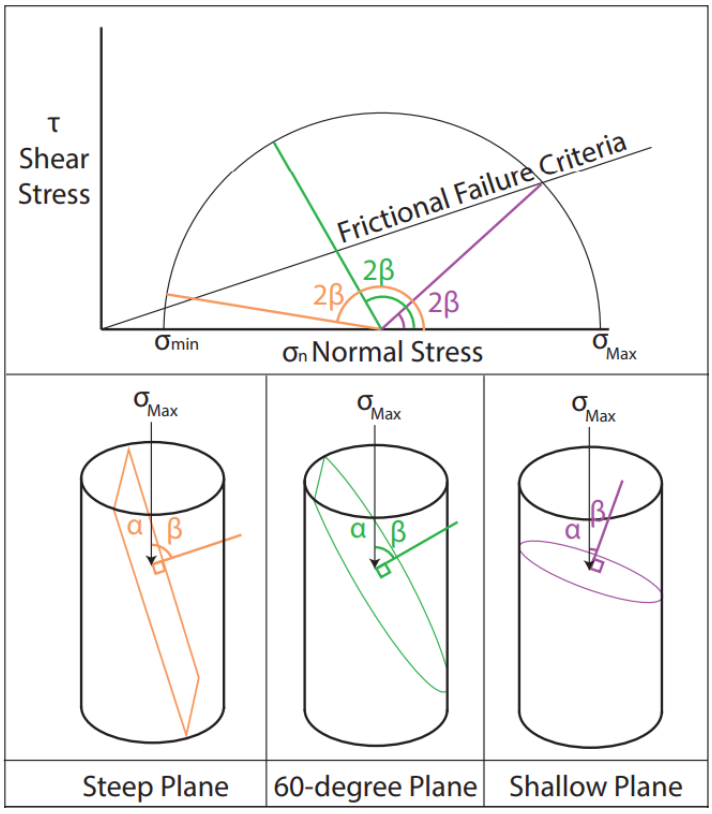

Figure 6.6 Mohr diagram corresponding to faulting at different angles, 90 - α = β

Results and Discussions

Polyacrylamide solution demonstrated non-Newtonian fluid behavior as increasing shear stress was applied to the samples. Fig. 6.7 demonstrates the pseudoplastic relationship between viscosity and shear rate of aqueous CO_2-SPAM at 1.0 wt% and 1.5 wt%. Both PAM samples experience a decrease in viscosity as shear rate increases. This can be explained by a phenomenon called "entanglement of polymer chains." This phenomenon causes a disentanglement of polymer chains as shear rate increases.[223,224] The increase of movement or flow keeps the polymer from orienting at random and entangling at rest[223]. As expected, higher weight percent of polyacrylamide exhibited higher viscosity than lower weight percent PAM sample because of the increase in the molecules' intermolecular attractions and strong hydrogen bonding that ultimately leads to resistance to flow.[225] The power law model for both PAM concentrations is obtained and will further be used to calculate the effective shear rate.

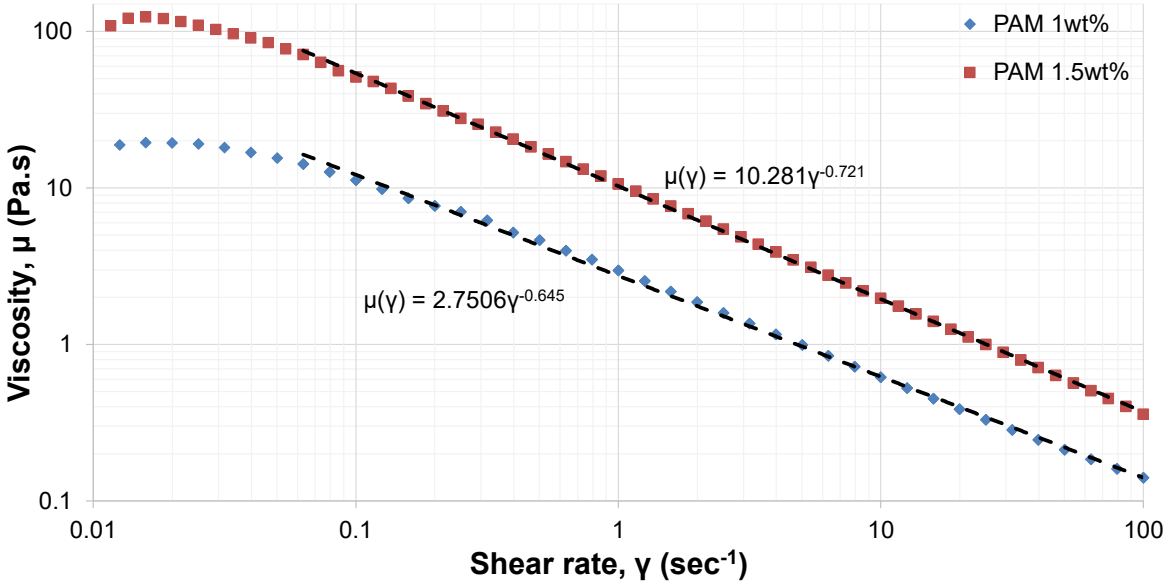

Figure 6.7 Viscosity vs. shear rate study on polyacrylamide with a concentration of 1.0 wt% and 1.5 wt%.

The pseudoplastic behavior can also be appreciated in Fig. 6.8. Here, the change in viscosity and shear rate are identified as the gel solution travels from the well to the fault. High shear rates near wellbore results in low gel viscosity near the wellbore. As the gel travels radially away from the wellbore, the shear rate decreases and viscosity increases.

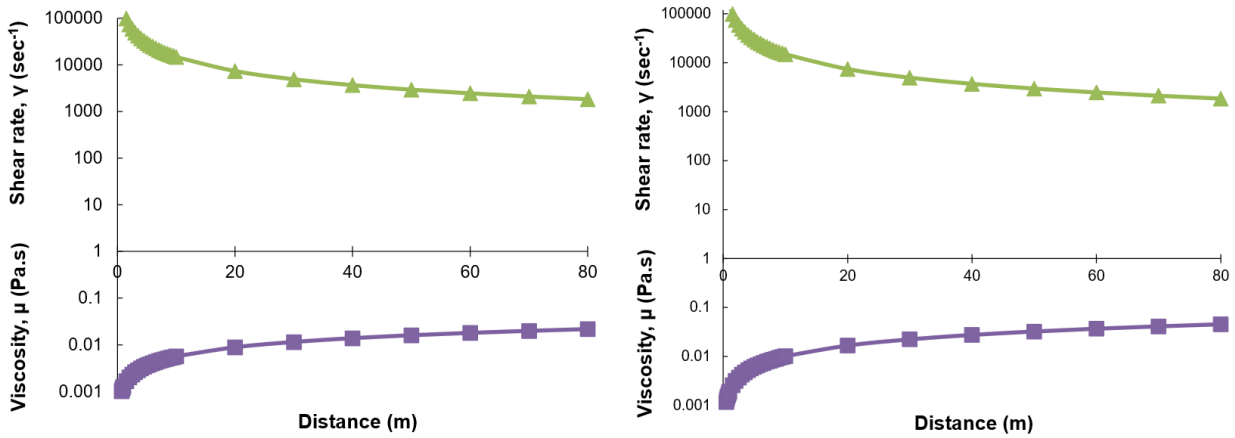

Figure 6.8 Shear rate and viscosity as a function of distance from wellbore to fault for (a) CO_2-SPAM at 1.0 wt% and (b) CO_2-SPAM at 1.5 wt%.

Pore Pressure at the Fault

At a depth of approximately ~6754 ft, the maximum pore pressure at the fault (P_f) calculated for 1.0 wt% and 1.5 wt% CO_2-SPAM solutions are 4,543 psi and 3,135 psi respectively as seen in Fig. 6.9. Viscosity increases as it flows radially and shear rate decreases; therefore, the pore pressure profile below illustrates the maximum pore pressure that will be experienced at a depth of 6754 ft. The increase in pore pressure will induce seismicity in the Raton Basin but, the range of angle of frictional sliding, or dipping plane angle, will define what planes will be affected or safe from reactivation.

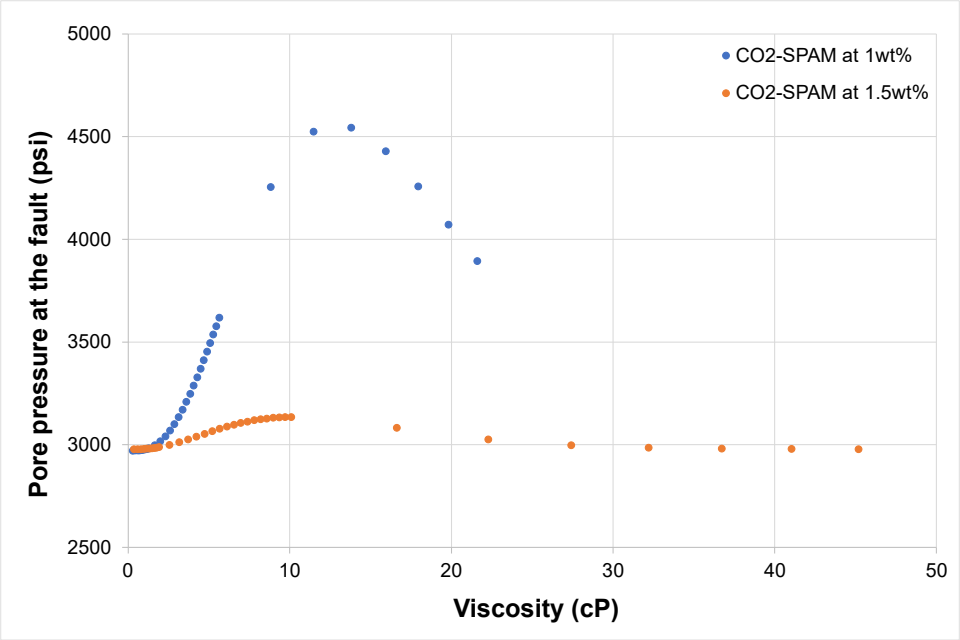

Figure 6.9 Pore pressure profile as a function of viscosity and radius.

Mohr Circle – Stress Analysis

The Mohr circle is a two-dimensional graphical tool that illustrates the normal and shear stresses causing failure along a plane at a certain orientation to σ_1.[220] These diagrams help illustrate the magnitude of the principal stresses at depth where all stresses are assumed to be compressive.[220] As mentioned before, this study is based on a normal faulting regime and all stress calculations are based the vertical (overburden) stress S_v, and the least horizontal stress S_{hmin}. The vertical stress and the least horizontal stresses were calculated using Eq. 6.13 and 6.15, which assume that faulting is happening at a single angle (usually 30° to the maximum principal stress). As pore pressure is applied, the stresses (S_n) become effective stresses (σ_n) and are plotted as a new Mohr circle. Eq. 6.16 shows the effective stress formula.

$$\sigma_1 = S_1 - P_p \tag{6.16}$$

There are two fractions to understanding pore pressure stress coupling. Fraction A discusses how rocks at failure equilibrium can only fail when the Mohr circle meets the failure envelope and no additional failure can be indicated (extending past the failure envelope) because the tangent point between the Mohr circle and the failure envelope specifies exactly where does failure occur.[220] A conventional triaxial strength tests on sandstone and limestone was performed by Handin et al. (1963)[226] and the strength tests data was used to find the dependence of rock strength on confining pressure in the absence of pore pressure using the strength at failure (S_1) as a function of confining pressure (S_3) as seen in Eq. 6.17.

$$S_1 = C_o + nS_3 \tag{6.17}$$

Where C_o in cohesion and n is the slope of the failure line. To take pore pressure into account, the total stresses will be replaced by the effective stresses and the rearranged equation reflects the strength of the rock as a function on the simple form of effective stress (see Eq. 6.18).

$$S_1 - S_3 = C_o + (1 - n)P_p - (1 - n)S_3 \tag{6.18}$$

Where S_1-S_3 is the differential stress (also referred to as the width of the Mohr circle and Pp is pore pressure. Their results showed that the effect of pore pressure on rock strength is described by the Terzaghi form of the effective stress.[227] Terzaghi (1943) demonstrated that the rock strength of saturated rock is controlled by the effective stress.[227] Handin et al. (1963) plotted the differential pressure ($S_1 – S_3$) against Pp, and their results indicated that as pore pressure increases, the differential stress decreases.[226] This means that when fluid is injected into the subsurface, pore pressure increases and slides the Mohr circle to the left but also decreases the width of the circle. Fraction B, which is used in this study, focuses on how pore pressure slides

the Mohr circle to the left and rock failure can be seen at a wider range of angles. Many fault angles are observed to be active in basins; therefore, knowing which faults could be reactivated is important.

Fig. 6.10 illustrates the effect of pore pressure on the stress distribution at a depth of approximately 6753.5 ft. The red Mohr Circle (labelled 'No Pore Pressure') indicates the stress distribution when pore pressure is not being applied. In this scenario, the Mohr circle touched the failure envelope ($\tau = 0.6004\sigma$) at one angle. When pore pressure taken into consideration and is reduced from the principal stresses, the Mohr circle shifts to the left (labelled 'With Pore Pressure') and crosses the failure envelope. The new stress distribution demonstrates an array of new angle ($2\alpha = 151°$) at which the failure will occur for CO_2-SPAM solution of 1.0 wt%.

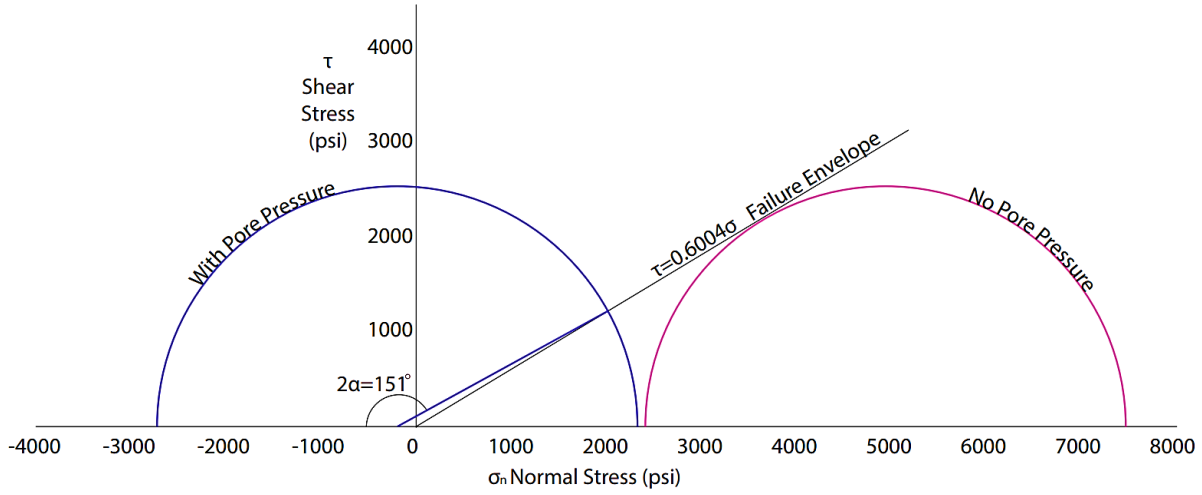

Figure 6.10 Mohr Circle stress distribution from pore pressure influence caused by CO_2-SPAM at 1.0 wt% injection at ~6753.5 ft depth.

At approximately 6753.5 ft, vertical fault planes (very steep plane) up to planes dipping at 14.5° are expected to activate. CO_2-SPAM at 1.5 wt% demonstrates very similar behavior in

the stress distribution as seen in Fig. 6.11. The range of angle between plane of failure and vertical stress indicates that failure is expected in vertical planes and dipping planes up to 27.5°.

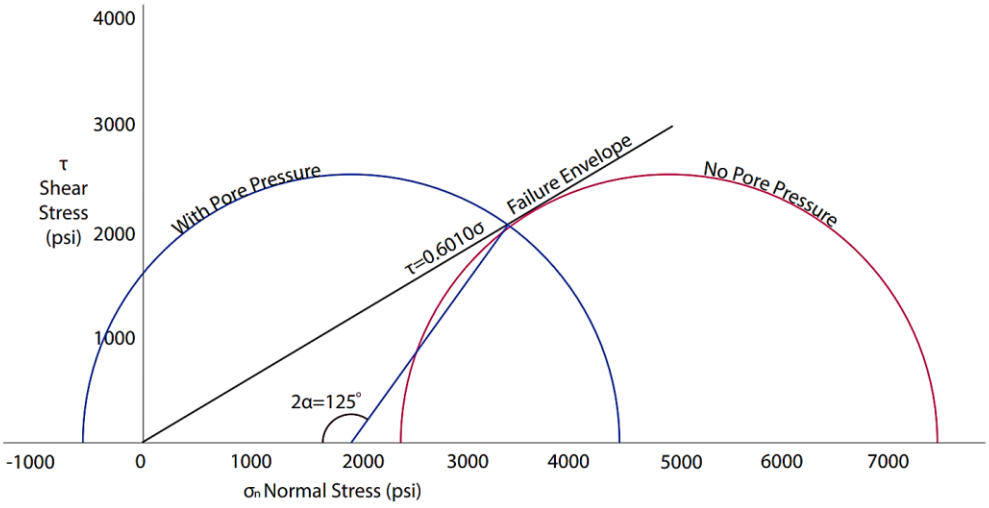

Figure 6.11 Mohr Circle stress distribution from pore pressure influence caused by CO_2-SPAM at 1.5 wt% injection at ~6753.5 ft depth.

The range of angles at which the fault can slip has increased significantly as pore pressure is increased. Additionally, the dipping angles from CO_2-SPAM at 1.0 wt% and 1.5 wt% were close due to the similar range of 2α angles. Fig. 6.12 shows a clear schematic of the wide range of angles for frictional sliding where the fault slip will occur. In other words, only extremely shallow dipping faults are safe from reactivations. Thrust faults have a shallow dipping plane and are the only planes that will not fail in this scenario.

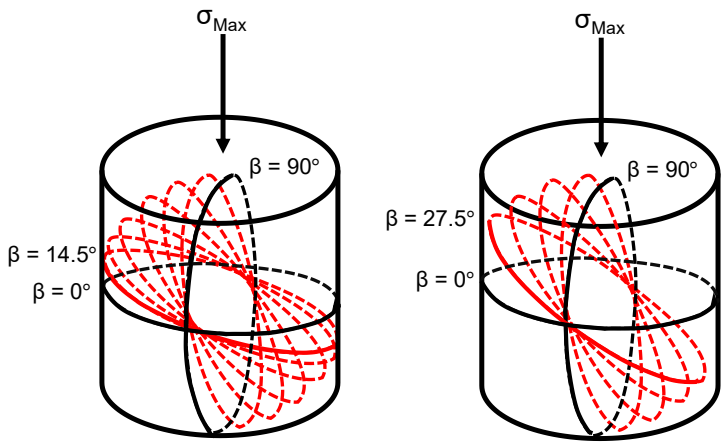

Figure 6.12 Schematic of the range of dipping angles prone to slippage by the injection of CO_2-SPAM at (a) 1.0 wt% and (b) 1.5 wt%. Not draw to scale.

Non-Active Faulting Zone Potential Activation from Pore Pressure Incrementation

As previously mentioned, the Raton Basin is in fact a very active zone with recent seismic activity caused by current wastewater injections. This scenario is very common because the Earth is at a constant state of failure equilibrium. This mean that any small change in pressure will affect the stress state in the subsurface and lead to failure. Nevertheless, there are situations where existing faults are not active and would need a significant change in pore pressure to reactive the fault. In this scenario, a normal non-active faulting zone will be used to derive an expression for the pore pressure necessary to induce faulting. Firstly, the least principal stress (S_{hmin}) will need to be measured though different testing methods (e.g., leak-off tests). A non-active faulting zone is represented in Fig. 6.13.

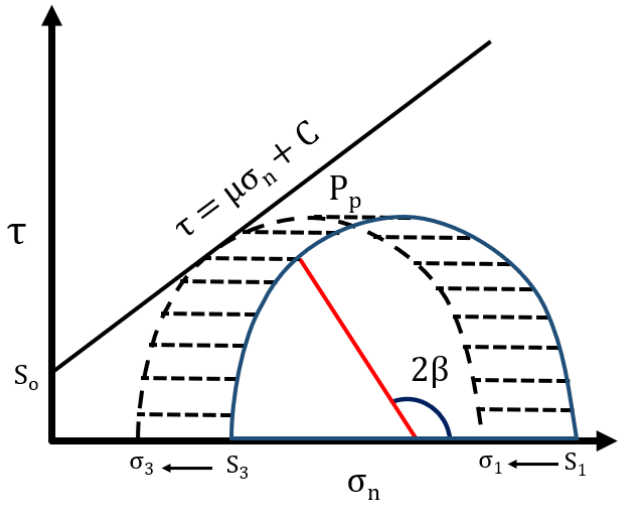

Figure 6.13 Mohr circle shift influenced by increased pore pressure.

Note that because this zone is intact, cohesion is non-zero and the failure envelope passes through the shear axis above the origin. This failure envelope is referred to as the Mohr Coulomb Failure Envelope. Pore pressure is deducted from the principal stress magnitudes (S_1 and S_3) to show the effective stresses (σ_1 and σ_3). To find the point at which the Mohr circle touches the Mohr Coulomb Failure Envelope, the normal stress and shear stress at failure expression is utilized.[228]

$$\tau = (\sigma_1 - \sigma_3)\frac{sin2\beta}{2} \tag{6.19}$$

$$\sigma_n = \left(\frac{\sigma_1 + \sigma_3}{2}\right) + cos2\beta\left(\frac{\sigma_1 - \sigma_3}{2}\right) \tag{6.20}$$

In most cases it can be assumed that $2\theta = 120°$ because normal faults are expected to form in conjugate pairs that dip approximately 60° and strike parallel to the direction of S_{Hmax}.[220]

Additionally, Anderson et al. (1951) had established the idea that rocks normally fail at 30° to σ1; therefore, θ = 60°. Eq. 6.19 and 6.20 can be further simplified to:

$$\tau = 0.2903(S_v - S_{hmin}) \tag{6.21}$$

$$\sigma_n = \left(\frac{S_v + S_{hmin}}{2}\right) + 0.8142\left(\frac{S_v - S_{hmin}}{2}\right) - P_p \tag{6.22}$$

For failure to happen the y-value (shear stress) does not change but normal stress is reduced by pore pressure. Additionally, the Mohr Coulomb Failure Criterion can be substituted for σ_n.

$$\frac{\tau - C}{\mu} = \left(\frac{S_v + S_{hmin}}{2}\right) + 0.8142\left(\frac{S_v - S_{hmin}}{2}\right) - P_p \tag{6.23}$$

Eq. 6.20 represents the normal effective stress at failure. Let C = 0 because cohesion strength is very low compared to the stresses typically necessary to induce failure, μ = 0.6 because of extensive relevant data that point to 0.6 as the best fit for coefficient of friction for most materials (also known as Byerlee's law).[220,221]

$$\frac{\tau}{0.6} = \left(\frac{S_v + S_{hmin}}{2}\right) + 0.8142\left(\frac{S_v - S_{hmin}}{2}\right) - P_p \tag{6.24}$$

Shear stress (Eq. 6.21) can now be substituted into Eq. 6.24 and further simplification leads to the development of a new criterion for normal faulting zones.

$$P_p = 0.5(S_v + S_{hmin}) - 0.0768(S_v - S_{hmin}) \tag{6.25}$$

Eq. 6.25 is a novel and original equation derived from the shear stress and effective normal stress on the fault that forms during the failure process in terms of the applied effective principal stresses. This is a relationship between the maximum principal stress, the least principal stress, and pore pressure from fluid injection. If pore pressure Pp is equal or greater than the right-hand side of this equation, in a normal faulting zone, the fault will be reactivated, and induced seismicity will occur. Eq. 6.25 can be called the Quan-Crane Criterion. This equation can be utilized of predict anthropogenic seismicity in normal faulting zone when geological stress values are provided from well data. Dike Mountain Unit #7-7 lacked stress studies and no values of the least principal horizontal stress in the area were recorded but based on the results of our stress analysis, induced seismicity is projected to occur.

Conclusions

Global warming and its ripple effects across the globe has kick-started several initiatives that have resulted in new and innovative GHG technologies. Carbon capture and storage has a great potential to take on the task of alleviating the excess CO_2 from emitting power plants. Limitations to CCS arise when the geological storage sites are compromised by leakage pathways that serve as escape routes. Sealing agents such as CO_2-sensitive polyacrylamide may play a role in the sustainability of CO_2 storage. The injection of sealing agents into the CO_2 storing site, however, might induce seismic activity; therefore, further stress analyses must be performed to understand the extent of fault activation. In this study, a formerly gas-producing well located in a normal faulting zone in the Raton Basin was used as the basis of our induced seismicity study. The well ‘Dike Mountain Unit #7-7’ is in close proximity to the North Abeyta Creek Fault which cuts through the Dakota formation. Pore pressure was calculated based on conventional core analysis results and the image well technique. The effect of pore pressure on

geological stresses was captured through the stress distribution represented by Mohr circles. The Frictional Faulting Criterion was utilized on the Raton Basin and based on the stress distribution caused by the gel solution injection. It was found that the increase in pore pressure from gel solution injection will cause fault slip at all angles ranging from vertical fractured plane to planes dipping 14.5 and 27.5° for a CO_2-SPAM concentration of 1.0 wt% and 1.5 wt%, respectively.

Based on these results, CO_2-SPAM with a PAM concentration of 1.5 wt% would be more ideal candidate for injection because of the larger number of dipping angles that are safe from reactivation compared to CO_2-SPAM at 1.0 wt% as illustrated in Fig. 6.12. In conclusion, only very shallow dipping faults, such as thrust faults, will not be activated and are safe from fault slip.

CHAPTER VII

CONCLUSIONS AND RECOMMENDATIONS

Conclusions

The main focus of this research lies in the advancement of the knowledge in GHG technologies, specifically carbon capture and storage. Exploring new methods and technologies to remediate CO_2 leakage is imperative for future applications and successful storage. Chapter 3 discussed which CO_2-sensitive chemicals have the potential to mitigate CO_2 leakage in subsurface formations. Gel, precipitated minerals, microgels and resins demonstrate advantages and limitations to their usage for CCS applications. Fast precipitation of minerals is desirable to seal leakage pathways, but additional studies are required in regards the resistance of these minerals to weak acids for long periods of time. Resins are great alternatives because of their resistance to weak acids and high concentrations of salt. However, resins are difficult and costly to inject, and their subsurface flow and mobility is questionable. Gel and microgels are agile blocking agents that have proven to be thermally resistant and salt tolerant. Specifically, CO_2-sensitive polyacrylamide is the suitable compound for CCS applications because it is cost effective, does not require an intensive synthesis, is commercially available, and most importantly, has been proven to efficiently block porous leakage pathways.

CO_2-sensitive polyacrylamide is a gel system that consists of methenamine, resorcinol and polyacrylamide. Under high temperatures and an acidic environment (pH = 5.5) methenamine decomposes into formaldehyde and ammonia when water is introduced to the

system. The formaldehyde further reacts with the resorcinol and forms hydroxymethyl group and ultimately forms phenolic resin. Formaldehyde also further reacts with polyacrylamide through polycondensation. Finally, the phenolic resin will further react with the polyacrylamide through deeper polycondensation and create the gel. CO_2 at reservoir conditions provide the necessary environment for CO_2-sensitive polyacrylamide to form it into a deformable non-flowing gel.

As mentioned before, reservoir-like conditions with the addition of CO_2 create the appropriate environment for the gel to form, but the subsurface also contains harsh substances that can possibly affect the gel's gelation time, strength, and viscosity. Salinity varies amongst formations and regions; therefore, understanding its impact is crucial. Based on the studies performed in Chapter 5, salt has a retarding effect on gelation time. High concentrations of salt in the solution elongate the gelation time. There are several explanations to this phenomenon which include the decrease in the dielectric constant and reduction of energy from hydrogen bonds as salt content is increased. The electrostatic repulsion of the polymer chain is affected by the excess metal ions in the solution which causes the molecular chains to curl and shrink. In other words, the negatively charged carboxylate group's interaction with the dissolved metal ions ultimately decreases the hydrodynamic volume of the polymer and decreases viscosity. Also, the shrinking and curling of the polymer chain tightens the micro-network structure of the gel which is covered by a layer of salt crystals. This interaction prevents the polymer from developing faster and therefore increases the gelation time. Lastly, it is also believed that the thickness of the electric double layer decreases as salt concentration increases which negatively affects the formation of an ordered structure and decreases the viscosity. Additionally, Chapter 5 also focuses on the effects of PAM concentrations on gelation time which is quite the opposite from salinity. It was found that gelation time, viscosity, and gel strength increase as PAM

concentration increases. Viscosity and gel strength increase as PAM concentration increases because higher polymer concentration results in a denser structure and higher cross-linking density. Also, the increase in viscosity is caused by the increase in drag force exerted by larger polymer molecules and the extensive network formed. Moreover, gelation time decreases because as PAM concentration increases, so does the number of accessible sites for cross-linking, which in turn accelerates cross-linking reaction and, hence, speeds up the gel formation.

Finally, CO_2-SPAM is intended to be injected into the subsurface as an aqueous solution to seal leakage pathways after CO_2 injection. Fluid injection into the subsurface has the potential to induce seismicity as it has been recorded in the past with wastewater injections. Chapter 6 demonstrates that CO_2-SPAM will induce seismicity in a normal faulting zone in the Raton basin at various angles in plane of failure. It was found that the injection of CO_2-SPAM at PAM concentration of 1.0 wt% and 1.5 wt %, will increase the pore pressure enough to activate any faults with fracture planes dipping 14.5° and 27.5° to 90°, respectively. This means that very shallow dipping planes are safe from fault activation and fault slip. Additionally, other scenarios were taken into consideration to properly evaluate the necessary pore pressure to activate a non-active faulting zone. A new equation was derived from the Mohr Coulomb Failure Envelope equation in addition to the expression for normal stress and shear stress at failure. The Quan-Crane Criterion establishes the relationship between the pore pressure needed from fluid injection to the maximum principal stress and least principal stress in the region. If the relationship is true in a normal faulting zone, then the fault will be reactivated, and seismic activity is expected. This is an issue when CCS efforts are undertaken in populated areas.

Recommendations

This dissertation has demonstrated that an in depth understanding of CO_2-SPAM's synthesis, rheological behavior and influence on geomechanical stresses due to its injection into subsurface formations is critical to the future applications of GHG technologies. The framework and findings in this dissertation will enable further expansion of the present knowledge of CO_2-sensitive chemicals and their role in real-life applications. As CCS technologies develop and improve, further studies are recommended on improving the mobility and injectivity of CO_2-SPAM in fractured cores. Due to the unforeseen difficulties brought by the SARS-CoV-2 pandemic, a core flooding experimental set up was not available to evaluate the gel's sealing performance and rheological behavior under high pressures. As a result, this dissertation focused mainly on rheological properties of the gel that contribute to adequate sealing properties such a high gel strength. Furthermore, permeability reduction in porous media has been reported in the past with PAM-based polymers but it is recommended that further studies are performed to determine the maximum fracture width this polymer gel system can successfully seal through a core flooding experiment with fractured core samples. Lastly, with regards to the relative movement of CO_2-SPAM and CO_2 in the reservoir and potential loss of pore space that could be used for CO_2 storage, a numerical multiphase flow simulation is the best tool that can accurately determine the extents of this loss and the effect of injection parameters on it. Core flooding experimental data and results can be used as inputs to determine an optimum sequence of injections to minimize lost storage space.

In Chapter 4, the chemical mechanisms happening during CO_2-SPAM synthesis were discussed. Even though resorcinol-formaldehyde resin, PAM-formaldehyde, and PAM-hydroxymethyl-resorcinol are formed during the process, it still unclear whether these polymer

chains are copolymerized and creating a complex gel network or physically entangle with one another resulting in an interpenetrating network. Copolymerization is when different species of monomers polymerize into a multicomponent polymer chain while a semi-interpenetrated network involves the penetration or interlacing of polymer networks and linear/branched polymers on a molecular scale but are not covalently bonded. A way to determine if copolymerization is happening is by using a combination of Soxhlet extraction and Raman microscopy or infrared spectroscopy (IR spectroscopy).[229] Firstly, the CO_2-SPAM gel will be subjected to Soxhlet extraction, where the cross-linked (gel) and linear (solvent-soluble) fractions will be separated. This method will remove any unreacted monomer and linear polymer chains. Secondly, Raman spectroscopy or IR spectroscopy will be used to determine the presence of phenolic resin and PAM-formaldehyde before and after Soxhlet extraction. If a multifunctional network is formed, the ether functional group (which is unique to the resorcinol-formaldehyde resin's ether bridge) (C–O) will show as a strong peak in IR spectra or a moderate peak in Raman microscopy between a wavelength of 1000 and 1250 cm^{-1} and a wavelength of 932 cm^{-1}, respectively.[230–233] If the ether functional group is absent, IF spectrometry can be used to identify the phenol group in PAM-hydroxymethyl-resorcinol. The phenol functional group will have a medium peak at a frequency between 1390 and 1310 cm^{-1}.[234] These functional groups will provide a strong marker in the spectra and will demonstrate if the polymer chains copolymerize.

The gel's rheological behavior was tested before and after gelation in both Chapter 5 and 6, but a dynamic study of the CO_2-SPAM solution as it gels can provide insight of the crossover modulus. Due to the nature of the gelation process, a glovebox or a sealed container is needed. This apparatus can be attached to the rheometer allowing the testing atmosphere to be flooded

with CO_2. The crossover modulus is the single point in the material's viscoelastic spectrum where G' and G'' cross. Initially, an aqueous solution is prepared and eventually changes into a semi-solid. The crossover modulus will be the specific point where the gel becomes less of a liquid and more of a solid (G'' decreases and G' increases). The crossover point indicates the moment the CO_2-SPAM gel solution displays more solid-like characteristics after being exposed to high concentrations of CO_2. This is an important characteristic worth to be noted to improve the sequence of injection and the gel's mobility across the reservoir. Finally, it is necessary to expand the study of CO_2-SPAM to encompass the full range of pressures, temperatures, and salinities encountered in subsurface CO_2 storage sites as depicted in Fig. 3.8 and 5.21.

REFERENCES

(1) US EPA, O. *Climate Change Indicators: U.S. Greenhouse Gas Emissions*. https://www.epa.gov/climate-indicators/climate-change-indicators-us-greenhouse-gas-emissions (accessed 2022-05-31).

(2) US EPA, O. *Inventory of U.S. Greenhouse Gas Emissions and Sinks*. https://www.epa.gov/ghgemissions/inventory-us-greenhouse-gas-emissions-and-sinks (accessed 2022-05-31).

(3) Girard, J. E. *Principles of Environmental Chemistry*; Jones & Bartlett Publishers, 2009.

(4) Boggs, S. *Principles of Sedimentology and Stratigraphy*; Pearson Prentice Hall, 2006.

(5) NOAA US Department of Commerce. *Global Monitoring Laboratory - Carbon Cycle Greenhouse Gases*. https://gml.noaa.gov/ccgg/trends/monthly.html (accessed 2022-05-31).

(6) Budinis, S.; Krevor, S.; Dowell, N. M.; Brandon, N.; Hawkes, A. An Assessment of CCS Costs, Barriers and Potential. *Energy Strategy Rev.* **2018**, *22*, 61–81. https://doi.org/10.1016/j.esr.2018.08.003.

(7) Raza, A.; Gholami, R.; Rezaee, R.; Rasouli, V.; Rabiei, M. Significant Aspects of Carbon Capture and Storage – A Review. *Petroleum* **2018**, *5*. https://doi.org/10.1016/j.petlm.2018.12.007.

(8) Størset, S. Ø.; Tangen, G.; Berstad, D.; Eliasson, P.; Hoff, K. A.; Langørgen, Ø.; Munkejord, S. T.; Roussanaly, S.; Torsæter, M. Profiting from CCS Innovations: A Study to Measure Potential Value Creation from CCS Research and Development. *Int. J. Greenh. Gas Control* **2019**, *83*, 208–215. https://doi.org/10.1016/j.ijggc.2019.02.015.

(9) Teir, S.; Tsupari, E.; Arasto, A.; Koljonen, T.; Kärki, J.; Lehtilä, A.; Kujanpää, L.; Aatos, S.; Nieminen, M. Prospects for Application of CCS in Finland. *Energy Procedia* **2011**, *4*, 6174–6181. https://doi.org/10.1016/j.egypro.2011.02.628.

(10) Wennersten, R.; Sun, Q.; Li, H. The Future Potential for Carbon Capture and Storage in Climate Change Mitigation – an Overview from Perspectives of Technology, Economy and Risk. *J. Clean. Prod.* **2015**, *103*, 724–736. https://doi.org/10.1016/j.jclepro.2014.09.023.

(11) Ni, Y.; Eskeland, G. S.; Giske, J.; Hansen, J.-P. The Global Potential for Carbon Capture and Storage from Forestry. *Carbon Balance Manag.* **2016**, *11* (1), 3. https://doi.org/10.1186/s13021-016-0044-y.

(12) Yáñez, E.; Ramírez, A.; Núñez-López, V.; Castillo, E.; Faaij, A. Exploring the Potential of Carbon Capture and Storage-Enhanced Oil Recovery as a Mitigation Strategy in the Colombian Oil Industry. *Int. J. Greenh. Gas Control* **2020**, *94*, 102938. https://doi.org/10.1016/j.ijggc.2019.102938.

(13) Miocic, J. M.; Gilfillan, S. M. V.; Frank, N.; Schroeder-Ritzrau, A.; Burnside, N. M.; Haszeldine, R. S. 420,000 Year Assessment of Fault Leakage Rates Shows Geological Carbon Storage Is Secure. *Sci. Rep.* **2019**, *9* (1), 769. https://doi.org/10.1038/s41598-018-36974-0.

(14) Li, D.; Zhang, L.; Ren, B.; Ren, S. Experimental Study of CO2-Sensitive Chemicals for Enhanced Sealing of Leakage Pathways in CO2 Geological Storage Process. *Energy Procedia* **2014**, *63*, 4646–4657. https://doi.org/10.1016/j.egypro.2014.11.498.

(15) Yang, F.; Bai, B.; Tang, D.; Shari, D.-N.; David, W. Characteristics of CO2 Sequestration in Saline Aquifers. *Pet. Sci.* **2010**, *7* (1), 83–92. https://doi.org/10.1007/s12182-010-0010-3.

(16) Celia, M. A.; Bachu, S.; Nordbotten, J. M.; Bandilla, K. W. Status of CO2 Storage in Deep Saline Aquifers with Emphasis on Modeling Approaches and Practical Simulations. *Water Resour. Res.* **2015**, *51* (9), 6846–6892. https://doi.org/10.1002/2015WR017609.

(17) Wei, N.; Li, X.; Jiao, Z.; Stauffer, P. H.; Liu, S.; Ellett, K.; Middleton, R. S. A Hierarchical Framework for CO2 Storage Capacity in Deep Saline Aquifer Formations. *Front. Earth Sci.* **2022**, *9*.

(18) Bachu, S. Review of CO2 Storage Efficiency in Deep Saline Aquifers. *Int. J. Greenh. Gas Control* **2015**, *40*, 188–202. https://doi.org/10.1016/j.ijggc.2015.01.007.

(19) Wang, K.; Xu, T.; Tian, H.; Wang, F. Impacts of Mineralogical Compositions on Different Trapping Mechanisms during Long-Term CO2 Storage in Deep Saline Aquifers. *Acta Geotech.* **2016**, *11* (5), 1167–1188. https://doi.org/10.1007/s11440-015-0427-3.

(20) Rathnaweera, T. D.; Ranjith, P. G.; Perera, M. S. A. Experimental Investigation of Geochemical and Mineralogical Effects of CO2 Sequestration on Flow Characteristics of Reservoir Rock in Deep Saline Aquifers. *Sci. Rep.* **2016**, *6* (1), 19362. https://doi.org/10.1038/srep19362.

(21) Upstill, G.; Hall, P. Estimating the Learning Rate of a Technology with Multiple Variants: The Case of Carbon Storage. *Energy Policy* **2018**, *121*, 498–505. https://doi.org/10.1016/j.enpol.2018.05.017.

(22) MagentaGreen. *Scheme of an Oil Trap*; 2014.

(23) Dake, L. P. *Fundamentals of Reservoir Engineering*; Elsevier, 1983.

(24) Tunio, S. Q.; Tunio, A. H.; Ghirano, N. A. Comparison of Different Enhanced Oil Recovery Techniques for Better Oil Productivity. **2011**, *1* (5), 12.

(25) Hamza, A.; Hussein, I. A.; Al-Marri, M. J.; Mahmoud, M.; Shawabkeh, R.; Aparicio, S. CO2 Enhanced Gas Recovery and Sequestration in Depleted Gas Reservoirs: A Review. *J. Pet. Sci. Eng.* **2021**, *196*, 107685. https://doi.org/10.1016/j.petrol.2020.107685.

(26) Office of Fossil Energy and Carbon Management. *Enhanced Oil Recovery*. Energy.gov. https://www.energy.gov/fecm/science-innovation/oil-gas-research/enhanced-oil-recovery (accessed 2022-05-31).

(27) Schlumberger. *Schlumberger New Energy, Chevron, and Microsoft Collaborate on Carbon Negative Bioenergy*. https://www.slb.com/newsroom/press-release/2021/pr-2021-0304-slb-newenergy-chevron-mendota (accessed 2022-05-31).

(28) Halliburton. *Energean Selects Halliburton for Carbon Storage Subsurface Study in Greece*. https://www.halliburton.com/en/about-us/press-release/energean-selects-halliburton-carbon-storage-subsurface-study-greece (accessed 2022-05-31).

(29) Chevron. *Carbon Capture and Storage Project*. chevron.com. https://www.chevron.com/newsroom/2022/q2/chevron-launches-carbon-capture-and-storage-project-in-san-joaquin-valley (accessed 2022-05-31).

(30) Abe, M.; Tanaka, S.; Noguchi, M.; Yamasaki, A. Investigation of Mineral Carbonation with Direct Bubbling into Concrete Sludge. *ACS Omega* **2021**, *6* (24), 15564–15571. https://doi.org/10.1021/acsomega.0c04758.

(31) Matter, J. M.; Kelemen, P. B. Permanent Storage of Carbon Dioxide in Geological Reservoirs by Mineral Carbonation. *Nat. Geosci.* **2009**, *2* (12), 837–841. https://doi.org/10.1038/ngeo683.

(32) Prigiobbe, V.; Hänchen, M.; Werner, M.; Baciocchi, R.; Mazzotti, M. Mineral Carbonation Process for CO2 Sequestration. *Energy Procedia* **2009**, *1* (1), 4885–4890. https://doi.org/10.1016/j.egypro.2009.02.318.

(33) Zarrouk, S. J.; McLean, K. Chapter 5 - Advanced Analytical Pressure-Transient Analysis Relevant to Geothermal Wells. In *Geothermal Well Test Analysis*; Zarrouk, S. J., McLean, K., Eds.; Academic Press, 2019; pp 89–111. https://doi.org/10.1016/B978-0-12-814946-1.00005-0.

(34) Min, T.; Gao, Y.; Chen, L.; Kang, Q.; Tao, W.-Q. *Changes in Porosity, Permeability and Surface Area during Rock Dissolution: Effects of Mineralogical Heterogeneity*; arXiv:1511.04295; arXiv, 2015. https://doi.org/10.48550/arXiv.1511.04295.

(35) Singh, K.; Anabaraonye, B. U.; Blunt, M. J.; Crawshaw, J. Partial Dissolution of Carbonate Rock Grains during Reactive CO2-Saturated Brine Injection under Reservoir Conditions. *Adv. Water Resour.* **2018**, *122*, 27–36. https://doi.org/10.1016/j.advwatres.2018.09.005.

(36) Verdon, J. P.; Stork, A. L. Carbon Capture and Storage, Geomechanics and Induced Seismic Activity. *J. Rock Mech. Geotech. Eng.* **2016**, *8* (6), 928–935. https://doi.org/10.1016/j.jrmge.2016.06.004.

(37) Chang, K. W.; Minkoff, S. E.; Bryant, S. L. Modeling Leakage Through Faults of CO2 Stored in an Aquifer; OnePetro, 2008. https://doi.org/10.2118/115929-MS.

(38) Peng, S. Overview of CO_2 Leakage Problems and Sealants for CO_2 Leakage Remediation. *Masters Theses* **2017**.

(39) Nicol, A.; Seebeck, H.; Field, B.; McNamara, D.; Childs, C.; Craig, J.; Rolland, A. Fault Permeability and CO2 Storage. *Energy Procedia* **2017**, *114*, 3229–3236. https://doi.org/10.1016/j.egypro.2017.03.1454.

(40) Oldenburg, C. M.; Bryant, S. L.; Nicot, J.-P. Certification Framework Based on Effective Trapping for Geologic Carbon Sequestration. *Int. J. Greenh. Gas Control* **2009**, *3* (4), 444–457. https://doi.org/10.1016/j.ijggc.2009.02.009.

(41) Zhang, Y.; Oldenburg, C. M.; Finsterle, S.; Jordan, P.; Zhang, K. Probability Estimation of CO2 Leakage through Faults at Geologic Carbon Sequestration Sites. *Energy Procedia* **2009**, *1* (1), 41–46. https://doi.org/10.1016/j.egypro.2009.01.008.

(42) Gholami, R.; Raza, A.; Iglauer, S. Leakage Risk Assessment of a CO2 Storage Site: A Review. *Earth-Sci. Rev.* **2021**, *223*, 103849. https://doi.org/10.1016/j.earscirev.2021.103849.

(43) Watson, T. L.; Bachu, S. Evaluation of the Potential for Gas and CO2 Leakage Along Wellbores. *SPE Drill. Complet.* **2009**, *24* (01), 115–126. https://doi.org/10.2118/106817-PA.

(44) Davidovits, J. Geopolymer Cement a Review. *Geopolymer Sci. Tech.* **2013**, 1–11.

(45) L′Orange Seigo, S.; Dohle, S.; Siegrist, M. Public Perception of Carbon Capture and Storage (CCS): A Review. *Renew. Sustain. Energy Rev.* **2014**, *38*, 848–863. https://doi.org/10.1016/j.rser.2014.07.017.

(46) Wallquist, L.; Visschers, V. H. M.; Siegrist, M. Impact of Knowledge and Misconceptions on Benefit and Risk Perception of CCS. *Environ. Sci. Technol.* **2010**, *44* (17), 6557–6562. https://doi.org/10.1021/es1005412.

(47) Jia, H.; Ren, Q.; Li, Y. M.; Ma, X. P. Evaluation of Polyacrylamide Gels with Accelerator Ammonium Salts for Water Shutoff in Ultralow Temperature Reservoirs: Gelation Performance and Application Recommendations. *Petroleum* **2016**, *2* (1), 90–97. https://doi.org/10.1016/j.petlm.2015.12.003.

(48) Li, D.; Zhang, L.; Liu, Y.-M.; Kang, W.-L.; Ren, S.-R. CO2-Triggered Gelation for Mobility Control and Channeling Blocking during CO2 Flooding Processes. *Pet. Sci.* **2016**, *13* (2), 247–258. https://doi.org/10.1007/s12182-016-0090-9.

(49) Al-Hamairi, A.; AlAmeri, W. Development of a Novel Model to Predict HPAM Viscosity with the Effects of Concentration, Salinity and Divalent Content. *J. Pet. Explor. Prod. Technol.* **2020**, *10* (5), 1949–1963. https://doi.org/10.1007/s13202-020-00841-4.

(50) Al-Muntasheri, G. A.; Nasr-El-Din, H. A.; Zitha, P. L. J. Gelation Kinetics and Performance Evaluation of an Organically Crosslinked Gel at High Temperature and Pressure. *SPE J.* **2008**, *13* (03), 337–345. https://doi.org/10.2118/104071-PA.

(51) Al-Muntasheri, G. A.; Nasr-El-Din, H. A.; Al-Noaimi, K. R.; Zitha, P. L. J. A Study of Polyacrylamide-Based Gels Crosslinked With Polyethyleneimine. *SPE J.* **2009**, *14* (02), 245–251. https://doi.org/10.2118/105925-PA.

(52) Amir, Z.; Said, I. M.; Jan, B. M. In Situ Organically Cross-Linked Polymer Gel for High-Temperature Reservoir Conformance Control: A Review. *Polym. Adv. Technol.* **2019**, *30* (1), 13–39. https://doi.org/10.1002/pat.4455.

(53) Deng, Q.; Li, H.; Li, Y.; Cao, X.; Yang, Y.; Song, X.; Deng, Q.; Li, H.; Li, Y.; Cao, X.; Yang, Y.; Song, X. Rheological Properties and Salt Resistance of a Hydrophobically Associating Polyacrylamide. *Aust. J. Chem.* **2014**, *67* (10), 1396–1402. https://doi.org/10.1071/CH14204.

(54) Durucan, S.; Korre, A.; Shi, J.-Q.; Govindan, R.; Mosleh, M. H.; Syed, A. The Use of Polymer-Gel Solutions for CO2 Flow Diversion and Mobility Control within Storage Sites. *Energy Procedia* **2016**, *86*, 450–459. https://doi.org/10.1016/j.egypro.2016.01.046.

(55) Jia, H.; Ren, Q.; Li, Y. M.; Ma, X. P. Evaluation of Polyacrylamide Gels with Accelerator Ammonium Salts for Water Shutoff in Ultralow Temperature Reservoirs: Gelation Performance and Application Recommendations. *Petroleum* **2016**, *2* (1), 90–97. https://doi.org/10.1016/j.petlm.2015.12.003.

(56) Jia, H.; Pu, W.-F.; Zhao, J.-Z.; Liao, R. Experimental Investigation of the Novel Phenol−Formaldehyde Cross-Linking HPAM Gel System: Based on the Secondary Cross-Linking Method of Organic Cross-Linkers and Its Gelation Performance Study after Flowing through Porous Media. *Energy Fuels* **2011**, *25* (2), 727–736. https://doi.org/10.1021/ef101334y.

(57) Aizebeokhai, A. P. Global Warming and Climate Change: Realities, Uncertainties and Measures. *Int. J. Phys. Sci.* **2009**, *4* (13), 868–879. https://doi.org/10.5897/IJPS.9000283.

(58) Sun, Y.; Li, Q.; Yang, D.; Liu, X. Laboratory Core Flooding Experimental Systems for CO2 Geosequestration: An Updated Review over the Past Decade. *J. Rock Mech. Geotech. Eng.* **2016**, *8* (1), 113–126. https://doi.org/10.1016/j.jrmge.2015.12.001.

(59) Sun, X.; Bai, B.; Long, Y.; Wang, Z. A Comprehensive Review of Hydrogel Performance under CO2 Conditions for Conformance Control. *J. Pet. Sci. Eng.* **2020**, *185*, 106662. https://doi.org/10.1016/j.petrol.2019.106662.

(60) Mosleh, M. H.; Govindan, R.; Shi, J.-Q.; Durucan, S.; Korre, A. The Use of Polymer-Gel Remediation for CO2 Leakage through Faults and Fractures in the Caprock. *Energy Procedia* **2017**, *114*, 4164–4171. https://doi.org/10.1016/j.egypro.2017.03.1557.

(61) Nagai, D.; Suzuki, A.; Kuribayashi, T. Synthesis of Hydrogels from Polyallylamine with Carbon Dioxide as Gellant: Development of Reversible CO2 Absorbent. *Macromol. Rapid Commun.* **2011**, *32* (4), 404–410. https://doi.org/10.1002/marc.201000601.

(62) George, M.; Weiss, R. G. Chemically Reversible Organogels: Aliphatic Amines as "Latent" Gelators with Carbon Dioxide. *J. Am. Chem. Soc.* **2001**, *123* (42), 10393–10394. https://doi.org/10.1021/ja016819+.

(63) Carretti, E.; Dei, L.; Baglioni, P.; Weiss, R. G. Synthesis and Characterization of Gels from Polyallylamine and Carbon Dioxide as Gellant. *J. Am. Chem. Soc.* **2003**, *125* (17), 5121–5129. https://doi.org/10.1021/ja034399d.

(64) Carretti, E.; Dei, L.; Weiss, R. G. Soft Matter and Art Conservation. Rheoreversible Gels and Beyond. *Soft Matter* **2005**, *1* (1), 17–22. https://doi.org/10.1039/B501033K.

(65) Yu, G.; Lu, Y.; Liu, X.; Wang, W.-J.; Yang, Q.; Xing, H.; Ren, Q.; Li, B.-G.; Zhu, S. Polyethylenimine-Assisted Extraction of α-Tocopherol from Tocopherol Homologues and CO2-Triggered Fast Recovery of the Extractant. *Ind. Eng. Chem. Res.* **2014**, *53* (41), 16025–16032. https://doi.org/10.1021/ie502568h.

(66) Yu, B.; Fan, W.; Zhao, Y. Gelation of Triblock Copolymers in Aqueous Solution through CO2-Triggered Electrostatic Interaction. *Macromol. Chem. Phys.* **2017**, *218* (17), 1700146. https://doi.org/10.1002/macp.201700146.

(67) Lin, S.; Theato, P. CO2-Responsive Polymers. *Macromol. Rapid Commun.* **2013**, *34* (14), 1118–1133. https://doi.org/10.1002/marc.201300288.

(68) Raje, M.; Asghari, K.; Vossoughi, S.; Green, D. W.; Willhite, G. P. Gel Systems for Controlling CO2 Mobility in Carbon Dioxide Miscible Flooding; Society of Petroleum Engineers, 1996. https://doi.org/10.2118/35379-MS.

(69) Li, D.; Zhang, L.; Ren, S.; Rui, H. Leakage Mitigation During CO2 Geological Storage Process Using CO2 Triggered Gelation. *Ind. Eng. Chem. Res.* **2019**, *58* (8), 3395–3406. https://doi.org/10.1021/acs.iecr.8b05049.

(70) Zhang, J.; Xu, D.; Guo, J.; Qian, W.; Yan, F. *CO2 Responsive Imidazolium-Type Poly(Ionic Liquid) Gels*. Wiley Online Library. https://onlinelibrary.wiley.com/doi/abs/10.1002/marc.201600069 (accessed 2022-05-31).

(71) Han, D.; Boissiere, O.; Kumar, S.; Tong, X.; Tremblay, L.; Zhao, Y. Two-Way CO_2 -Switchable Triblock Copolymer Hydrogels. *Macromolecules* **2012**, *45* (18), 7440–7445. https://doi.org/10.1021/ma3015189.

(72) Atashin, S. Mineral Sequestration for Permanent CO2 Storage. **2016**.

(73) Chang, R.; Kim, S.; Lee, S.; Choi, S.; Kim, M.; Park, Y. *Calcium Carbonate Precipitation for CO2 Storage and Utilization: A Review of the Carbonate Crystallization and Polymorphism*. Frontiers. https://www.frontiersin.org/articles/10.3389/fenrg.2017.00017/full (accessed 2022-05-31).

(74) Kim, B.-J.; Park, E.-H.; Choi, K.; Kang, K.-S. Synthesis of CaCO3 Using CO2 at Room Temperature and Ambient Pressure. *Mater. Lett.* **2017**, *190*, 45–47. https://doi.org/10.1016/j.matlet.2016.12.030.

(75) Domingo, C.; García-Carmona, J.; Loste, E.; Fanovich, A.; Fraile, J.; Gómez-Morales, J. Control of Calcium Carbonate Morphology by Precipitation in Compressed and Supercritical Carbon Dioxide Media. *J. Cryst. Growth* **2004**, *271* (1), 268–273. https://doi.org/10.1016/j.jcrysgro.2004.07.060.

(76) Czaplicka, N.; Konopacka-Łyskawa, D.; Kościelska, B.; Łapiński, M. Effect of Selected Ammonia Escape Inhibitors on Carbon Dioxide Capture and Utilization via Calcium Carbonate Precipitation. *J. CO2 Util.* **2020**, *42*, 101298. https://doi.org/10.1016/j.jcou.2020.101298.

(77) Korchef, A. Effect of Iron Ions on the Crystal Growth Kinetics and Microstructure of Calcium Carbonate. *Cryst. Growth Des.* **2019**, *19* (12), 6893–6902. https://doi.org/10.1021/acs.cgd.9b00503.

(78) Korchef, A. *Effect of Operating Parameters and Foreign Ions on the Crystal Growth of Calcium Carbonate during Scale Formation: An Overview*; IntechOpen, 2020. https://doi.org/10.5772/intechopen.94121.

(79) Shen, D.; Li, W.; Xu, S.; Wu, P. Fabrication of BaCO3 Sheaves Tailored by Carboxymethyl Cellulose under Compressed CO2. *J. Cryst. Growth* **2012**, *353*, 101–107. https://doi.org/10.1016/j.jcrysgro.2012.05.019.

(80) Montes-Hernandez, G.; Daval, D.; Chiriac, R.; Renard, F. Growth of Nanosized Calcite through Gas−Solid Carbonation of Nanosized Portlandite under Anisobaric Conditions. *Cryst. Growth Des.* **2010**, *10* (11), 4823–4830. https://doi.org/10.1021/cg100714m.

(81) Fricker, K. J.; Park, A.-H. A. Investigation of the Different Carbonate Phases and Their Formation Kinetics during Mg(OH)2 Slurry Carbonation. *Ind. Eng. Chem. Res.* **2014**, *53* (47), 18170–18179. https://doi.org/10.1021/ie503131s.

(82) Van Lopik, J. H. Feasibility of EcoGrout: Modelling of in-Situ Calcite Precipitation and CO2 Degassing in Porous Medium. Master's Thesis, 2014.

(83) Beckingham, L. E. Evaluation of Macroscopic Porosity-Permeability Relationships in Heterogeneous Mineral Dissolution and Precipitation Scenarios. *Water Resour. Res.* **2017**, *53* (12), 10217–10230. https://doi.org/10.1002/2017WR021306.

(84) Wetzel, M.; Kempka, T.; Kühn, M. Hydraulic and Mechanical Impacts of Pore Space Alterations within a Sandstone Quantified by a Flow Velocity-Dependent Precipitation Approach. *Materials* **2020**, *13* (14), 3100. https://doi.org/10.3390/ma13143100.

(85) Pallardy, S. G. CHAPTER 8 - Lipids, Terpenes, and Related Substances. In *Physiology of Woody Plants (Third Edition)*; Pallardy, S. G., Ed.; Academic Press: San Diego, 2008; pp 217–232. https://doi.org/10.1016/B978-012088765-1.50009-9.

(86) Zhu, D.; Peng, S.; Zhao, S.; Wei, M.; Bai, B. Comprehensive Review of Sealant Materials for Leakage Remediation Technology in Geological CO_2 Capture and Storage Process. *Energy Fuels* **2021**, *35* (6), 4711–4742. https://doi.org/10.1021/acs.energyfuels.0c04416.

(87) Lu, H.; Liu, Y.; Jiang, J.; Huang, Z. Use of a CO2-Switchable Hydrophobic Associating Polymer to Enhance Viscosity–Response. *J. Appl. Polym. Sci.* **2015**, *132* (7). https://doi.org/10.1002/app.41468.

(88) Pang, S.; Sharma, M. M. A Model for Predicting Injectivity Decline in Water-Injection Wells. *SPE Form. Eval.* **1997**, *12* (03), 194–201. https://doi.org/10.2118/28489-PA.

(89) Han, D.; Tong, X.; Boissière, O.; Zhao, Y. General Strategy for Making CO2-Switchable Polymers. *ACS Macro Lett.* **2012**, *1* (1), 57–61. https://doi.org/10.1021/mz2000175.

(90) Zhao, C.; Zhang, J.; Yuan, G.; Han, C. C. CO2-Triggered Liquid–Solid Switching through a Jamming Mechanism. *RSC Adv.* **2013**, *3* (25), 9645–9648. https://doi.org/10.1039/C3RA41004H.

(91) Zhang, L.; Khan, N.; Pu, C. A New Method of Plugging the Fracture to Enhance Oil Production for Fractured Oil Reservoir Using Gel Particles and the HPAM/Cr3+ System. *Polymers* **2019**, *11* (3), 446. https://doi.org/10.3390/polym11030446.

(92) Brattekas, B.; Fernø, M. New Insight from Visualization of Mobility Control for Enhanced Oil Recovery Using Polymer Gels and Foams; 2016. https://doi.org/10.5772/64586.

(93) Tian, Q.; Han, P.; Li, B.; Feng, Y. Thermo- and CO2-Triggered Swelling Polymer Microgels for Reducing Water-Cut during CO2 Flooding. *J. Appl. Polym. Sci.* **2020**, *137* (4), 48305. https://doi.org/10.1002/app.48305.

(94) *Reservoir pressure and temperature*. PetroWiki. https://petrowiki.spe.org/Reservoir_pressure_and_temperature (accessed 2022-06-17).

(95) *Average Depth of Crude Oil and Natural Gas Wells*. https://www.eia.gov/dnav/pet/pet_crd_welldep_s1_a.htm (accessed 2022-06-17).

(96) Sheng, J.; Chen, K. Evaluation of the EOR Potential of Gas and Water Injection in Shale Oil Reservoirs. *J. Unconv. Oil Gas Resour.* **2014**, *5*, 1–9. https://doi.org/10.1016/j.juogr.2013.12.001.

(97) Michael, K.; Golab, A.; Shulakova, V.; Ennis-King, J.; Allinson, G.; Sharma, S.; Aiken, T. Geological Storage of CO2 in Saline Aquifers—A Review of the Experience from Existing Storage Operations. *Int. J. Greenh. Gas Control* **2010**, *4* (4), 659–667. https://doi.org/10.1016/j.ijggc.2009.12.011.

(98) Chuajiw, W.; Nakano, M.; Takatori, K.; Kojima, T.; Wakimoto, Y.; Fukushima, Y. Effects of Amine, Amine Salt and Amide on the Behaviour of Carbon Dioxide Absorption into Calcium Hydroxide Suspension to Precipitate Calcium Carbonate. *J. Environ. Sci.* **2013**, *25* (12), 2507–2515. https://doi.org/10.1016/S1001-0742(12)60284-8.

(99) Peng, S. OVERVIEW OF CO2 LEAKAGE PROBLEMS AND SEALANTS FOR CO2 LEAKAGE REMEDIATION. 101.

(100) Li, D.; Zhang, L.; Ren, B.; Ren, S. Experimental Study of CO2-Sensitive Chemicals for Enhanced Sealing of Leakage Pathways in CO2 Geological Storage Process. *Energy Procedia* **2014**, *63*, 4646–4657. https://doi.org/10.1016/j.egypro.2014.11.498.

(101) Lashari, Z.; Kang, W.; Yang, H.; Zhang, H.; Sarsenbekuly, B. Macro-Rheology and Micro-Rheological Study of Composite Polymer Gel at High Salinity and Acidic Conditions for CO2 Shut Off Treatment in Harsh Reservoirs for Improving Oil Recovery; 2019. https://doi.org/10.2118/201175-MS.

(102) Li, D.; Zhang, L.; Ren, S.; Rui, H. Leakage Mitigation During CO2 Geological Storage Process Using CO2 Triggered Gelation. *Ind. Eng. Chem. Res.* **2019**, *58* (8), 3395–3406. https://doi.org/10.1021/acs.iecr.8b05049.

(103) *Progress in Study and Application of Drilling Fluid Viscosifier at Home--《Guangzhou Chemical Industry》2012年12期*. https://en.cnki.com.cn/Article_en/CJFDTotal-GZHA201212006.htm (accessed 2022-03-07).

(104) Kurenkov, V. F.; Hartan, H.; Lobanov, F. I. *Application of Polyacrylamide Flocculants for Water Treatment*.

(105) Long, Y.; You, X.; Chen, Y.; Hong, H.; Liao, B.-Q.; Lin, H. Filtration Behaviors and Fouling Mechanisms of Ultrafiltration Process with Polyacrylamide Flocculation for Water Treatment. *Sci. Total Environ.* **2020**, *703*, 135540. https://doi.org/10.1016/j.scitotenv.2019.135540.

(106) Ma, J.; Wang, R.; Wang, X.; Zhang, H.; Zhu, B.; Lian, L.; Lou, D. Drinking Water Treatment by Stepwise Flocculation Using Polysilicate Aluminum Magnesium and Cationic Polyacrylamide. *J. Environ. Chem. Eng.* **2019**, *7* (3), 103049. https://doi.org/10.1016/j.jece.2019.103049.

(107) Solberg, D.; Wågberg, L. On the Mechanism of Cationic-Polyacrylamide-Induced Flocculation and Re-Dispersion of a Pulp Fiber Dispersion. *Nord. Pulp Pap. Res. J.* **2003**, *18* (1), 51–55.

(108) Wong, S. S.; Teng, T. T.; Ahmad, A. L.; Zuhairi, A.; Najafpour, G. Treatment of Pulp and Paper Mill Wastewater by Polyacrylamide (PAM) in Polymer Induced Flocculation. *J. Hazard. Mater.* **2006**, *135* (1), 378–388. https://doi.org/10.1016/j.jhazmat.2005.11.076.

(109) Wu, R.; Wang, Q.; Wang, G. Immobilized Enzyme on Pulp Fiber through Layer-by-Layer Technique Using Cationic Polyacrylamide for Whitewater Treatment from Papermaking. *Bioprocess Biosyst. Eng.* **2019**, *42* (10), 1583–1589. https://doi.org/10.1007/s00449-019-02155-0.

(110) Djafari Petroudy, S. R.; Syverud, K.; Chinga-Carrasco, G.; Ghasemain, A.; Resalati, H. Effects of Bagasse Microfibrillated Cellulose and Cationic Polyacrylamide on Key Properties of Bagasse Paper. *Carbohydr. Polym.* **2014**, *99*, 311–318. https://doi.org/10.1016/j.carbpol.2013.07.073.

(111) Mosleh, M. H.; Govindan, R.; Shi, J.-Q.; Durucan, S.; Korre, A. The Use of Polymer-Gel Remediation for CO2 Leakage through Faults and Fractures in the Caprock. *Energy Procedia* **2017**, *114*, 4164–4171. https://doi.org/10.1016/j.egypro.2017.03.1557.

(112) Jia, H.; Pu, W.-F.; Zhao, J.-Z.; Liao, R. Experimental Investigation of the Novel Phenol−Formaldehyde Cross-Linking HPAM Gel System: Based on the Secondary Cross-Linking Method of Organic Cross-Linkers and Its Gelation Performance Study after Flowing through Porous Media. *Energy Fuels* **2011**, *25* (2), 727–736. https://doi.org/10.1021/ef101334y.

(113) Ren, Q.; Jia, H.; Yu, D.; Pu, W.-F.; Wang, L.-L.; Li, B.; Yang, J.-J.; Ni, J.-H.; Chen, L. New Insights into Phenol–Formaldehyde-Based Gel Systems with Ammonium Salt for Low-Temperature Reservoirs. *J. Appl. Polym. Sci.* **2014**, *131* (16). https://doi.org/10.1002/app.40657.

(114) Yadav, U. S.; Mahto, V. Investigating the Effect of Several Parameters on the Gelation Behavior of Partially Hydrolyzed Polyacrylamide–Hexamine–Hydroquinone Gels. *Ind. Eng. Chem. Res.* **2013**, *52* (28), 9532–9537. https://doi.org/10.1021/ie400488a.

(115) Hamza, A.; Shamlooh, M.; Hussein, I. A.; Nasser, M.; Salehi, S. Polymeric Formulations Used for Loss Circulation Materials and Wellbore Strengthening Applications in Oil and Gas Wells: A Review. *J. Pet. Sci. Eng.* **2019**, *180*, 197–214. https://doi.org/10.1016/j.petrol.2019.05.022.

(116) Wong, S. S.; Jameson, D. M. *Chemistry of Protein and Nucleic Acid Cross-Linking and Conjugation*; CRC Press, 2011.

(117) Zhang, Q.; Zhou, J.; Zhai, Y.; Liu, F.; Gao, G. Effect of Salt Solutions on Chain Structure of Partially Hydrolyzed Polyacrylamide. *J. Cent. South Univ. Technol.* **2008**, *15* (S1), 80–83. https://doi.org/10.1007/s11771-008-0319-x.

(118) Jia, H.; Pu, W.-F.; Zhao, J.-Z.; Jin, F.-Y. Research on the Gelation Performance of Low Toxic PEI Cross-Linking PHPAM Gel Systems as Water Shutoff Agents in Low Temperature Reservoirs. *Ind. Eng. Chem. Res.* **2010**, *49* (20), 9618–9624. https://doi.org/10.1021/ie100888q.

(119) Jia, H.; Zhao, J.-Z.; Jin, F.-Y.; Pu, W.-F.; Li, Y.-M.; Li, K.-X.; Li, J.-M. New Insights into the Gelation Behavior of Polyethyleneimine Cross-Linking Partially Hydrolyzed Polyacrylamide Gels. *Ind. Eng. Chem. Res.* **2012**, *51* (38), 12155–12166. https://doi.org/10.1021/ie301818f.

(120) Jin, F.-Y.; Yuan, C.-D.; Pu, W.-F.; Zhang, Y.-Y.; Tang, S.; Dong, Y.; Zhao, T.; Li, Y.-B. Investigation on Gelation Process and Microstructure for Partially Hydrolyzed Polyacrylic Amide (HPAm)–Cr(III) Acetate–Methanal Compound Crosslinked Weak Gel. *J. Sol-Gel Sci. Technol.* **2015**, *73* (1), 181–191. https://doi.org/10.1007/s10971-014-3509-z.

(121) Singh, R.; Talukdar, P. Study the Rheological Behaviour and Effectiveness of Partially Hydrolyzed Polyacrylamide-Zirconium Acetate Gel System for Enhanced Oil Recovery. *Int. J. Appl. Eng. Res.* **2018**, *13*, 13672–13676.

(122) Ma, J.; Yu, P.; Xia, B.; An, Y. Effect of Salt and Temperature on Molecular Aggregation Behavior of Acrylamide Polymer. *E-Polym.* **2019**, *19* (1), 594–606. https://doi.org/10.1515/epoly-2019-0063.

(123) Sarsenbekuly, B.; Kang, W.; Fan, H.; Yang, H.; Dai, C.; Zhao, B.; Aidarova, S. Study of Salt Tolerance and Temperature Resistance of A Hydrophobically Modified Polyacrylamide Based Novel Functional Polymer for EOR. *Colloids Surf. Physicochem. Eng. Asp.* **2016**, *514*. https://doi.org/10.1016/j.colsurfa.2016.10.051.

(124) Lyu, Y.; Gu, C.; Tao, J.; Yao, X.; Zhao, G.; Dai, C. Thermal-Resistant, Shear-Stable and Salt-Tolerant Polyacrylamide/Surface-Modified Graphene Oxide Composite. *J. Mater. Sci.* **2019**, *54* (24), 14752–14762. https://doi.org/10.1007/s10853-019-03967-x.

(125) DREYFORS, J. M.; JONES, S. B.; SAYED, Y. Hexamethylenetetramine: A Review. *Am. Ind. Hyg. Assoc. J.* **1989**, *50* (11), 579–585. https://doi.org/10.1080/15298668991375191.

(126) Moldoveanu, S. C. Chapter 16 - Pyrolysis of Aromatic Heterocyclic Compounds. In *Pyrolysis of Organic Molecules (Second Edition)*; Moldoveanu, S. C., Ed.; Elsevier, 2019; pp 715–762. https://doi.org/10.1016/B978-0-444-64000-0.00016-0.

(127) Dressler, H. *Resorcinol: Its Uses and Derivatives*; Springer Science & Business Media, 2013.

(128) Li, D.; Zhang, L.; Ren, S.; Rui, H. Leakage Mitigation During CO_2 Geological Storage Process Using CO_2 Triggered Gelation. *Ind. Eng. Chem. Res.* **2019**, *58* (8), 3395–3406. https://doi.org/10.1021/acs.iecr.8b05049.

(129) *Partial dissolution of carbonate rock grains during reactive CO2-saturated brine injection under reservoir conditions | Elsevier Enhanced Reader*. https://reader.elsevier.com/reader/sd/pii/S0309170818305311?token=4B6E52B8651DDF3D3F191E4350062ED51FA9E18D5914C26C09770C04DCAA7C07FE3ED14D8766813248FF9A180C3DAE72&originRegion=us-east-1&originCreation=20211025185038 (accessed 2021-10-25). https://doi.org/10.1016/j.advwatres.2018.09.005.

(130) Lashari, Z.; Kang, W.; Yang, H.; Zhang, H.; Sarsenbekuly, B. Macro-Rheology and Micro-Rheological Study of Composite Polymer Gel at High Salinity and Acidic Conditions for CO2 Shut Off Treatment in Harsh Reservoirs for Improving Oil Recovery; 2019. https://doi.org/10.2118/201175-MS.

(131) He, H.; Wang, Y.; Zhang, J.; Xu, X.; Zhu, Y.; Bai, S. Comparison of Gelation Behavior and Morphology of Resorcinol–Hexamethylenetetramine–HPAM Gel in Bulk and Porous Media. *Transp. Porous Media* **2015**, *109* (2), 377–392. https://doi.org/10.1007/s11242-015-0524-7.

(132) Gaca, K.; Sefcik, J. Mechanism and Kinetics of Nanostructure Evolution during Early Stages of Resorcinol-Formaldehyde Polymerisation. *J. Colloid Interface Sci.* **2013**. https://doi.org/10.1016/j.jcis.2013.05.062.

(133) Durairaj, R. B. *Resorcinol Based Polymers*; Springer: Berlin, Heidelberg, 2005. https://doi.org/10.1007/3-540-28090-1_7.

(134) Šebenik, A.; Osredkar, U.; Vizovišek, I. Study of the Reaction between Resorcinol and Formaldehyde. *Polymer* **1981**, *22* (6), 804–806. https://doi.org/10.1016/0032-3861(81)90019-7.

(135) Prostredny, M.; Ballantine, J.; Sefcik, J.; Fletcher, A. *The impact of deuterium oxide on the properties of resorcinol-formaldehyde gels*. https://1library.net/document/4zpv1mrz-impact-deuterium-oxide-properties-resorcinol-formaldehyde-gels.html (accessed 2022-06-26).

(136) Mohamed, M. A.; Mohd Hir, Z. A.; Wan Mokthar, W. N. A.; Osman, N. S. 6 - Features of Metal Oxide Colloidal Nanocrystal Characterization. In *Colloidal Metal Oxide Nanoparticles*; Thomas, S., Tresa Sunny, A., Velayudhan, P., Eds.; Metal Oxides; Elsevier, 2020; pp 83–122. https://doi.org/10.1016/B978-0-12-813357-6.00008-5.

(137) Alonso-Buenaposada, I. D.; Rey-Raap, N.; Calvo, E. G.; Menéndez, J. A.; Arenillas, A. Acid-Based Resorcinol-Formaldehyde Xerogels Synthesized by Microwave Heating. *J. Sol-Gel Sci. Technol.* **2017**, *84* (1), 60–69. https://doi.org/10.1007/s10971-017-4475-z.

(138) Ma, Q.; Shuler, P. J.; Aften, C. W.; Tang, Y. Theoretical Studies of Hydrolysis and Stability of Polyacrylamide Polymers. *Polym. Degrad. Stab.* **2015**, *121*, 69–77. https://doi.org/10.1016/j.polymdegradstab.2015.08.012.

(139) Kennepohl, D.; Farmer, S.; Reusch, W.; Neils, T. *Acidity of Carboxylic Acids*. Chemistry LibreTexts. https://chem.libretexts.org/Courses/Nassau_Community_College/Organic_Chemistry_I_and_II/19%3A_Carboxylic_Acids/19.02%3A_Acidity_of_Carboxylic_Acids (accessed 2022-07-03).

(140) Al-Muntasheri, G. A.; Nasr-El-Din, H. A.; Peters, J. A.; Zitha, P. L. J. Investigation of a High-Temperature Organic Water-Shutoff Gel: Reaction Mechanisms. *SPE J.* **2006**, *11* (04), 497–504. https://doi.org/10.2118/97530-PA.

(141) Albonico, P.; Bartosek, M.; Malandrino, A.; Bryant, S.; Lockhart, T. P. Studies on Phenol-Formaldehyde Crosslinked Polymer Gels in Bulk and in Porous Media; OnePetro, 1995. https://doi.org/10.2118/28983-MS.

(142) Moradi-Araghi, A. A Review of Thermally Stable Gels for Fluid Diversion in Petroleum Production. *J. Pet. Sci. Eng.* **2000**, *26* (1), 1–10. https://doi.org/10.1016/S0920-4105(00)00015-2.

(143) Bongiovanni, R.; Vitale, A. 8 - Smart Multiphase Polymer Coatings for the Protection of Materials. In *Smart Composite Coatings and Membranes*; Montemor, M. F., Ed.; Woodhead Publishing Series in Composites Science and Engineering; Woodhead Publishing, 2016; pp 213–234. https://doi.org/10.1016/B978-1-78242-283-9.00008-7.

(144) Liu, Y.; Hsu, Y.-H.; Huang, A. P.-H.; Hsu, S. Semi-Interpenetrating Polymer Network of Hyaluronan and Chitosan Self-Healing Hydrogels for Central Nervous System Repair. *ACS Appl. Mater. Interfaces* **2020**, *12* (36), 40108–40120. https://doi.org/10.1021/acsami.0c11433.

(145) Stille, J. K. Step-Growth Polymerization. *J. Chem. Educ.* **1981**, *58* (11), 862. https://doi.org/10.1021/ed058p862.

(146) Pinner, S. H. *Functionality of non-equivalent mixtures*. Journal of Polymer Science - Wiley Online Library. https://onlinelibrary.wiley.com/doi/epdf/10.1002/pol.1956.120219718 (accessed 2022-07-19).

(147) Sydansk, R. D. A New Conformance-Improvement-Treatment Chromium(III) Gel Technology; OnePetro, 1988. https://doi.org/10.2118/17329-MS.

(148) Wu, X.; Fan, M.; Shen, X.; Cui, S.; Tan, G. Silica Aerogels Formed from Soluble Silicates and Methyl Trimethoxysilane (MTMS) Using CO2 Gas as a Gelation Agent. *Ceram. Int.* **2018**, *44* (1), 821–829. https://doi.org/10.1016/j.ceramint.2017.10.005.

(149) Floren, M. L.; Spilimbergo, S.; Motta, A.; Migliaresi, C. Carbon Dioxide Induced Silk Protein Gelation for Biomedical Applications. *Biomacromolecules* **2012**, *13* (7), 2060–2072. https://doi.org/10.1021/bm300450a.

(150) Gurikov, P.; Smirnova, I. Non-Conventional Methods for Gelation of Alginate. *Gels* **2018**, *4* (1), 14. https://doi.org/10.3390/gels4010014.

(151) Nguele, R.; Omondi, B. A.; Yamasaki, S.; Mandai, S.; Sugai, Y.; Sasaki, K. Evaluation of CO2-Triggered and Thermo-Responsive Gels for Heterogeneous Oil Formations. *Colloids Surf. Physicochem. Eng. Asp.* **2021**, *622*, 126688. https://doi.org/10.1016/j.colsurfa.2021.126688.

(152) Aminzadeh, F.; Dasgupta, S. N. Chapter 2 - Fundamentals of Petroleum Geology. In *Developments in Petroleum Science*; Aminzadeh, F., Dasgupta, S. N., Eds.; Geophysics for Petroleum Engineers; Elsevier, 2013; Vol. 60, pp 15–36. https://doi.org/10.1016/B978-0-444-50662-7.00002-0.

(153) Dusseault, M. B.; Maury, V.; Sanfilippo, F.; Santarelli, F. J. Drilling Through Salt: Constitutive Behavior And Drilling Strategies; OnePetro, 2004.

(154) Onajite, E. Chapter 1 - Sedimentation and Oil/Gas Formation. In *Seismic Data Analysis Techniques in Hydrocarbon Exploration*; Onajite, E., Ed.; Elsevier: Oxford, 2014; pp 3–16. https://doi.org/10.1016/B978-0-12-420023-4.00001-0.

(155) Romero-Zerón, L.; Manalo, F.; Kantzas, A. Characterization of Crosslinked Gel Kinetics and Gel Strength by Use of NMR. *SPE Reserv. Eval. Eng.* **2008**, *11* (03), 439–453. https://doi.org/10.2118/86548-PA.

(156) Dai, C.; Zhao, G.; You, Q.; Zhao, M. A Study on Environment-Friendly Polymer Gel for Water Shut-off Treatments in Low-Temperature Reservoirs. *J. Appl. Polym. Sci.* **2014**, *131* (8). https://doi.org/10.1002/app.40154.

(157) Reddy, B. R.; Crespo, F.; Eoff, L. Water Shutoff at Ultralow Temperatures Using Organically Crosslinked Polymer Gels; OnePetro, 2012. https://doi.org/10.2118/153155-MS.

(158) Al-Muntasheri, G. A.; Nasr-El-Din, H. A.; Hussein, I. A. A Rheological Investigation of a High Temperature Organic Gel Used for Water Shut-off Treatments. *J. Pet. Sci. Eng.* **2007**, *59* (1), 73–83. https://doi.org/10.1016/j.petrol.2007.02.010.

(159) Mohamed, A. I. A.; Hussein, I. A.; Sultan, A. S.; Al-Muntasheri, G. A. Gelation of Emulsified Polyacrylamide/Polyethylenimine under High-Temperature, High-Salinity Conditions: Rheological Investigation. *Ind. Eng. Chem. Res.* **2018**, *57* (36), 12278–12287. https://doi.org/10.1021/acs.iecr.8b02571.

(160) Al-Hajri, S.; Mahmood, S. M.; Akbari, S.; Abdulelah, H. Gelation Behavior as a Function of Concentration of Sodium Thiosulfate for PAM Gels Cross-Linked with Chromium. *J. Pet. Explor. Prod. Technol.* **2019**, *9* (2), 1539–1546. https://doi.org/10.1007/s13202-018-0566-9.

(161) Shamlooh, M. S. Development of Polymeric Crosslinkable Formulations for Conformance Control In Oil and Gas Reservoirs. **2020**.

(162) Yin, H.; Yin, X.; Cao, R.; Zeng, P.; Wang, J.; Wu, D.; Luo, X.; Zhu, Y.; Zheng, Z.; Feng, Y. In Situ Crosslinked Weak Gels with Ultralong and Tunable Gelation Times for Improving Oil Recovery. *Chem. Eng. J.* **2022**, *432*, 134350. https://doi.org/10.1016/j.cej.2021.134350.

(163) Igunnu, E. T.; Chen, G. Z. Produced Water Treatment Technologies. *Int. J. Low-Carbon Technol.* **2014**, *9* (3), 157–177. https://doi.org/10.1093/ijlct/cts049.

(164) Mohammad Salehi, M.; Omidvar, P.; Naeimi, F. Salinity of Injection Water and Its Impact on Oil Recovery Absolute Permeability, Residual Oil Saturation, Interfacial Tension and Capillary Pressure. *Egypt. J. Pet.* **2017**, *26* (2), 301–312. https://doi.org/10.1016/j.ejpe.2016.05.003.

(165) Li, D.-X.; Zhang, L.; Liu, Y.-M.; Kang, W.-L.; Ren, S.-R. CO2-Triggered Gelation for Mobility Control and Channeling Blocking during CO2 Flooding Processes. *Pet. Sci.* **2016**, *13* (2), 247–258. https://doi.org/10.1007/s12182-016-0090-9.

(166) Li, D.; Zhang, L.; Ren, S.; Rui, H. Leakage Mitigation During CO2 Geological Storage Process Using CO2 Triggered Gelation. *Ind. Eng. Chem. Res.* **2019**, *58* (8), 3395–3406. https://doi.org/10.1021/acs.iecr.8b05049.

(167) Sydansk, R. D. Well Kill Treatment for Oil Field Wellbore Operations. US4995461A, February 26, 1991.

(168) Sydansk, R. D. Foamed Gel for Permeability Reduction or Mobility Control in a Subterranean Hydrocarbon-Bearing Formation. US5834406A, November 10, 1998.

(169) Syed, A.; Pantin, B.; Durucan, S.; Korre, A.; Shi, J.-Q. The Use of Polymer-Gel Solutions for Remediation of Potential CO2 Leakage from Storage Reservoirs. *Energy Procedia* **2014**, *63*, 4638–4645. https://doi.org/10.1016/j.egypro.2014.11.497.

(170) Gu, C.; Lv, Y.; Fan, X.; Zhao, C.; Dai, C.; Zhao, G. Study on Rheology and Microstructure of Phenolic Resin Cross-Linked Nonionic Polyacrylamide (NPAM) Gel for Profile Control and Water Shutoff Treatments. *J. Pet. Sci. Eng.* **2018**, *169*, 546–552. https://doi.org/10.1016/j.petrol.2018.06.016.

(171) Sydansk, R. D.; Southwell, G. P. More Than 12 Years' Experience With a Successful Conformance-Control Polymer-Gel Technology. *SPE Prod. Facil.* **2000**, *15* (04), 270–278. https://doi.org/10.2118/66558-PA.

(172) Otero-Espinar, F. J.; Fernández-Ferreiro, A.; González-Barcia, M.; Blanco-Méndez, J.; Luzardo, A. Chapter 6 - Stimuli Sensitive Ocular Drug Delivery Systems. In *Drug Targeting and Stimuli Sensitive Drug Delivery Systems*; Grumezescu, A. M., Ed.; William Andrew Publishing, 2018; pp 211–270. https://doi.org/10.1016/B978-0-12-813689-8.00006-9.

(173) Coussot, P. *Rheometry of Pastes, Suspensions, and Granular Materials: Applications in Industry and Environment*; John Wiley & Sons, 2005.

(174) Berret, J.-F. Rheology of Wormlike Micelles: Equilibrium Properties and Shear Banding Transitions. In *Molecular Gels*; Weiss, R. G., Terech, P., Eds.; Springer-Verlag: Berlin/Heidelberg, 2006; pp 667–720. https://doi.org/10.1007/1-4020-3689-2_20.

(175) *Rubbery Plateau*. http://polymerdatabase.com/polymer%20physics/RubberyPlateau.html (accessed 2022-06-27).

(176) Bertasa, M.; Dodero, A.; Alloisio, M.; Vicini, S.; Riedo, C.; Sansonetti, A.; Scalarone, D.; Castellano, M. Agar Gel Strength: A Correlation Study between Chemical Composition and Rheological Properties. *Eur. Polym. J.* **2020**, *123*, 109442. https://doi.org/10.1016/j.eurpolymj.2019.109442.

(177) Tang, J.; Tung, M. A.; Zeng, Y. Compression Strength and Deformation of Gellan Gels Formed with Mono- and Divalent Cations. *Carbohydr. Polym.* **1996**, *29* (1), 11–16. https://doi.org/10.1016/0144-8617(95)00124-7.

(178) Hamza, A.; Shamlooh, M.; Hussein, I. A.; Nasser, M.; Salehi, S. Polymeric Formulations Used for Loss Circulation Materials and Wellbore Strengthening Applications in Oil and Gas Wells: A Review. *J. Pet. Sci. Eng.* **2019**, *180*, 197–214. https://doi.org/10.1016/j.petrol.2019.05.022.

(179) Green, D. W.; Willhite, G. P. *Enhanced Oil Recovery*; Henry L. Doherty Memorial Fund of AIME, Society of Petroleum Engineers, 1998.

(180) Mao, J.; Tan, H.; Yang, B.; Zhang, W.; Yang, X.; Zhang, Y.; Zhang, H. Novel Hydrophobic Associating Polymer with Good Salt Tolerance. *Polymers* **2018**, *10* (8), 849. https://doi.org/10.3390/polym10080849.

(181) Karsani, K. S. M. E.; Al-Muntasheri, G. A.; Sultan, A. S.; Hussein, I. A. Impact of Salts on Polyacrylamide Hydrolysis and Gelation: New Insights. *J. Appl. Polym. Sci.* **2014**, *131* (23). https://doi.org/10.1002/app.41185.

(182) El-karsani, K.; Al-Muntasheri, G.; Sultan, A.; Hussein, I. Impact of Salts on Polyacrylamide Hydrolysis and Gelation: New Insights. *J. Appl. Polym. Sci.* **2014**, *131*. https://doi.org/10.1002/app.41185.

(183) Jiang, J.; Lu, J. Impact of Temperature on the Linear Viscoelastic Region of Wood. *Can. J. For. Res.-Rev. Can. Rech. For. - CAN J For. RES* **2009**, *39*, 2092–2099. https://doi.org/10.1139/X09-119.

(184) Kar, F.; Arslan, N. Effect of Temperature and Concentration on Viscosity of Orange Peel Pectin Solutions and Intrinsic Viscosity–Molecular Weight Relationship. *Carbohydr. Polym.* **1999**, *40* (4), 277–284. https://doi.org/10.1016/S0144-8617(99)00062-4.

(185) Kulicke, W. M.; Böse, N.; Bouldin, M. The Role of Polymers in Enhanced Oil Recovery. In *Water-Soluble Polymers for Petroleum Recovery*; Stahl, G. A., Schulz, D. N., Eds.; Springer US: Boston, MA, 1988; pp 1–17. https://doi.org/10.1007/978-1-4757-1985-7_1.

(186) *Water-Soluble Polymers for Petroleum Recovery*; Stahl, G. A., Schulz, D. N., Eds.; Springer US: Boston, MA, 1988. https://doi.org/10.1007/978-1-4757-1985-7.

(187) Thiel, G. P.; Lienhard, J. H. Treating Produced Water from Hydraulic Fracturing: Composition Effects on Scale Formation and Desalination System Selection. *Desalination* **2014**, *346*, 54–69. https://doi.org/10.1016/j.desal.2014.05.001.

(188) Environmental, M. *Green Remediation Technologies that Address Climate Change*. Munirem Environmental. https://www.munirem.com/green-remediation-technologies-that-address-climate-change/ (accessed 2022-02-24).

(189) Dewan, A. *G20 agrees on key climate goals around global warming limits and coal financing, but lacks firm commitments*. CNN. https://www.cnn.com/2021/10/31/politics/g20-climate-communique/index.html (accessed 2022-02-24).

(190) Matthews, H. D.; Zickfeld, K. Climate Response to Zeroed Emissions of Greenhouse Gases and Aerosols. *Nat. Clim. Change* **2012**, *2* (5), 338–341. https://doi.org/10.1038/nclimate1424.

(191) Noureldin, M.; Allinson, W. G.; Cinar, Y.; Baz, H. Coupling Risk of Storage and Economic Metrics for CCS Projects. *Int. J. Greenh. Gas Control* **2017**, *60*, 59–73. https://doi.org/10.1016/j.ijggc.2017.03.008.

(192) Gholami, R.; Raza, A.; Iglauer, S. Leakage Risk Assessment of a CO2 Storage Site: A Review. *Earth-Sci. Rev.* **2021**, *223*, 103849. https://doi.org/10.1016/j.earscirev.2021.103849.

(193) Tongwa, P.; Nygaard, R.; Blue, A.; Bai, B. Evaluation of Potential Fracture-Sealing Materials for Remediating CO2 Leakage Pathways during CO2 Sequestration. *Int. J. Greenh. Gas Control* **2013**, *18*, 128–138. https://doi.org/10.1016/j.ijggc.2013.06.017.

(194) Watson, T. L.; Bachu, S. Evaluation of the Potential for Gas and CO2 Leakage Along Wellbores. *SPE Drill. Complet.* **2009**, *24* (01), 115–126. https://doi.org/10.2118/106817-PA.

(195) Glasgow, M. E.; Schmandt, B.; Wang, R.; Zhang, M.; Bilek, S. L.; Kiser, E. *Raton Basin Induced Seismicity Is Hosted by Networks of Short Basement Faults and Mimics Tectonic Earthquake Statistics*; preprint; Geophysics, 2021. https://doi.org/10.1002/essoar.10507748.1.

(196) Evans, D. M. The Denver Area Earthquakes and the Rocky Mountain Arsenal Disposal Well. In *Engineering Seismology*; Adams, WM. M., Ed.; Geological Society of America: U.S.A., 1970; pp 25–32. https://doi.org/10.1130/Eng-Case-8.25.

(197) Johnson, R.; Finn, T. *Potential for a Basin-Centered Gas Accumulation in the Raton Basin, Colorado and New Mexico*; 2001. https://doi.org/10.3133/b2184B.

(198) Baltz, E. H. Stratigraphy and History of Raton Basin and Notes on San Luis Basin, Colorado-New Mexico1. *AAPG Bull.* **1965**, *49* (11), 2041–2075. https://doi.org/10.1306/A6633882-16C0-11D7-8645000102C1865D.

(199) Woodward, L. A. *Chapter 14: Role of Regional Tectonic Analysis in Exploration for Fracture Reservoirs in Cretaceous Source Rocks of the Raton Basin, New Mexico*. https://archives.datapages.com/data/rocky-mtn-geologist-pubs/data/003/003001/219_rmag-bk0030219.htm (accessed 2022-02-23).

(200) Lund Snee, J.-E.; Zoback, M. D. Multiscale Variations of the Crustal Stress Field throughout North America. *Nat. Commun.* **2020**, *11* (1), 1951. https://doi.org/10.1038/s41467-020-15841-5.

(201) Nakai, J. S.; Weingarten, M.; Sheehan, A. F.; Bilek, S. L.; Ge, S. A Possible Causative Mechanism of Raton Basin, New Mexico and Colorado Earthquakes Using Recent Seismicity Patterns and Pore Pressure Modeling. *J. Geophys. Res. Solid Earth* **2017**, *122* (10), 8051–8065. https://doi.org/10.1002/2017JB014415.

(202) Brown, M. R. M.; Ge, S. Earthquake Interactions in the Raton Basin, Colorado and New Mexico, USA. **2018**, *2018*, S32A-04.

(203) Scott, J. *New study links Raton Basin earthquakes to oil and gas wastewater injections - TheCivilEngineer.org*. https://www.thecivilengineer.org/news-center/latest-news/item/1455-new-study-links-raton-basin-earthquakes-to-oil-and-gas-wastewater-injections (accessed 2022-02-23).

(204) Rubinstein, J. L.; Ellsworth, W. L.; McGarr, A.; Benz, H. M. The 2001–Present Induced Earthquake Sequence in the Raton Basin of Northern New Mexico and Southern Colorado. *Bull. Seismol. Soc. Am.* **2014**, *104* (5), 2162–2181. https://doi.org/10.1785/0120140009.

(205) Richfield Company. *Dike Mountain Unit Well Completion Diagram*. COGIS - WELL INFORMATION. https://cogcc.state.co.us/schematic/055/0550604700.gif (accessed 2022-04-12).

(206) Richfield Company. *Dike Mountain Well Documentation*. COGCC. https://cogcc.state.co.us/cogisdb/Resources/Docs?ID=05506047&uni=2324847 (accessed 2022-04-12).

(207) Johnson, R. B. Geologic Map of the Trinidad Quadrangle, South-Central Colorado. *IMAP* **1969**. https://doi.org/10.3133/i558.

(208) Vine, J. D. Geologic Map and Cross Sections of the La Veta Pass, La Veta, and Ritter Arroyo Quadrangles, Huerfano and Costilla Counties, Colorado. *IMAP* **1974**. https://doi.org/10.3133/i833.

(209) Petex. *MOVE Core*. http://www.petex.com/products/move-suite/move/ (accessed 2022-06-15).

(210) Flew, S.; Sellin, R. H. J. Non-Newtonian Flow in Porous Media-a Laboratory Study of Polyacrylamide Solutions. *J. Non-Newton. Fluid Mech.* **1993**, *47*, 169–210. https://doi.org/10.1016/0377-0257(93)80050-L.

(211) Shin, S.; Cho, Y. I. Temperature Effect on the Non-Newtonian Viscosity of an Aqueous Polyacrylamide Solution. *Int. Commun. Heat Mass Transf.* **1993**, *20* (6), 831–844. https://doi.org/10.1016/0735-1933(93)90037-V.

(212) Odell, J. A.; Müller, A. J.; Keller, A. Non-Newtonian Behaviour of Hydrolysed Polyacrylamide in Strong Elongational Flows: A Transient Network Approach. *Polymer* **1988**, *29* (7), 1179–1190. https://doi.org/10.1016/0032-3861(88)90042-0.

(213) Kizilkan, Ö.; Dincer, I. Evaluation of Thermal Characteristics of a Borehole Thermal Energy Storage System. In *Progress in Exergy, Energy, and the Environment*; Dincer, I., Midilli, A., Kucuk, H., Eds.; Springer International Publishing: Cham, 2014; pp 385–398. https://doi.org/10.1007/978-3-319-04681-5_34.

(214) Habibi, M.; Aligolzadeh, F.; Hakkaki-Fard, A. A Techno-Economic Analysis of Geothermal Ejector Cooling System. *Energy* **2020**, *193*, 116760. https://doi.org/10.1016/j.energy.2019.116760.

(215) Habibi, M.; Hakkaki-Fard, A. Long-Term Energy and Exergy Analysis of Heat Pumps with Different Types of Ground and Air Heat Exchangers. *Int. J. Refrig.* **2019**, *100*, 414–433. https://doi.org/10.1016/j.ijrefrig.2019.02.021.

(216) Odell, J. A.; Müller, A. J.; Keller, A. Non-Newtonian Behaviour of Hydrolysed Polyacrylamide in Strong Elongational Flows: A Transient Network Approach. *Polymer* **1988**, *29* (7), 1179–1190. https://doi.org/10.1016/0032-3861(88)90042-0.

(217) Flew, S.; Sellin, R. H. J. Non-Newtonian Flow in Porous Media-a Laboratory Study of Polyacrylamide Solutions. *J. Non-Newton. Fluid Mech.* **1993**, *47*, 169–210. https://doi.org/10.1016/0377-0257(93)80050-L.

(218) Eberhard, U.; Seybold, H. J.; Floriancic, M.; Bertsch, P.; Jiménez-Martínez, J.; Andrade, J. S.; Holzner, M. Determination of the Effective Viscosity of Non-Newtonian Fluids Flowing Through Porous Media. *Front. Phys.* **2019**, *7*.

(219) Cannella, W. J.; Huh, C.; Seright, R. S. Prediction of Xanthan Rheology in Porous Media; OnePetro, 1988. https://doi.org/10.2118/18089-MS.

(220) Zoback, M. D. *Reservoir Geomechanics*; Cambridge University Press: Cambridge, 2007. https://doi.org/10.1017/CBO9780511586477.

(221) Byerlee, J. Friction of Rocks. In *Rock Friction and Earthquake Prediction*; Byerlee, J. D., Wyss, M., Eds.; Contributions to Current Research in Geophysics (CCRG); Birkhäuser: Basel, 1978; pp 615–626. https://doi.org/10.1007/978-3-0348-7182-2_4.

(222) Zoback, M.; Healy, J. Friction, Faulting and «in Situ» Stress. **1984**. https://doi.org/10.1016/0148-9062(85)93053-0.

(223) de Gennes, P. G.; Leger, L. Dynamics of Entangled Polymer Chains. *Annu. Rev. Phys. Chem.* **1982**, *33* (1), 49–61. https://doi.org/10.1146/annurev.pc.33.100182.000405.

(224) Wu, S. Chain Structure and Entanglement. *J. Polym. Sci. Part B Polym. Phys.* **1989**, *27* (4), 723–741. https://doi.org/10.1002/polb.1989.090270401.

(225) Yadav, S.; Shire, S. J.; Kalonia, D. S. Factors Affecting the Viscosity in High Concentration Solutions of Different Monoclonal Antibodies. *J. Pharm. Sci.* **2010**, *99* (12), 4812–4829. https://doi.org/10.1002/jps.22190.

(226) Handin, J.; Hager, R. V.; Jr; Friedman, M.; Feather, J. N. Experimental Deformation of Sedimentary Rocks Under Confining Pressure: Pore Pressure Tests. *AAPG Bull.* **1963**, *47* (5), 717–755.

(227) Terzaghi, K. *Theoretical Soil Mechanics*; Chapman and Hall, 1951.

(228) Turcotte, D. L.; Schubert, G. *Geodynamics*; Cambridge University Press, 2002.

(229) Kaalberg, S. M.; Schissel, S. M.; Soumounthong, M.; Jessop, J. L. P. Elucidation of Network Structure in Cationic Photopolymerization of Cyclic Ether Comonomers. *Polym. Chem.* **2021**, *12* (41), 5999–6008. https://doi.org/10.1039/D1PY00824B.

(230) Smith, B. The C-O Bond III: Ethers By a Knockout. *Spectroscopy* **2017**, *32* (5), 22–26.

(231) Murray, M. J.; Cleveland, F. F. Raman Spectra of Some Ethers Containing One or More Phenyl Groups. *J. Chem. Phys.* **1941**, *9* (2), 129–132. https://doi.org/10.1063/1.1750864.

(232) Magnotti, G.; Kc, U.; Varghese, P. L.; Barlow, R. S. Raman Spectra of Methane, Ethylene, Ethane, Dimethyl Ether, Formaldehyde and Propane for Combustion Applications. *J. Quant. Spectrosc. Radiat. Transf.* **2015**, *163*, 80–101. https://doi.org/10.1016/j.jqsrt.2015.04.018.

(233) Spec_ir_nmr_spectra_tables.Pdf.

(234) *IR Spectrum Table*. https://www.sigmaaldrich.com/US/en/technical-documents/technical-article/analytical-chemistry/photometry-and-reflectometry/ir-spectrum-table (accessed 2022-06-29).

(235) Tsau, J.; Barati, R. A Review of the Current Progress of CO2 Injection EOR and Carbon Storage in Shale Oil Reservoirs. *Fuel* **2019**, *236*, 404–427. https://doi.org/10.1016/j.fuel.2018.08.103.

(236) Jin, L.; Hawthorne, S.; Sorensen, J.; Pekot, L.; Kurz, B.; Smith, S.; Heebink, L.; Herdegen, V.; Bosshart, N.; Torres, J.; Dalkhaa, C.; Peterson, K.; Gorecki, C.; Steadman, E.; Harju, J. Advancing CO2 Enhanced Oil Recovery and Storage in Unconventional Oil Play—Experimental Studies on Bakken Shales. *Appl. Energy* **2017**, *208* (C). https://doi.org/10.1016/j.apenergy.2017.10.054.

(237) Jin, L.; Sorensen, J. A.; Hawthorne, S. B.; Smith, S. A.; Pekot, L. J.; Bosshart, N. W.; Burton-Kelly, M. E.; Miller, D. J.; Grabanski, C. B.; Gorecki, C. D.; Steadman, E. N.; Harju, J. A. Improving Oil Recovery by Use of Carbon Dioxide in the Bakken Unconventional System: A Laboratory Investigation. *SPE Reserv. Eval. Eng.* **2016**, *20* (03), 602–612. https://doi.org/10.2118/178948-PA.

(238) Jia, B.; Tsau, J.-S.; Barati, R. Measurement of CO2 Diffusion Coefficient in the Oil-Saturated Porous Media. *J. Pet. Sci. Eng.* **2019**, *181*, 106189. https://doi.org/10.1016/j.petrol.2019.106189.

(239) Gao, H.; Zhang, B.; Fan, L.; Zhang, H.; Chen, G.; Tontiwachwuthikul, P.; Liang, Z. Study on Diffusivity of CO2 in Oil-Saturated Porous Media under High Pressure and Temperature. *Energy Fuels* **2019**, *33* (11), 11364–11372. https://doi.org/10.1021/acs.energyfuels.9b01947.

(240) Song, L.; Kantzas, A.; Bryan, J. Experimental Measurement of Diffusion Coefficient of CO2 in Heavy Oil Using X-Ray Computed-Assisted Tomography Under Reservoir Conditions; OnePetro, 2010. https://doi.org/10.2118/137545-MS.

(241) Upreti, S.; Mehrotra, A. Diffusivity of CO2, CH4, C2H6 and N2 in Athabasca Bitumen. *Can. J. Chem. Eng.* **2002**, *80*, 116–125. https://doi.org/10.1002/cjce.5450800112.

(242) Zhang, Y. P.; Hyndman, C. L.; Maini, B. B. Measurement of Gas Diffusivity in Heavy Oils. *J. Pet. Sci. Eng. Amst.* **2000**, *25*. https://doi.org/10.1016/S0920-4105(99)00031-5.

(243) Tharanivasan, A. K.; Yang, C.; Gu, Y. Measurements of Molecular Diffusion Coefficients of Carbon Dioxide, Methane, and Propane in Heavy Oil under Reservoir Conditions. *Energy Fuels* **2006**, *20* (6), 2509–2517. https://doi.org/10.1021/ef060080d.

(244) Riazi, M. *A new method for experimental measurement of diffusion coefficients in reservoir fluids*. https://www.semanticscholar.org/paper/A-new-method-for-experimental-measurement-of-in-Riazi/e9b9a611bc3f6aa6f997e8a43000b27e5f1aa5a1 (accessed 2022-06-01).

(245) Kavousi, A.; Torabi, F.; Chan, C. Experimental Measurement of CO2 Solubility in Heavy Oil and Its Diffusion Coefficient Calculation at Both Static and Dynamic Conditions; OnePetro, 2013. https://doi.org/10.2118/165559-MS.

(246) Wang, L.-S.; Lang, Z.-X.; Guo, T.-M. Measurement and Correlation of the Diffusion Coefficients of Carbon Dioxide in Liquid Hydrocarbons under Elevated Pressures. *Fluid Phase Equilibria* **1996**, *117* (1), 364–372. https://doi.org/10.1016/0378-3812(95)02973-7.

(247) Zhang, X.; Shaw, J. M. Liquid-Phase Mutual Diffusion Coefficients for Heavy Oil + Light Hydrocarbon Mixtures. *Pet. Sci. Technol.* **2007**, *25* (6), 773–790. https://doi.org/10.1080/10916460500411796.

(248) Song, L.; Kantzas, A.; Bryan, J. Investigation of CO2 Diffusivity in Heavy Oil Using X-Ray Computer-Assisted Tomography Under Reservoir Conditions; OnePetro, 2010. https://doi.org/10.2118/138205-MS.

(249) Do, H. D.; Pinczewski, W. V. Diffusion-Controlled Swelling of Reservoir Oil by Indirect Contact with Injection Gas. *Chem. Eng. Sci.* **1993**, *48* (18), 3243–3252. https://doi.org/10.1016/0009-2509(93)80208-8.

(250) Jamialahmadi, M.; Emadi, M.; Müller-Steinhagen, H. Diffusion Coefficients of Methane in Liquid Hydrocarbons at High Pressure and Temperature. *J. Pet. Sci. Eng.* **2006**, *53* (1), 47–60. https://doi.org/10.1016/j.petrol.2006.01.011.

(251) Yang, C.; Gu, Y. A New Method for Measuring Solvent Diffusivity in Heavy Oil by Dynamic Pendant Drop Shape Analysis (DPDSA). *SPE J.* **2006**, *11* (01), 48–57. https://doi.org/10.2118/84202-PA.

(252) Luo, H.; Kantzas, A. Investigation of Diffusion Coefficients of Heavy Oil and Hydrocarbon Solvent Systems in Porous Media; OnePetro, 2008. https://doi.org/10.2118/113995-MS.

(253) Renner, T. A. Measurement and Correlation of Diffusion Coefficients for CO2 and Rich-Gas Applications. *SPE Reserv. Eng.* **1988**, *3* (02), 517–523. https://doi.org/10.2118/15391-PA.

(254) Unatrakarn, D.; Asghari, K.; Condor, J. Experimental Studies of CO2 and CH4 Diffusion Coefficient in Bulk Oil and Porous Media. *Energy Procedia* **2011**, *4*, 2170–2177. https://doi.org/10.1016/j.egypro.2011.02.103.

(255) Li, Z.; Dong, M. Experimental Study of Carbon Dioxide Diffusion in Oil-Saturated Porous Media under Reservoir Conditions. *Ind. Eng. Chem. Res.* **2009**, *48* (20), 9307–9317. https://doi.org/10.1021/ie900145c.

(256) Li, S.; Li, Z.; Dong, Q. Diffusion Coefficients of Supercritical CO2 in Oil-Saturated Cores under Low Permeability Reservoir Conditions. *J. CO2 Util.* **2016**, *14*, 47–60. https://doi.org/10.1016/j.jcou.2016.02.002.

(257) Kim, H.-T.; Huh, D.-G.; Kim, S.-J.; Kim, I.-K.; Sung, W.-M. Improvement of a high pressure capillary tube viscometer for incompressible crude oil. *J. Korean Inst. Miner. Energy Resour. Eng.* **2000**, *37*.

(258) Vilarrasa, V.; Bolster, D.; Dentz, M.; Olivella, S.; Carrera, J. Effects of CO2 Compressibility on CO2 Storage in Deep Saline Aquifers. *Transp. Porous Media* **2010**, *85* (2), 619–639. https://doi.org/10.1007/s11242-010-9582-z.

(259) Bird, B.; Stewart, W.; Lightfoot, E. *Transport Phenomena*, 2nd ed.; John Wiley & Sons, 2006.

APPENDIX A

CO_2 DIFFUSION IN OIL-SATURATED POROUS MEDIA

Objective

To understand the behavior of the CO_2-SPAM, it is imperative to understand the transport properties of CO_2 diffusion. Appendix A focuses on CO_2 diffusion in a homogenous rock sample and at high pressures and temperatures. The governing equations are derived from the equations of continuity and Fick's Second Law of Diffusion. Furthermore, the concentration profile of CO_2 in the porous media is obtained and discussed further.

Introduction

As mentioned before in Chapter 1 and 3, CO_2 is known to be a very influential GHG whose excess has had a detrimental effect on the environment. Also, CO_2 has been used in the oil and gas industry to reduce the oil's viscosity and enhance oil displacement in EOR practices. Redirecting the impact of excess CO_2 might be the answer industries are looking for. CO_2 produced from energy plants can be recycled and injected into oil reservoir as a cost-effective oil recovery agent. This technique has not only demonstrated to have high oil recovery rates at a lesser cost, but it is also actively contributing to long-term CO_2 sequestration. Various studies demonstrate that the miscibility development between oil and gas and the conventional reservoir pressure maintenance has a great impact on the oil recovery performance during injection.[235–237] It is important to note that for both EOR involving the use of CO_2, and carbon capture and storage, the coefficient of molecular diffusion is paramount to determine mixing rates of injected oil and gas as well as the parting rate of lighter gases from both the oil and formation water.[238] Moreover, it is important to develop an adequate method to establish a dependable diffusion coefficient because molecular diffusion is a vital recovery mechanism in fractured reeservoirs.[239]

There are two methods that are used to determine the diffusion coefficient. Firstly, a direct measurement and analysis of a sample at various distances and times can be used to determine the concentration gradient of gas in an oil sample.[240,241] An indirect method used before focuses on monitoring any changes in the pressure of the diffusing gas,[241–246] the liquid phase density,[247,248] the liquid-gas interface,[249,250] the swelling of a pendant droplet,[251] and other physical properties of the oil-gas system to determine diffusivity. Many technological improvements have been made to testing methods for diffusion coefficients and indirect methods have gained popularity amongst several research groups. Indirect methods such as the pressure-decay technique is normally conducted in a PVT cell and has provided great results in determining the molecular diffusion coefficient of an oil-gas system.[242,244] Challenges arise when this study is performed in a porous medium due to the influences of tortuosity. In porous mediums, the effective flow paths are much longer than the apparent length. Thus, instead of the fluid flowing in a straight path, it flows along tortuous paths which can interfere with the diffusion process. Under reservoir-like conditions, the molecular diffusion coefficient of an oil-CO_2 systems determined using the pressure decay technique in a PVT cell may deviate from measured effective diffusion coefficients in sand packs. Although many studies have attempted to accurately determine the diffusion coefficient from an oil- CO_2 system, few have demonstrated the true value of diffusivity in porous media under high pressures.[252–256]

Due to the increasing usage of CO_2 in several industrial applications, new studies on CO_2's behavior under reservoir-like conditions has the potential to advance the knowledge in the field and improve fluid mechanics simulators such as OpenFOAM, UTCHEM, ECLIPSE, AD-GPRS by Stanford University, MRST by Sintef, and Dynamo/MoReS by Shell. Research on the mass transport properties of CO_2 in porous media is necessary as CCS and EOR project design,

risk assessment and performance forecast highly depend on it. Hence, the CO_2 concentration profile in a porous media using the continuity equation in an unsteady state situation is discussed and derived.

Oil-Gas System

For this system, consider a homogeneous core sample of length L. The core sample is saturated in diesel (oil phase) and CO_2 (gas phase) is being diffused from the top of the core sample. It is desired to determine the diffusion of CO_2 at high pressures and high temperatures. Fig. A.1 demonstrates the schematic of the system where CO_2 is species A, and the oil is species B.

For this problem it is desired to use the cartesian coordinate system where CO_2 is flowing in the z-direction.

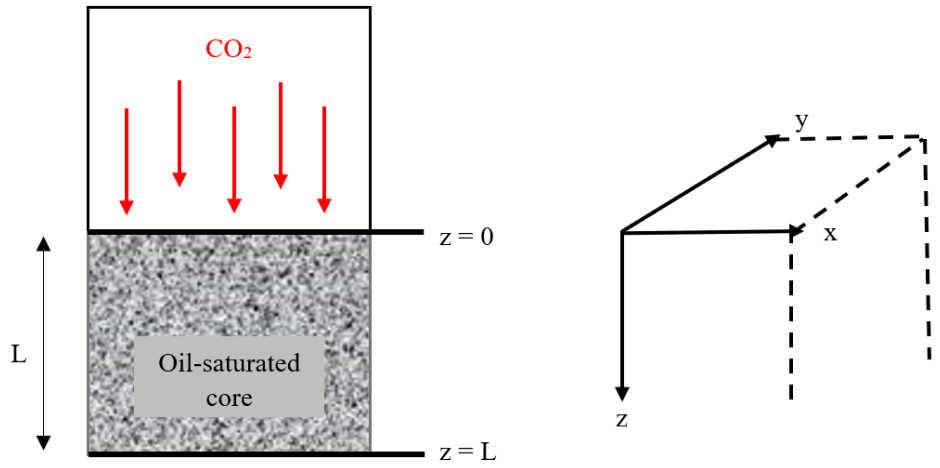

Figure A.1 Oil-CO_2 system in heterogenous porous medium.

Assumptions

Several assumptions were made to simplify the mass transport profile for this specific problem. The assumptions are as follows:

1. Velocity is assumed to be zero in the continuity equations.
2. No chemical reaction is taking place between the oil and CO_2.
3. Natural convection is negligible.
4. The diffusion coefficient is constant.
5. Density is constant.
6. The core sample is homogeneous.
7. Diffusion is uniform across the core sample.

These assumptions are justified because based on the experimental set-up (Fig. A.1), the oil is at rest inside the core: therefore, velocity is equal to zero. Also, no chemical reaction is happening because CO_2 is no reacting with the oil but mixes entirely with the oil to form one miscible mixture. Natural convection is negligible because this system uses external sources (i.e., pump) to generate fluid motion. Petroleum fluids are relatively incompressible fluids but CO_2 is a highly compressible which can lead in viscosity variations.[257,258] Some of the shortcomings of these assumptions is that in the field, rock are rarely homogeneous. Additionally, the diffusion coefficient is dependent on the molecule's size and environments' temperature and pressure. Geological formations have temperature and pressure gradients associated with depth, and as a result, the diffusion coefficient changes as function of depth as well.

Other assumptions made by Gao et al. (2019)[239] are as follows:

1. Mass transfer resistance is negligible.
2. Concentration is constant at the gas-liquid interface.
3. Volume expansion is negligible.

4. Evaporation of oil into the has phase is negligible.

Derivation of the Governing Equations

For this system, the equation of continuity (Eq. A.1) is:

$$\frac{\partial \rho}{\partial t} + (\boldsymbol{\nabla} \cdot \rho \boldsymbol{v}) = 0 \tag{A.1}$$

The equation of continuity can be rewritten in terms of cartesian coordinates (Eq. A.2) to fit the Fig. A.1.

$$\frac{\partial \rho}{\partial t} + \frac{\partial}{\partial x}(\rho \boldsymbol{v_x}) + \frac{\partial}{\partial y}\left(\rho \boldsymbol{v_y}\right) + \frac{\partial}{\partial z}(\rho \boldsymbol{v_z}) = 0 \tag{A.2}$$

Since this is a multi-component system, the equation of continuity is written in terms of species A (CO_2) and species B (oil). As a result, our two component (binary) system can be expressed as:

Species A: $$\frac{\partial \rho_A}{\partial t} + (\boldsymbol{\nabla} \cdot n_A) = r_A \tag{A.3}$$

Species B: $$\frac{\partial \rho_B}{\partial t} + (\boldsymbol{\nabla} \cdot n_B) = r_B \tag{A.4}$$

Where n is $\rho \boldsymbol{v}$ of its respective species.

If species A and B are added together, then Eq. A.5 is obtained:

$$\frac{\partial \rho_A}{\partial t} + (\boldsymbol{\nabla} \cdot (n_A + n_B)) = r_A + r_B \tag{A.5}$$

In this situation, the addition of the reaction rates will be equal to zero because the summation is done per mass basis. For most cases, it is preferrable to consider this equation in a molar basis. The molar form of the continuity equation is as follow:

Species A: $$\frac{\partial c_A}{\partial t} + (\boldsymbol{\nabla} \cdot N_A) = R_A \quad \text{(A.6)}$$

Species B: $$\frac{\partial c_B}{\partial t} + (\boldsymbol{\nabla} \cdot N_B) = R_B \quad \text{(A.7)}$$

When species A and B are added together:

$$\frac{\partial c_A}{\partial t} + (\boldsymbol{\nabla} \cdot (N_A + N_B)) = R_A + R_B \quad \text{(A.8)}$$

Unlike in the mass basis, the addition of $R_A \; and \; R_B$ is not always equal to zero. To simplify this equation, it is desired to use the molar average velocity.

$$v^* = \sum x_i v_i = x_A v_A + x_B v_B \quad \text{(A.9)}$$

Now, the equation of continuity can be rewritten for a constant density and diffusion coefficient as:

$$\frac{\partial c_A}{\partial t} + \nabla \cdot c_A v^* = c D_{AB} \cdot \nabla x_A + R_A \quad \text{(A.10)}$$

Eq. A.10 is in cartesian coordinates and includes both the velocity and concentration components. It also contains the reaction rate, molecular diffusion, and convection due to bulk motion. Note that in this system no reaction is taking place, therefore; the term R_A will be zero. Based on the assumptions made to simplify the oil-CO_2 system, the continuity equation is as follows:

$$\frac{dc_A}{dt} = D_{AB}\left(\frac{\partial^2 c_A}{\partial x^2} + \frac{\partial^2 c_A}{\partial y^2} + \frac{\partial^2 c_A}{\partial z^2}\right) \quad \text{(A.11)}$$

Eq. A.11 is known as Fick's Second Law of Diffusion, and it can also be written with the Laplacian operator.

$$\frac{dc_A}{dt} = D_{AB}(\nabla^2 c_A) \tag{A.12}$$

Derivation of the Oil- CO_2 System's Concentration Profile

The equation of continuity (Eq. A.10) will be expanded to demonstrate in detail what elements are discarded, and which ones are being kept.

$$\frac{dc_A}{dt} + \left(v_x \frac{\partial c_A}{\partial x} + v_y \frac{\partial c_A}{\partial y} + v_z \frac{\partial c_A}{\partial z}\right) = D_{AB}\left(\frac{\partial^2 c_A}{\partial x^2} + \frac{\partial^2 c_A}{\partial y^2} + \frac{\partial^2 c_A}{\partial z^2}\right) + R_A \tag{A.13}$$

It is assumed that no fluid flows across the core sample and that the oil is at rest. As a result, the velocity gradient in the left-hand side is equal to zero. In addition to that, it is assumed that any reaction in the oil-gas interface is so small, it can be neglected. Therefore, the reaction rate is equal to zero. Now Eq. A.13 can be reduced to:

$$\frac{dc_A}{dt} = D_{AB}\left(\frac{\partial^2 c_A}{\partial x^2} + \frac{\partial^2 c_A}{\partial y^2} + \frac{\partial^2 c_A}{\partial z^2}\right) \tag{A.14}$$

Based on the schematic, it is assumed that the concentration of CO_2 will be evenly distributed across the core sample in the z direction. Thus, concentration variations of CO_2 in the x and y directions are equal to zero. Eq. A.14 simplifies to the governing equation:

$$\frac{dc_A}{dt} = D_{AB}\left(\frac{\partial^2 c_A}{\partial z^2}\right) \tag{A.15}$$

Before initiating the CO_2 diffusion experiment (t = 0), the concentration of CO_2 inside the core sample will be equal to zero. This is because the core sample is fully saturated with oil and no diffusion has happened yet. Hence, the initial condition is as follows:

I.C. $t < 0$ $C_A = 0$ $0 < z < L$

As for the boundary conditions, the concentration of CO_2 at z = 0 is considered to be the concentration in the gas-oil interface and the concentration of CO_2 at z = L to be the change in concentration as a function of z.

B.C. 1 $t > 0$ $C_A = C_{Ao}$ $z = 0$

B.C. 2 $t > 0$ $\frac{dc_A}{dz} = 0$ $z = L$

To simplify the mathematical derivation process, dimensionless values are utilized.

Dimensionless concentration

$$c = \frac{C_A}{C_{Ao}}$$

Dimensionless time

$$\tau = \frac{tD_{AB}}{L^2}$$

Dimensionless length

$$\xi = \frac{z}{L}$$

After successfully determining the dimensionless values, it is very important to evaluate the governing equation (Eq. A.15) and make it dimensionless.

$$\frac{dc}{d\tau} = \left(\frac{\partial^2 c}{\partial \xi^2}\right) \tag{A.16}$$

For this type of unsteady state problem, it is convenient to split the solution into two terms. These terms are the steady state (c_∞) and transient (c_t) terms.

$$c = c_\infty - c_t \tag{A.17}$$

For the steady state term, τ will go to infinity, therefore:

$$\frac{dc_\infty}{d\tau} = \left(\frac{\partial^2 c}{\partial \xi^2}\right) \tag{A.18}$$

$$0 = \left(\frac{\partial^2 c}{\partial \xi^2}\right) \tag{A.19}$$

After differentiating, Eq. A.20 is obtained:

$$C_\infty = C_1 \xi + C_2 \tag{A.20}$$

Once the boundary conditions have been applied, the steady state dimensionless concentration of CO_2 will be equal to 1. This means that at infinity, the concentration inside the core sample will be the same as the concentration of the CO_2 in the outside.

Now for the transient term, the boundary condition are as follows:

I.C.	τ = 0	c = 0	0 = c∞ - ct	ct = 1
B.C. 1	ξ = 0	c = 1	1 = c∞ - ct	ct = 0
B.C. 2	ξ = 1	$\frac{dc}{d\xi}$ = 0	1 = $\frac{dc_\infty}{d\xi}$ - $\frac{dc_t}{d\xi}$	$\frac{dc_\infty}{d\xi}$ = $\frac{dc_t}{d\xi}$

Now, separation of variables (A.21) is used.

$$c = \psi(\xi) T(\tau) \tag{A.21}$$

$$\psi \frac{dT}{d\tau} = T \frac{d^2\psi}{d\xi^2} = -\lambda^2 \tag{A.22}$$

The separation of variables was solved by separating the left-hand side and the right-hand side and setting them both equal to the constant. The solutions for the ordinary differential equation were found in Appendix C from the book Transport Phenomena 2nd Edition by Bird and Stewart.[259] The right-hand side was further simplified by using the following boundary conditions:

B.C. 1 $\xi = 0$ $c_t = 1$

B.C. 2 $\xi = 1$ $\frac{dc_t}{d\xi} = 0$

Once the boundary conditions have been applied, the transient concentration of CO_2 is expressed as:

$$c_t = \sum_{n=0}^{\infty} c_{5n} \exp(-\lambda_n^2 \tau) \sin(\lambda_n \xi) \tag{A.23}$$

Now, the initial condition will be applied.

I.C. $\tau = 0$ $c_t = 1$

This condition yields to,

$$1 = \sum_{n=0}^{\infty} c_{5n} \sin(\lambda_n \xi) \tag{A.24}$$

Here, $\sin(\lambda_n \xi)$ is the orthogonal function, therefore; $\sin(\lambda_m \xi)$ will be multiplied by both sides, where m is an integer and integrate from 0 to 1. After integration, there will be two conditions:

When m = n, then the right-side will equal to zero.

When m ≠ n, then $c_{5n} = 2/\lambda m$

These rules yield to our concentration profile,

$$C = 1 - \sum \frac{2}{\lambda_m} \exp(-\lambda_m^2 \tau) \sin(\lambda_m \xi) \quad \text{(A.25)}$$

CO_2 Concentration Profile

The final concentration profile (Eq. A.25) was plotted at n = 0, 1 and 3. The dimensionless length (ξ) was varied from zero to one and the dimensionless time (τ) was varied from several values between 0.05 to 1. All plots exhibited similar behaviors regarding the concentration behavior as time progresses along the length of the core sample as seen in Fig A.2, A.3, and A.4. For all plots it is observed that the concentration of CO_2 at $\tau = 0.1$ is very low as ξ reaches 1. This is because al the beginning stages of the experiment the CO_2 is just starting to diffuse through the core sample. As a result, the amount of CO_2 found at the end of the core sample will be minimal. As time goes by and the experiments reaches steady state, the concentration of CO_2 increases significantly. At $\tau = 1$ to and $\xi = 1$, the dimensionless concentration of CO_2 found in the core sample is 0.892. This means that at length L and steady state conditions, the concentration of CO_2 in the core sample is 89.2% of the CO_2 concentration being injected.

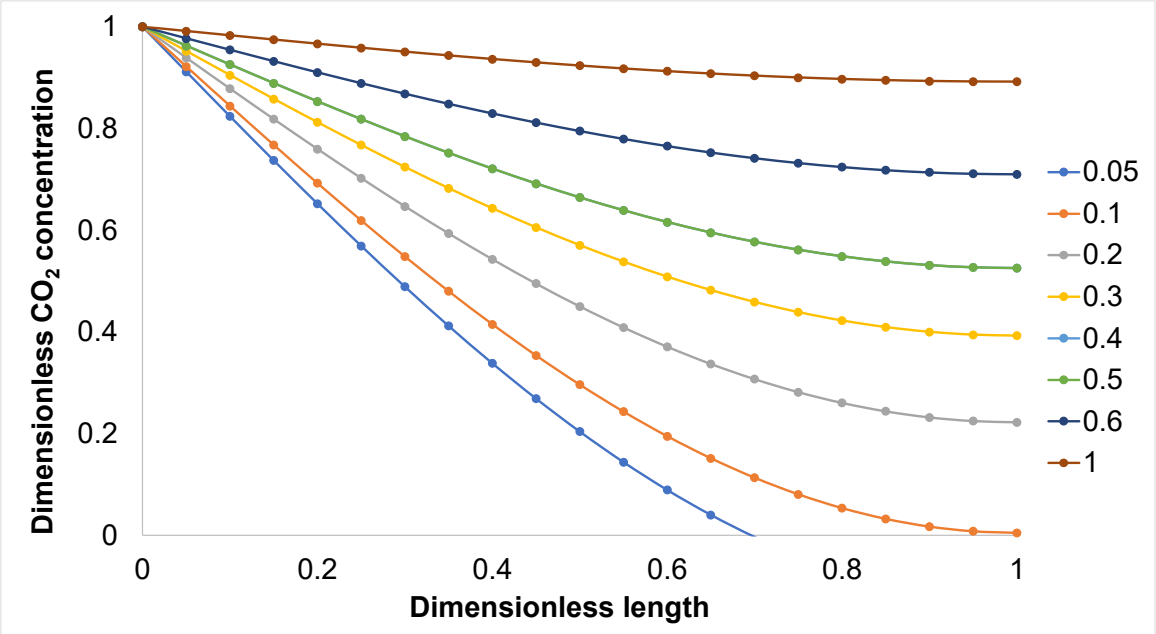

Figure A.2 Dimensionless concentration as a function of dimensionless time vs. dimensionless length at n = 0.

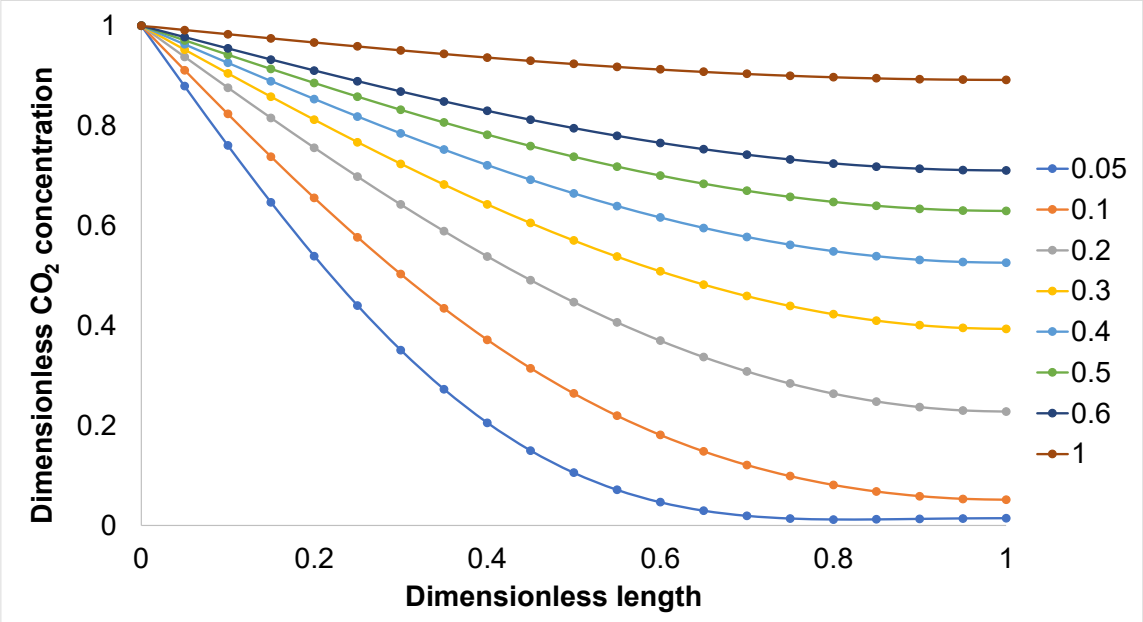

Figure A.3 Dimensionless concentration as a function of dimensionless time vs. dimensionless length at n = 1.

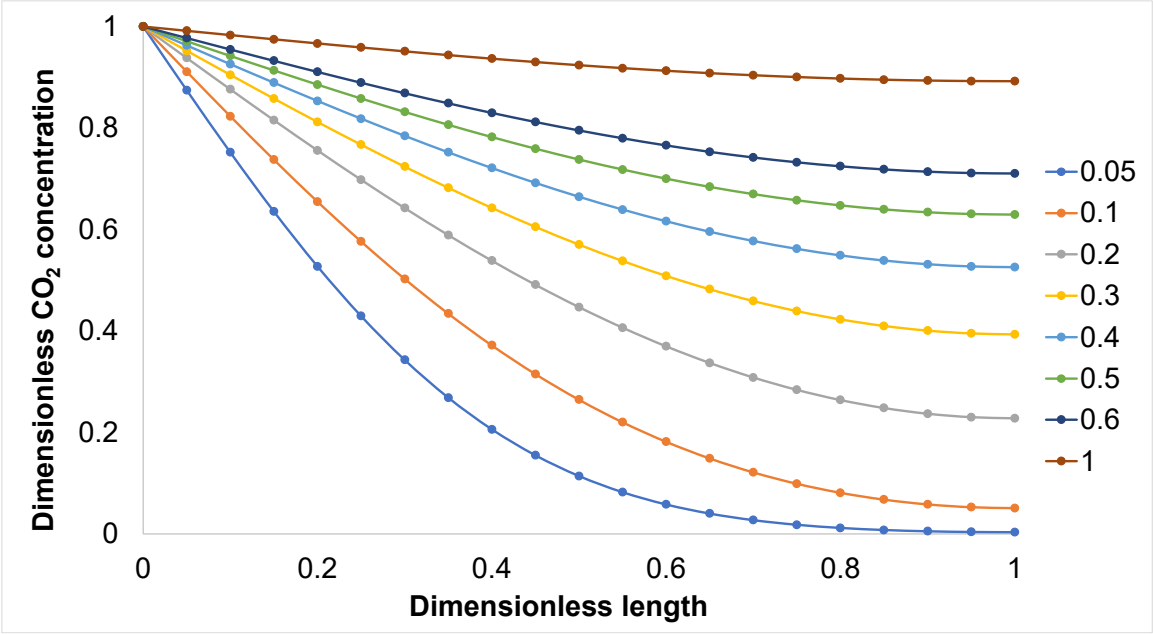

Figure A.4 Dimensionless concentration as a function of dimensionless time vs. dimensionless length at n = 3.

Results and Discussions

In this effort, the concentration profile of the diffused CO_2 in a porous medium was derived. According to past literature, it is known that tortuosity can highly deviate the accuracy of diffusion calculations. In this method, the tortuosity was not taken into consideration and neglecting it, could have influenced our ability to find the effective diffusivity. Porous media contains porous space that function as conduits. The total distance of these conduits is much longer than the straight paths. Fluid will always travel through tortuous channels and not straight lines; therefore, the molecular diffusion can potentially be very different than the effective diffusivity.

In comparison with Gao et al.'s article, the same concentration of CO_2 profile was derived. Gao et al., took a different approach to this problem and analytically solved the

governing equation by applying the Laplace transform. In contrast, dimensionless values were used to solve this problem. Additionally, the unsteady state equation was split into two terms (steady state and transient) and use both separations of variables and the orthogonal function to derive the equation.

Conclusions

In this mass transport study, the diffusion of CO_2 in oil-saturated core samples was investigated. The governing equation was derived based on the continuity equation on a molar basis. Several assumptions were made to simplify and solve the problem analytically. Ultimately, the author of this project and Gao et al. (2019) developed and derived the same concentration profile for an oil-gas system. Several assumptions where made that can potentially affect the outcome of the final derivation. The tortuosity has a great impact in the diffusivity due to the apparent and actual path length. Gao et al. (2019) stated that tortuosity has a great impact in diffusion of CO_2 in porous media. This is due to the increase in mass transfer resistance as tortuosity increases. Additionally, future studies should focus on CO_2 diffusion in oil-saturated porous media measured by utilizing multifunctional core displacement instruments and directly used to the results to model CO_2 injection. This practice has the potential to provide higher quality data that correlates to the practical gas injection procedure as it is also believed that an increase in tortuosity in the porous media can limit the CO_2 solubility.